Mammography Machine Compression Paddle Movement and Observer Performance Analysis

Wang Kei Ma

Thesis for the Degree of Doctor of Philosophy

PhD by Published Works

Directorate of Radiography

School of Health Sciences

University of Salford

Salford, UK

Table of Contents

List of Figures

Acknowledgements

I would like to thank my supervisors, Professor Peter Hogg, Dr John Thompson, and Dr Lucy Walton for their advice and support during the course of my authoring this thesis. I would like to offer my special thanks to Professor Richard Lawson for his insightful comments and suggestions. I am also immensely grateful to my co-authors, Professor David Howard, Dr Rob Aspin, Mrs Judith Kelly, Mrs Sara Millington, Dr Carla Lança, and Dr David Brettle for their contributions in the form of intellectual input, data collection, analysis, and co-authorship of the journal papers. I would like to extend my thanks to Mass Measuring Ltd and its staff members for granting me access to their equipment. Finally, I would like to thank my family and friends for their constant support.

Acronyms and Abbreviations

b	Damping coefficient
C_b	Breast viscous friction coefficient
C_p	Static position error coefficient
C_v	Static velocity error coefficient
CC	Craniocaudal view
d	Distance between object and the observer
D	Paddle and breast gain
DCIS	Ductal carcinoma in situ
DICOM	Digital imaging and communications in medicine
ECR	European Congress of Radiology
f	Focal spot size
F_p	Paddle force
FFDM	Full field digital mammography
FOM	Figure of merit
G	Gap between the support platform and the detector
H	Paddle and breast dynamics
IDC	Invasive ductal carcinoma
ILC	Invasive lobular carcinoma
k_b	Breast spring constant
k_p	Paddle spring constant
kVp	Kilovolt peak
mA	Milliamperes
m	Paddle mass
m_b	Effective mass of the breast and addle
MLO	Mediolateral oblique view
MP	Mega pixels
N	Newton
NHS	National health service
NHSBSP	National health service breast screening programme
O	Object size
OID	Object to image distance
PE	Polyethylene
PMMA	Poly methyl methacrylate
s	The Laplace variable
SD	Standard deviation

SFM	Screen film mammography
SID	Source to image distance
SOD	Source to object distance
T	Compressed breast thickness
Ug	Geometric unsharpness
US	United States
UK	United Kingdom
UKRC	United Kingdom Radiological Congress
WHO	World health organisation
x_p	Paddle displacement
$\ddot{x}_p$	Paddle acceleration
θ	Angular size
O_{min}	Eye resolution
τ	Machine drive time constant

Glossary

Paddle position	It refers to the position of the paddle as measured by the linear potentiometer and measured in mm
Paddle displacement	It refers to a change in paddle position and is determined by subtracting the final position of the paddle from its current position. It is measured in mm
Paddle motion or movement	It refers to a change in paddle position with time and measured in mm/s

Abstract

Full field digital mammography (FFDM) was introduced into the United Kingdom (UK) as a replacement for screen-film mammography (SFM) in 2005. Since then, individual breast screening centres have begun to report blurred images through local audits. Blurring was probably present in SFM as well, however the improvement in contrast resolution in FFDM may have made it more apparent. The sources of blurring include improper imaging techniques, patient movement caused by breathing and heart motion, the viscoelastic motion of the breast, and paddle motion. This thesis aims to test the hypothesis that paddle motion might cause image blur. It investigates whether blurring can be detected visually on technical review monitors and reporting grade monitors. The thesis presents a method to minimise paddle motion during X-ray exposure. Six papers have been published. Two of these (papers 1 and 2) investigated paddle displacement using linear potentiometers. Three investigated the influence of paddle motion on image quality. Paper 3 investigated whether paddle motion can cause image blur; paper 4 determined the minimum amount of simulated motion required for the visual detection of blurring; and paper 5 evaluated the practitioner's ability to identify blurring on monitors with different resolutions (2.3 MP and 5 MP). The final research paper (paper 6) investigated a way to reduce paddle displacement settling time; this involved the use of a closed-loop control system.

Results: In papers 1 and 2 paddle displacement followed a bi-exponential function with a settling time of approximately 40 s. The use of average paddle displacement to estimate the amount of paddle motion would underestimate the worst case of the three different runs of the experiment. The estimated paddle motion would be greatly reduced if the time of exposure is delayed from 5 to 10 s.

In paper 3 all metal ball bearings shown increased in diameters and the range of magnification varied from 1.04 to 1.21. T-test results shown that there was a significant difference ($p < 0.05$) in the ball bearing diameters between the intensity thresholding and the edge detection methods for all paddle/ compression force combinations. The ball bearing diameters calculated by the intensity thresholding method had higher variability than the edge detection method.

In paper 4 the soft-edged mask method best represented the physical process that caused the blurring effect and was chosen as the standard simulation approach for motion blurring. The ratio between the vertical paddle motion and the horizontal breast motion estimated by the mathematical model is approximately 1:0.3.

In paper 5 the angular size calculation shown that for a viewing distance of 75 cm the screen resolution for 5 MP and 12 MP monitors was better than the observer eyes' resolution. For a viewing distance of 30 cm the observer eyes' resolution was better than the screen resolution for 2.3 MP, 5 MP and 12 MP monitors. Among all three

monitors, image displayed on the 12 MP monitor has the lowest loss in image quality after interpolation.

In paper 6 the simulation results shown that force overshoot is possible for position control system. Force overshoot occurred almost instantaneously for step input and its magnitude is about 10 times larger than the ramp input. Force overshoot and steady-state error can be eliminated by the use of force control system.

Conclusion: The magnitude of calculated paddle motion is much lower than the minimum amount of simulated motion required for the visual detection of blurring. Mathematical models have shown that vertical paddle motion caused a smaller horizontal breast displacement when compressed. Therefore, there is no sufficient evidence to support the hypothesis that paddle motion is a cause of image blurring in FFDM.

Introduction

Since the introduction of full-field digital mammography (FFDM) in the National Health Service Breast Screening Programme (NHSBSP) in 2005 (Vinnicombe et al., 2009), individual breast screening centres have reported an increasing number of blurred images during image-quality audits (Kelly et al., 2011). Blurring was probably present in screen-film mammography (SFM), but due to the increase in contrast resolution in FFDM, it has become more apparent (Ikeda & Miyake, 2016). Seddon et al. (2000), in a study on SFM, found that 90% of their screening mammogram technical recalls were due to blurred images. A local audit conducted by Rourke et al. (2014) within breast screening centres in the Manchester area (UK) concurred with Seddon et al. (2000), finding that blurred images were a main reason for patient recall. Blurring can be technology-based, such as mammography paddle motion, or patient-based, such as heart motion, chest-wall motion, and breast motion (Geiser et al., 2011; Shah & Mandava, 2013). Breast motion is likely to occur due to the viscoelastic properties of the breast tissue while it is compressed (Insana et al., 2004; Carmichael et al., 2015). Image blurring could be the effect of both paddle and breast motion during exposure. Hauge et al. (2012) observed that paddle motion occurred after compression force ceased. However, whether this motion caused blurring in FFDM images and could be visually detected on technical review monitors or reporting grade monitors was

unknown. Due to the increasing importance of blurred images and the paucity of literature on it, this thesis presents the investigation of one possible causation of blurring paddle motion during exposure. It also considers how it visually affects image appearance as well as its potential solutions.

Aims

The aims were to test the hypothesis that paddle motion causes image blur in FFDM and to propose a novel method for minimising the effects of paddle motion.

Objectives

The objectives were to determine the following:

1. Whether image blur due to paddle motion can be detected in FFDM images

2. The minimum level of simulated motion required for blurring detection

3. Observer blurring detection performance

4. Whether using closed-loop control systems could reduce paddle displacement settling time

Rationale of the thesis

Image blur in FFDM is a widely recognised problem within the NHSBSP. Anecdotal evidence, together with observations by Hauge et al., suggests that paddle motion could be a source of image blur. Previous to and during the development of this thesis, no study had determined whether paddle motion could cause blurring in FFDM images or whether blur could be visually detected on monitors with different resolutions.

Therefore, this thesis seeks to evaluate the effect of paddle motion on FFDM.

Published works

Six peer-reviewed publications between 2014 and 2017 have been included in this portfolio, and my contributions to each paper are detailed in appendix 1. The papers have undergone peer review and were subsequently accepted for publication. The dates of publication do not reflect the order in which the research was undertaken. This is partly due to the labour-intensive nature of each and because some papers took varying amounts of time to move through the publication process. The Gantt chart in Figure 1 illustrates the timeline of research and writing activities. The flowchart in Figure 2 summarises the research process and timeline of each publication.

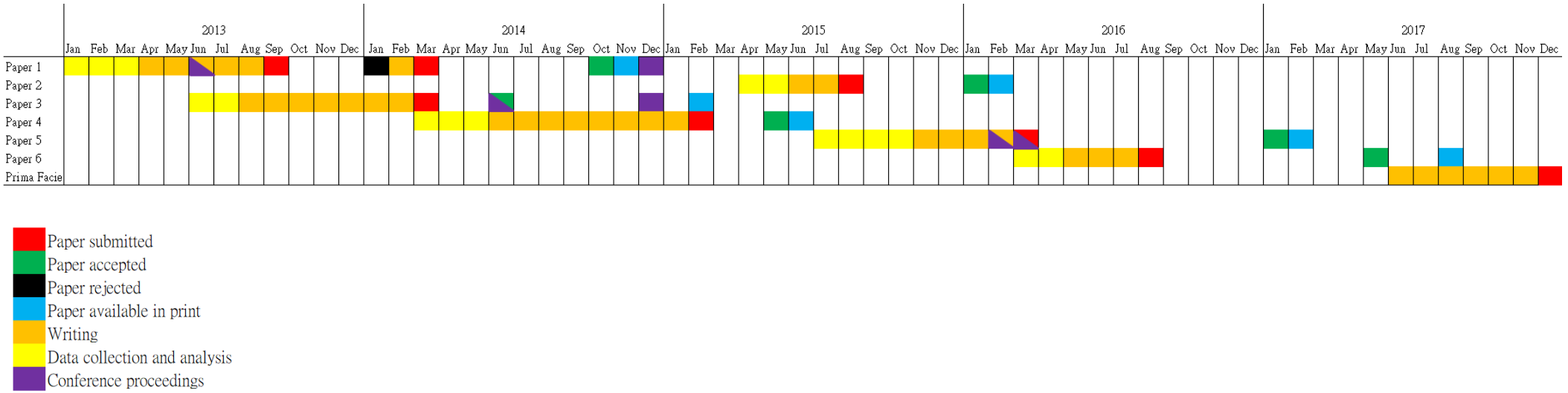

Figure 1. Gantt chart showing research and writing activities

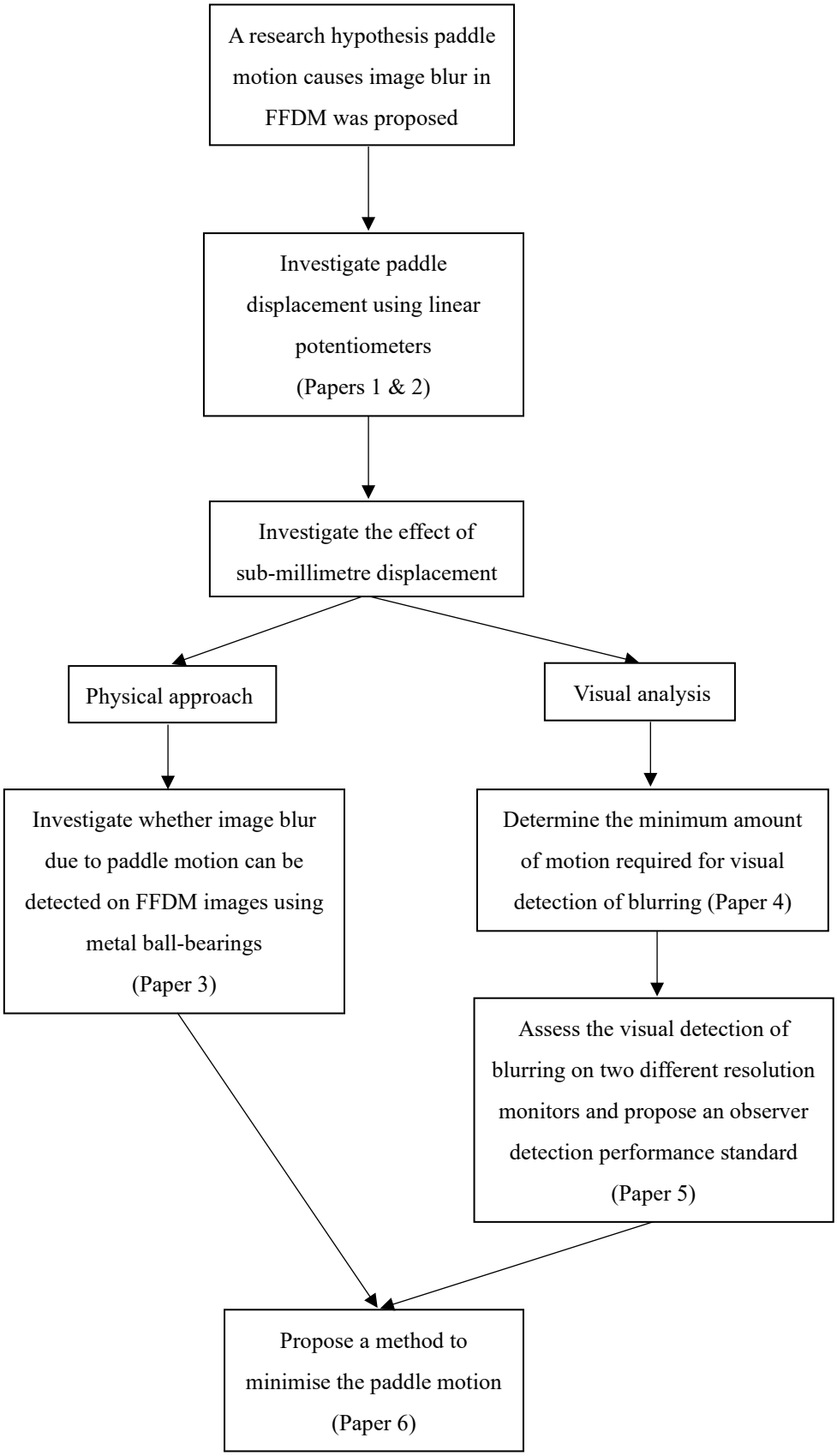

Figure 2. Research process and timeline of publication

Conference proceedings

Relevant posters and oral presentations at international conferences and seminars have been produced since 2013 to promote this research topic and bring the research findings to the attention of practitioners. Posters were presented at the United Kingdom Radiological Congress (UKRC) and European Congress of Radiology (ECR) in 2013, 2014, and 2016. The research was also presented as part of local mammography seminars in North West England. Oral presentations were delivered at research seminars at the University of Salford in 2014 and 2016. Table 1 summarises the contributions to international conferences and local seminars.

Table 1 Conference and seminar proceedings

Conferences/ Seminars	2013	2014	2016
Paper 1	UKRC Poster	Oral presentation at the University of Salford (Mammography Research Seminar)	
Paper 3		UKRC Poster Oral presentation at the University of Salford (Mammography Research Seminar)	
Paper 5			ECR poster Oral presentation at the University of Salford (Controversial Issues in Breast Cancer Diagnosis using FFDM Research Seminar)

What is breast cancer?

This section explains what breast cancer is and provides statistics to show the international prevalence of breast cancer among women. Breast cancer is an uncontrolled growth of breast cells leading to the formation of a lump, also known as a tumour (Cutter, 2018).

Breast cancers can be classified based on where they form and how they spread. Ductal carcinoma in situ (DCIS) is the most common type of non-invasive breast cancer and is responsible for 20 % of newly diagnosed breast cancer cases (Parikh, Chhor, &

Mercado, 2018). DCIS is formed in the lining of the breast milk ducts and does not spread outside of the duct (Welcsh, 2009). Cancers that spread into the surrounding breast tissue are known as invasive breast cancers and can be classified as either invasive ductal carcinoma (IDC) or invasive lobular carcinoma (ILC) (Goodman & Fuller, 2011). While IDC originates in the milk ducts (Figure 3) and constitutes approximately 80 % of breast cancers, ILC originates in the milk-producing gland lobules (Figure 4) and represents approximately 20 % of breast cancers (Odom-Forren, 2017).

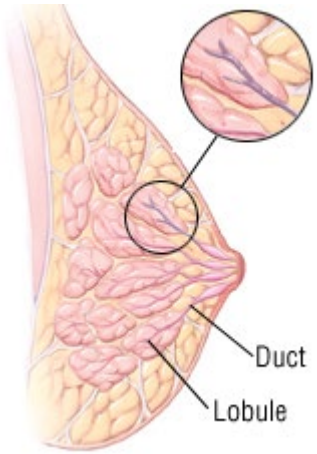

Figure 3. Illustration of invasive ductal Carcinoma (Harvard Health Publishing, 2014)

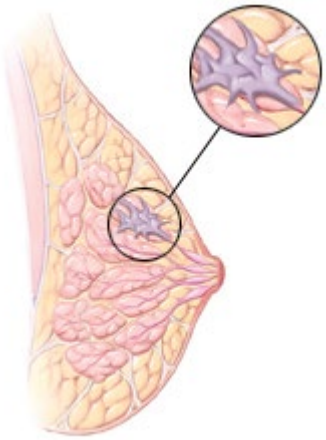

Figure 4. Illustration of invasive lobular carcinoma (Harvard Health Publishing, 2014)

Breast cancer is the most common cancer. It is the leading cause of cancer deaths in women worldwide (World Cancer Research Fund International, 2018). There were 2,088,849 new breast cancer cases diagnosed in women worldwide in 2018, constituting approximately 11.6 % of new cancer cases. Furthermore, there were

626,679 breast cancer deaths in women worldwide. This represents approximately 6.6 % of total cancer deaths (Bray et al., 2018).

Mammography

Before moving into how breast screening is organised, this short section explains the background information on how images were previously acquired and why there has been a move towards digital mammography. Mammography is a radiographic examination of the breast. It uses low energy X-rays (25-35 kVp) to enhance breast tissue contrast (Dendy & Heaton, 2012) to allow subtle breast cancer lesions to be detected visually. Mammography continues to be used in breast screening programmes because it is a low-cost and low-radiation procedure that offers reasonable sensitivity for the early detection of breast cancers (Shah & Guraya, 2017). Mammography is conducted in symptomatic women with breast abnormalities and in asymptomatic women as part of breast screening programmes (Whitley, 2015).

Digital mammography, also known as FFDM, first gained approval from the United States (US) Food and Drug Administration in 2000 (White, 2000). In the UK, FFDM was first introduced into the NHSBSP in 2005 at the St Bartholomew Hospital (London, England) (Vinnicombe et al., 2009).

Throughout many countries around the world, FFDM has replaced SFM in most breast cancer screening centres (deMunck et al., 2016) because the former provides a lower

radiation dose (in the case of large breasts), faster image acquisition, higher contrast resolution, and a wider dynamic range (Brant & Helms, 2012; Silverman, 2012). The dynamic range of the imaging system refers to the range of exposures that an image receptor can accurately detect (Johnston & Fauber, 2015). The wide dynamic range of FFDM means that even moderate underexposure or overexposure can still produce diagnostic images of acceptable quality (Fauber, 2013). In 2001, the American College of Radiology Imaging Network conducted a digital mammographic image screening trial to measure the diagnostic accuracy of FFDM and SFM. This was carried out for a screening population of 49,528 women over 25 months in 33 American and Canadian screening centres. It was found that the overall diagnostic accuracy of FFDM and SFM for breast cancer screening is similar, but that FFDM is more accurate in pre- or perimenopausal women younger than 50 years with dense breasts (Pisano et al., 2005, 2008).

Breast Screening Programmes

Breast screening programmes have been implemented in many countries throughout the world, each of recommending different beginning and ending ages and screening frequencies (Ali et al., 2015). A 2017 study by Altobelli et al. found that breast screening programmes are active in almost all World Health Organisation (WHO)

region European countries, except in Greece, the Czech Republic, and Slovakia, with screening participation levels varying from 20 % to 91 %.

The goal of breast screening programmes is to reduce breast cancer mortality rates through its early detection and treatment (Sardanelli et al., 2017). In a randomised controlled trial of 160,921 women in the UK, there was a 24 % reduction in breast cancer mortality compared with women who did not undergo screening (Moss et al., 2006). Notably, the findings by Marmot et al. (2013) were similar to those by Moss et al. (2006). Marmot et al. (2013) conducted an independent review of the benefits and potential harm associated with breast cancer screening via a meta-analysis of 11 randomised controlled breast screening trials with 13 years of follow-up. They found that a reduction of approximately 20 % in breast cancer mortality was achieved in women who participated in the breast screening programme.

Early detection of breast cancer has also been found to improve patient survival rates by the National Cancer Institute's Surveillance, Epidemiology, and End Results database (Noone et al., 2018), which represents approximately 10 % of the population of the US. The five-year survival rate for women diagnosed with early-stage breast cancer (Stages 0 to II) was more than 90 %, while the survival rate dropped to 22 % for those diagnosis with advanced-stage breast cancer (Stage IV or metastatic).

Mediolateral oblique (MLO) and craniocaudal (CC) views are standard projections

performed during routine screening mammograms (Sweeney et al., 2017). The MLO projection demonstrates the inframammary angle and all of the breast tissue in one image, while the CC projection demonstrates the majority of the breast tissue with the exclusion of the extreme portion and the axillary tail (Popli et al., 2014) .

Figure 5 presents the process of conducting a mammogram and the relative position of the patient, compression paddle, image receptor, and X-ray tube.

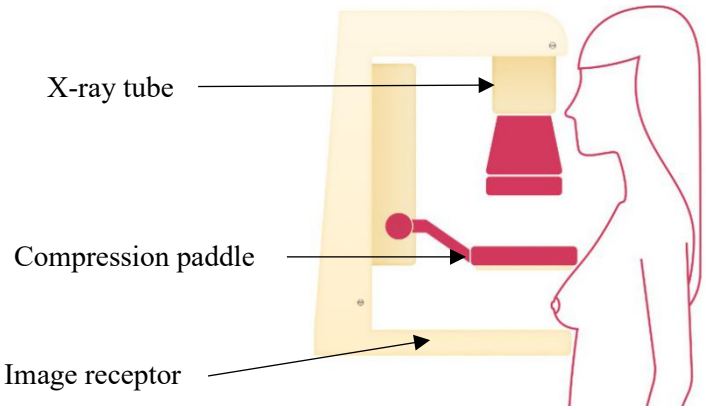

Figure 5. Schematic showing the process of conducting a mammogram (National Breast Cancer Foundation, 2016)

Technical Recall and Technical Repeat

FFDM images are examined to ensure that their technical quality is sufficient for diagnosis and that they are free from blurring or other unwanted artefacts before being sent for reporting. If image blur is identified at the time of attendance, the operator may repeat the examination while the patient is still in the clinical room (a technical repeat)

(NHSBSP, 2017a). If image blur is identified during reporting, the patient might be recalled for a new appointment (a technical recall) (NHSBSP, 2017a). If this occurs, the patient may have to wait several days for a repeat mammogram and this could lead to further anxiety in patients and their families (Hogg et al., 2015). Repeat mammograms also incur increased patient radiation dose (Hogg et al., 2015), increased cost attributed to NHSBSP for booking the appointments and reattendance (Rothschild, Lourenco, & Mainiero, 2013), and possibly a violation of the NHSBSP performance criteria of 3 % technical repeat and 70 % attendance rate (NHSBSP, 2017b).

What is Blurring?

Image blur is defined as the 'unsharpness' of well-defined boundaries in an object image (Hendee & Ritenour, 2002). In medical imaging there are three types of unsharpness, as follows: (i) geometric unsharpness, (ii) photographic unsharpness, and (iii) motion unsharpness (Allisy-Roberts & Williams, 2007).

Geometric unsharpness occurs due to the penumbra from the finite size of the X-ray source (Flower, 2012). The relationship between geometric unsharpness (Ug), focal spot size (f), object to image distance (OID), and source to object distance (SOD) is summarised in equation (1):

$$Ug = \frac{OID}{SID} f \quad (1)$$

Photographic unsharpness is dependent on the resolution of the image recording system in FFDM, specifically the size of the pixels (Dendy & Heaton, 2012). Motion unsharpness is caused by the movement of the patient or equipment during the exposure period (Lancaster & Hasegawa, 2016). These three types of unsharpness are interrelated: any change in one form of unsharpness will tend to provoke an increase in another form of as well (Whitley, 2015). For example, if the operator wants to reduce movement unsharpness for a restless patient by reducing the exposure time (s), the tube current (mA) must be increased correspondingly to maintain sufficient milliamperes for exposure. However, this increase in milliamperes may require an increase in focal spot size to cope with the increase in thermal loading on the anode, which will in turn increase the geometric unsharpness (Carlton & Adler, 2012).

Why blurring was missed

Operators do not always identify image blur, even though it exists. A study by Kinnear and Mercer (2016) performed in one UK screening centre for a 12-month period, showed that 0.88 % (40,954 clients) of mammographic examinations were recalled by the image reader and 1.16 % were repeated by the operators. They further analysed the recall data and found that more than half of the recalls were due to image blur, while only 5 % of the repeats were due to image blur. This indicated that blurring is often

missed by the operators at the time of examination.

There are many instances in which blurring is missed when images are checked for technical accuracy at the time of imaging, while the patient is still in the clinical room. Possible causes for this could be the lower quality technical review monitors used in the clinical room, sub-optimal viewing conditions and that blur recognition is not always covered in operator training (Kinnear & Mercer, 2016; Kelly & Hogg, 2018). Typically, clinical room monitors used for assessing image quality are 3 mega pixels (MP) or lower, while reporting grade monitors are 5 MP. Thus, subtle artefacts such as blurring could be being missed on the lower grade technical monitors.

Kinnear and Mercer (2016) compared the ability of six observers to detect blurring on FFDM images on 1 MP and 5 MP monitors. They compared the 1 MP and 5 MP monitors using the NHSBSP guidance on image display equipment (NHSBSP Equipment Report 0604, 2009), which states that high-resolution monitors within the mammography department for diagnostic reading must be at the 5 MP level, while the 'general' category display monitors in clinical rooms for image acquisition and reviewing could be lower than 3 MP. They found that higher resolution monitors resulted in a 16 % higher visual detection rate for blurred images compared with lower resolution monitors. They further concluded that the blurring detection rate could be improved if higher resolution monitors were used for image review in clinical rooms.

However, the limitation of this study is that only a small number of observers were involved in viewing the images and the order of the image display was not randomised between reads to reduce recall bias. As image assessment is subjective in its nature, different image readers may produce different results and the results produced from a relatively small number of observers may not accurately represent general image readers. Therefore, to produce more robust results, the number of observers could be increased and the order of images could be randomised between reads.

The effect of blurring

If blurring is not recognised at the time of imaging, the resulting suboptimal images may affect lesion detection performance (Abdullah et al., 2017). A study by Abdullah et al. (2017) demonstrated that motion blurring can significantly reduce the lesion detection performance of observers. In their study, they compared the lesion detection performance of seven observers in 248 cases (62 with masses, 62 with microcalcifications, and 124 normal cases) for three conditions: no blurring, 0.7 mm and 1.5 mm simulated blur, respectively. The motion blur was applied using a mathematical technique called convolution masking which produces a three-standard deviations (SD) distribution of blur in FFDM images. Abdullah et al. (2017) used the figure of merit (FOM) to represent the probability that lesion localisation would be

rated higher than non-lesion localisation in normal cases. They found a significant difference in lesion detection performance for both masses and microcalcifications. Furthermore, the FOM was reduced as the magnitude of simulated blurring increased. The FOM reduction indicated that motion blurring has a negative effect on lesion detection performance for the detection of masses and microcalcifications in FFDM images. The limitation of this study is that the blurring is imposed globally by the mathematical simulation software, but in clinical practice the motion blurring can be global or regional. Therefore, these results may not fully represent the effect of blurring on lesion detection performance. Unlike masses, microcalcifications are anatomical structures which have a low contrast to their background and slightly blurred edges (Linguraru, Brady, & Yam, 2001). Thus, the presence of regional blur may reduce the visibility of image details and limit the image reader's ability to detect the microcalcifications (Ekpo et al., 2018). This study may have potentially underestimated the effect of blur because it did not consider the effects of regional blur on the visual detection of microcalcifications.

Image blurring has the potential to increase the false-negative results, as it may obscure small lesions and affect the assessment of low-density microcalcifications in dense breast tissue (Hogg, Kelly, & Mercer, 2015). If the image reader does not recognise abnormalities, false-negative interval cancers could occur. False-negative interval

cancers are tumours that are visible on a mammogram but are not recognised by the image reader due to misinterpretation or technical error (Renart-Vicens et al., 2014). Many reasons exist for missed cancers, including image blur, as noted above in Abdullah's work. A retrospective study by Hoff et al. (2012), involving data from the Norwegian Breast Cancer Screening Programme from 2002 to 2008, showed that the percentage of interval breast cancers missed using FFDM can reach 33% (16/49). Knowing that blur is a problem in FFDM, it is possible that some of these cancers might have been missed due to this kind of artefact.

Rosen et al. (2002), in their retrospective study of 295 short-term mammographic follow-up cases, found that 41% (21/51) of malignancies that were identified as microcalcifications were not biopsied and were incorrectly followed up on. This was because the magnification views were compromised by blurring. Figures 6 and 7 show the FFDM images of the same patient with and without blurring. The fine microcalcification can be seen on the sharp image (Figure 6) but cannot be seen on the blurred image (Figure 7).

Figure 6. Image with blurring. The arrow indicates area of fine microcalcification (Kelly & Hogg, 2018)

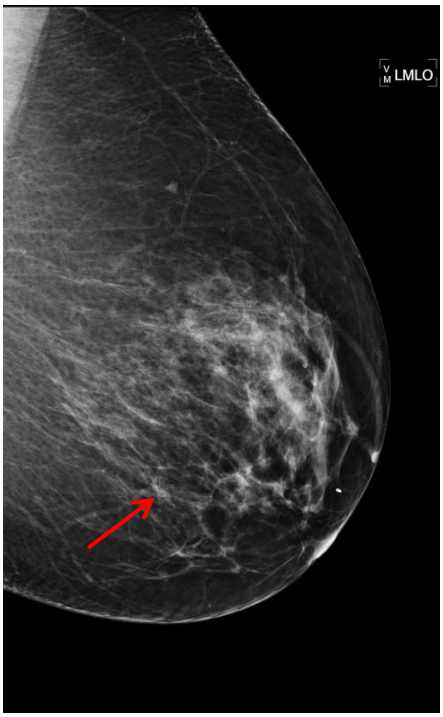

Figure 7. Image without blurring. The arrow indicates area of fine microcalcification (Kelly & Hogg, 2018)

Breast Compression

During mammography the breast is compressed with compression paddles which tend to be made of Lexan and have a right-angled edge at the chest-wall side (Bushberg et al., 2011). The intention of compression is to reduce and make uniform the breast thickness to reduce the breast radiation dose and improve image quality.

Compression provides lower attenuation to the incident X-rays and the radiation dose can be lower while still achieving a similar image quality (Analoui, Bronzino & Peterson, 2012). It reduces the breast tissue thickness and shortens the path for the X-

ray photons to travel before reaching the detector, this reduces the scatter radiation and lowers the radiation dose for the patient (Kuppusamy, 2017).

Compression improves the image quality by reducing both motion unsharpness and geometric unsharpness. This is because it immobilises the breast and brings the breast structures close to the image receptor, which reduces the OID (Brant & Helms, 2012; Carlton & Adler, 2012).

It is important to ensure adequate compression is applied to the breast to minimise motion blurring. A study by Seddon et al. (2000), which aimed to identify the causes of blurring on film images, found that more than 90 % of recalls were due to blurred images. To investigate the possible causes of blurring, Seddon et al. (2000) reviewed two groups of SFM with 45 randomly selected, technically adequate films and 45 blurred films. They found that breast thickness was significantly higher in the blurred group ($p < 0.01$) and that the average compression forces applied for the blurred and adequate films were 100 N and 130 N, respectively. They concluded that inadequate compression is the cause of blurring. The limitation of this study was that the authors only reviewed SFM images and that their results may not applicable in the case of FFDM.

Breast compression cycle

According to de Groot et al. (2013), breast compression consists of a deformation phase, for flattening the breast, and then a clamping phase, for its immobilisation. Figure 8 illustrates these phases. In the deformation phase, the breast is flattened gradually by the lowering of the paddle. This occurs alongside the increasing of compression force, up to a target force. In the clamping phase, the paddle is held at the same position to immobilise the breast. After the exposure, the paddle returns to its original position and releases the breast.

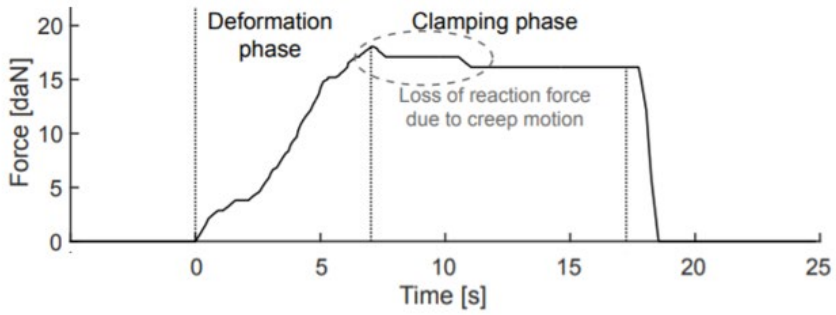

Figure 8. Typical breast compression cycle (de Groot et al., 2015)

Pressure standardised compression

The current compression practice is based on force-standardised compression in which each breast is compressed within the range of recommended compression forces (denBoer et al., 2018). As the force-standardised approach does not consider breast size, it may lead to a large variation in applied pressure (Branderhorst et al., 2015). The

problem with this approach is that the amount of applied pressure can be different for each breast, and that the pressure would be larger for smaller breasts compared with larger ones because the contact area between the breast and the paddle is smaller whilst still being under the same compression force (Bushberg et al., 2011). A study by de Groot et al. (2015) showed that force-standardised compression may result in women with smaller breasts being subjected to higher pressures and experiencing more pain during mammography compared to women with larger breasts. DeGroot et al. (2015) compared the use of a force-standardised protocol with a pressure-standardised protocol and found that the proportion of retakes (16.4 % for the force-standardised protocol and 16.0 % for the pressure-standardised protocol) and average glandular dose were similar for both protocols, but that pain was significantly reduced in the case of the pressure-standardised protocol (average pain scores were reduced by 10 % in MLO view and 17 % in CC view). Recently, a pressure-based compression paddle called the Sensitive Sigma paddle (Sigmascreening, Amsterdam, Netherlands; Figure 9) was developed to optimise breast compression during mammography. The Sensitive Sigma paddle has multiple pressure sensors to measure and calculate the pressure in real time to achieve an optimal compression pressure of 75 mmHg, which makes the procedure more predictable and reproducible (Sigmascreening, 2017).

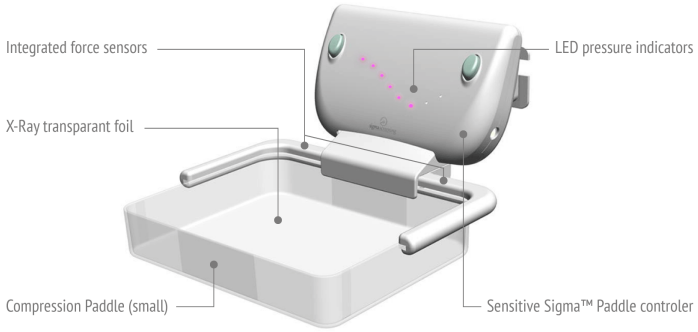

Figure 9. Illustration of Sensitive Sigma Paddle (Sigmascreening, 2017)

Previous studies on paddle motion

Paddle motion was first reported by Hauge et al. (2012) in their multicentre study. They evaluated breast thickness readout variations on a range of SFM and FFDM units (eight units and six different manufacturers) for two differently sized paddles (18 x 24 cm and 24 x 30 cm) and two compression forces (60 N and 100 N). A custom thickness measuring device was used with a breast phantom to measure the distance between the paddle and detector. They found that the maximum thickness variation was 16 mm in the 18 x 24 cm flexible paddle. The differences in readout and measured thickness suggested that bending and distortion occurred in the paddles after the compression force ceased. The authors hypothesised that paddle bend and distortion may be linked to motion artefacts. The limitation of this study, as noted by the authors, was that different readout thicknesses were achieved every time when the measurement was

repeated. This may have been due to positioning errors during repeats. Positioning errors can be reduced by using optical measuring technology because optical measuring devices can automatically detect the measurement points which reduces the risk of human error, as this step would typically be carried out by an operator (Metrios, 2020). Separately, Hogg et al. (2012) extended the work by Hauge et al. (2012) to consider the relationship between the applied compression force and the breast thickness readout. They generated composite compression graphs (Figures 10 and 11) using the female mammography compression data (131 compression sets for CC and 128 for MLO views). They observed unusual appearances in the compression graphs and found abnormal changes in breast thickness (i.e. reduced change in breast thickness magnitude when compression force increased) at compression forces of 7, 9, and 11 dN, which suggested that paddle/breast motion occurred during compression. They hypothesised that this could be due to paddle relaxation, breast relaxation or both. Relaxation is achieved when the breast and paddle have stopped moving.

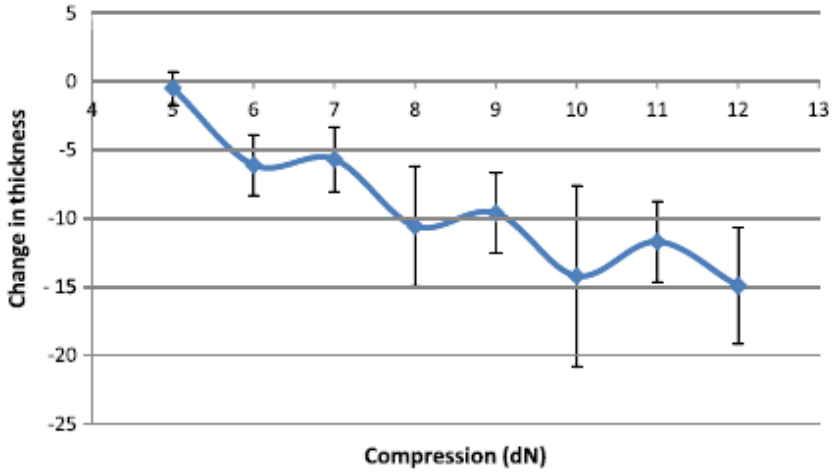

Figure 10. Change in breast thickness versus compression in CC view (Hogg, 2012)

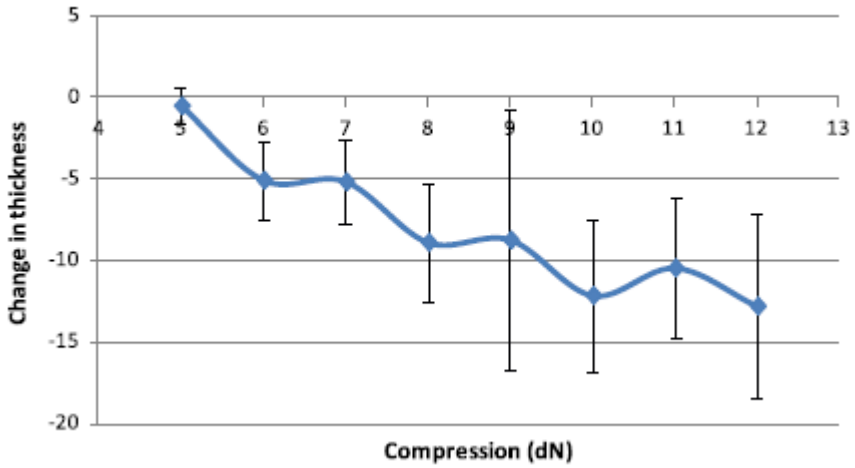

Figure 11. Change in breast thickness versus compression in MLO view (Hogg, 2012)

Having reviewed the literature relevant to this thesis, the papers presented along with this thesis will now be reviewed critically.

Critical review on paper 1 & 2

Paper 1. Ma, W. K., Brettle, D., Howard, D., Kelly, J., Millington, S., & Hogg, P. (2014). Extra patient movement during mammographic imaging: an experimental study. *The British journal of radiology, 87*(1044), 20140241.

Paper 2. Ma, W. K., McEntee, M. F., Mercer, C., Kelly, J., Millington, S., & Hogg, P. (2016). Analysis of motion during the breast clamping phase of mammography. *The British journal of radiology, 89*(1059), 20150715.

The novelty of paper 1 is that it is first time a mathematical model was used to analyse the paddle motion. Paper 1 suggests that the compression should be applied slowly to avoid sharp changes in compression force. The novelty of paper 2 is that it was the first multicentre study to investigate the paddle motion during the clamping phase. Paper 2 suggests that the exposure could be made a few seconds after the clamping phase commences. Both papers provide recommendations for clinical practice on how to reduce the possibility of image blurring. The following section will provide a critical review on papers 1 and 2.

Misinterpretation of movement

In paper 1, there was a mistake made in the labelling of the graphs in Figures 6, 7, 8 and 9 which show displacement against time, not movement against time. Therefore, the fitted bi-exponential paddle equations are equations of displacement against time rather than movement (or motion) against time. The implication of this

misinterpretation is that the actual amount of motion during a 2-second exposure is much less than the value calculated in paper 1. For example, in paper 1 the estimated "movement" for the 2 s limit at the 18x24 cm and 24x29 cm flexible paddles were 0.8 mm and 0.6 mm. This is in fact the displacement at 2 s after compression and thus these values need to compared with the displacement at 0 s (0.9 mm and 0.7 mm) to get the motion during a 2-second exposure, which are 0.1 mm and 0.1 mm. The implication of an overestimation in paddle motion is that the original hypothesis (paddle motion causes image blur in FFDM) may no longer be valid since the estimated paddle motion for the 2 s limit is greatly reduced from 0.9 mm to 0.1 mm for the 18x24 cm flexible paddle and from 0.7 mm to 0.1 mm for the 24x29 cm flexible paddle. The amount of paddle motion is now less than the threshold required for the visual detection of blur (≥ 0.7 mm).

In addition, the assumption made in the calculation of paddle motion may not be realistic because it assumes the exposure would take place immediately after compression had finished. In clinical practice, the operator needs time to move behind the screen before the exposure can be started.

A similar mistake was made in Tables 4 and 5 of paper 2, as the displacement was misidentified as motion. For example, in paper 2 the values in Tables 4 and 5 are only the displacement at 2, 4, 8, 16 and 32 s after clamping commencement. These values

would need to be compared with the displacement at 0 s to get the motion. The implication of this misinterpretation is that the vertical paddle motion for both small and large paddles was overestimated.

Single exponential or bi-exponential

In paper 1, the fitted results for the paddle displacement equations had identical values for λ1 and λ2 which implies a single exponential. As shown in Figure 12, the data is not a single exponential (green curve) because it does not fit well with the measurements (blue curve), while the bi-exponential fit (red curve) is much closer to the measurements.

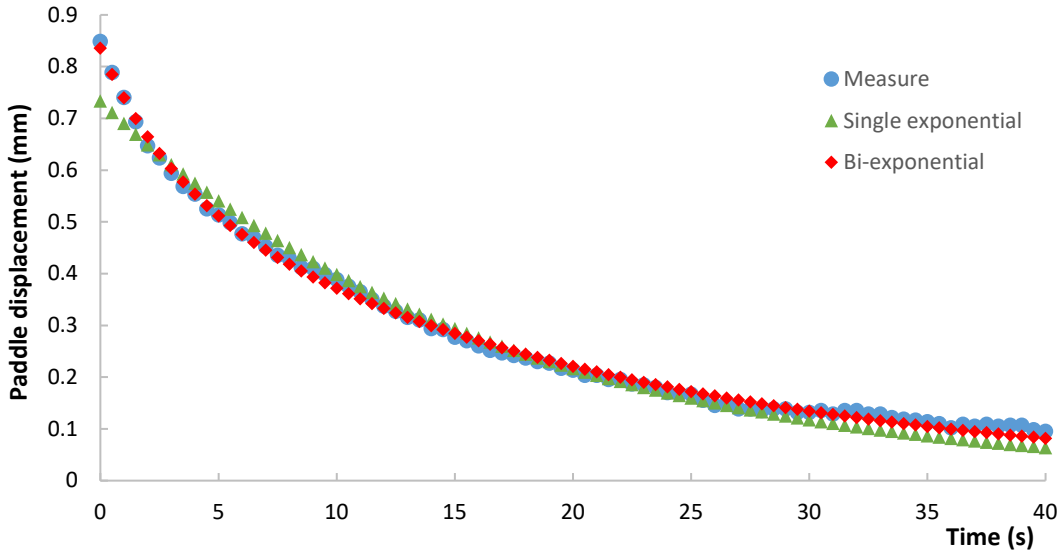

Figure 12. Single and bi-exponential fit for the displacement time curves

The reason why the bi-exponential was misidentified with the single exponential could be that the curve fitting program did not find the optimum solution. When the paddle displacement equations were derived using the 'Simplex' method in Excel Solver (Microsoft, Redmond, WA), it only found a local minimum rather than a global

minimum. This may have been because the target function may have a complicated landscape with several valleys. Therefore, the 'GRG Non-linear' method should have been used because it sets several starting points randomly over a landscape to ensure the curve fitting program can find a global minimum (McFedries, 2019).

Variations in starting position

In paper 1, the measurement was repeated three times to minimise the experimental uncertainties and the results were averaged to determine the average paddle displacement. Figure 13 shows how big the difference can be in the starting position of the paddle for three runs of the experiment. The first run of the experiment (blue curve) shows a greater paddle motion (steeper slope of the curve) than the average (yellow curve), while the second run of the experiment (orange curve) shows much less paddle motion than the average. The difference in starting position of the paddle may depend on small variations in how an operator performs a breast compression. For example, how quickly the paddle is moved, which area of the breast is compressed; and whether the compression is stopped at 79 N, 80 N or 81 N.

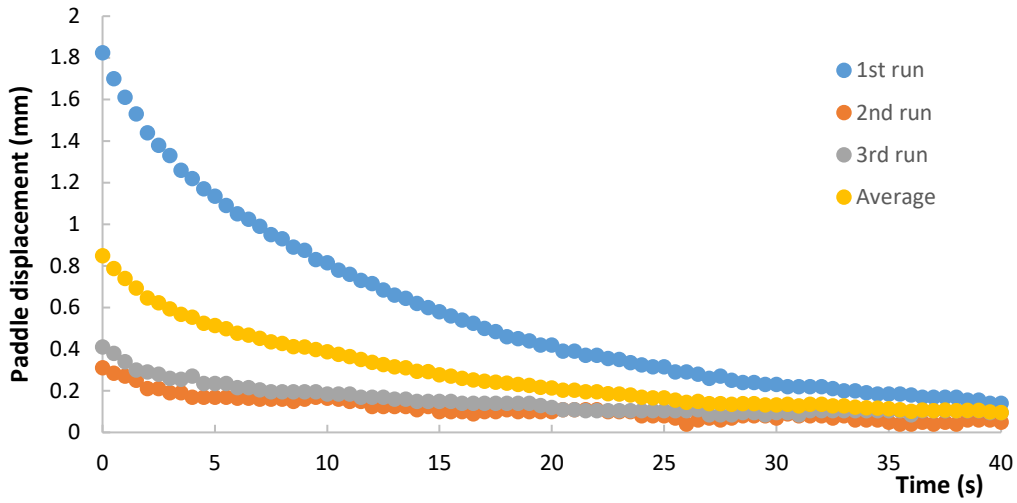

Figure 13. Displacement time curves for a 18x24 cm fixed paddle for three runs of the experiment

The displacement equations for the three runs of the experiment and the average can be found by curve fitting.

$$x(t)_{1st} = 0.34e^{-0.39t} + 1.48e^{-0.06t} \quad (2)$$

$$x(t)_{2nd} = 0.11e^{-0.67t} + 0.21e^{-0.04t} \quad (3)$$

$$x(t)_{3rd} = 0.24e^{-0.14t} + 0.13e^{-0.01t} \quad (4)$$

$$x(t)_{aver} = 0.24e^{-0.33t} + 0.60e^{-0.05t} \quad (5)$$

In theory, the three runs should all have similar values for λ1 and λ2 because they reflected same the physical properties - elasticity and damping of the system. However, the values for λ1 and λ2 are different in each run. One possible explanation is that the speed of the compression may affect the elasticity and damping of the system. For thixotropic material, the viscosity decreases under high shear rate (Ducheyne, 2017).

This is because breast phantoms have similar compression characteristics to the human female breast, which also exhibits thixotropic behaviour during compression. If the viscosity decreases with the speed of the compression, the damping of the system would also decrease.

In paper 1, the use of average value to estimate the amount of motion for the 2 s limit would inevitably underestimate the worst case of the three runs. For example, if an 18 x 24 cm fixed paddle was used for compression, the exposure was taken at 5 s, and a typical exposure lasts for 2 s, then using the displacement equation for the first run (2) and the average (5) to calculate the displacement at 5 s and 7 s would result in 1.13 mm and 0.97 mm for the first run and 0.51 mm and 0.44 mm for the average. The estimated paddle motion during the time of exposure (lasting from 5 s to 7 s) for the first run and the average would be 0.15 mm and 0.07 mm. Therefore, it would be more useful to look at the worst case rather than the average, which is more likely to produce blur. The implication of averaging the three runs is that the variation in the starting position would have been ignored.

Hypothesis on paddle motion

The hypothesis of this thesis was that paddle motion can cause image blur. This hypothesis was developed from the study by Hauge et al. (2012) who noticed that the paddle moved for a significant period after compression force had ceased. The paddle

motion study in paper 2 demonstrated that the paddle always moves during the clamping phase but that not every image is blurred. This can be explained by the moment of exposure and the amount of motion required for the visual detection of blurring. The effect of the moment of exposure can be explained using the paddle displacement equation (2):

$$x(t)_{1st} = 0.34e^{-0.39t} + 1.48e^{-0.06t} \quad (2)$$

According to de Groot et al. (2013), the clamping phase lasts approximately 12.8 s and exposure should be made within this time period. Assuming an 18 x 24 cm fixed paddle was used for compression and the exposure was made at 5 s and a typical exposure lasts 2 s, then by using the displacement equation (2) for the 18 x 24 cm fixed paddle (lasting from 5 s to 7 s) the motion would be 0.15 mm during the time of the exposure. On the other hand, if exposure was made at 10-12 s, the paddle would move 0.10 mm during the time of exposure. This illustrates that if exposure begins later, the change in displacement during the time of exposure smaller. If the change in displacement during the exposure is smaller than the minimum amount of motion required for the visual detection of blurring (Ma et al. 2015, Paper 3 of my PhD portfolio), which is 0.7 mm, there is a high possibility that the blur would not be noticeable to the naked eye.

Pilot study on linear potentiometers location

In papers 1 and 2, two calibrated linear potentiometers were placed at the anterior corners of the paddle to measure the paddle position. The rationale for doing this for 40s was based on a pilot study conducted on a Hologic Selenia Dimensions mammography unit (McGeever 2012). The pilot study by McGeever (2012) showed that the measured paddle position at the anterior corners is higher than it is the centre of the paddle, and that the value become stable after 30 s (Figures 14 and 15). As shown in Figure 15, the paddle position measured by potentiometer 1 is higher than that of potentiometer 2. This may be due to paddle tilt during the application of compression force, which results in linear potentiometers at slightly different levels.

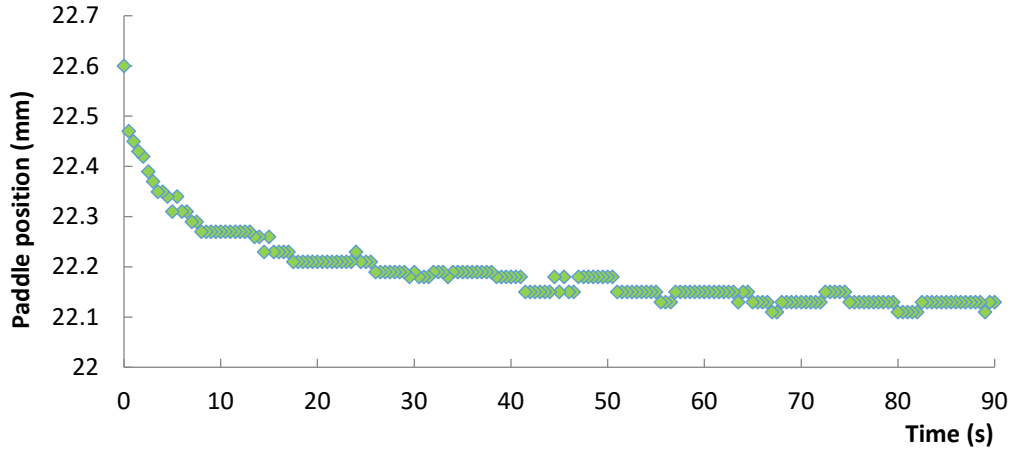

Figure 14. Paddle position against time for linear potentiometer at the centre of the paddle

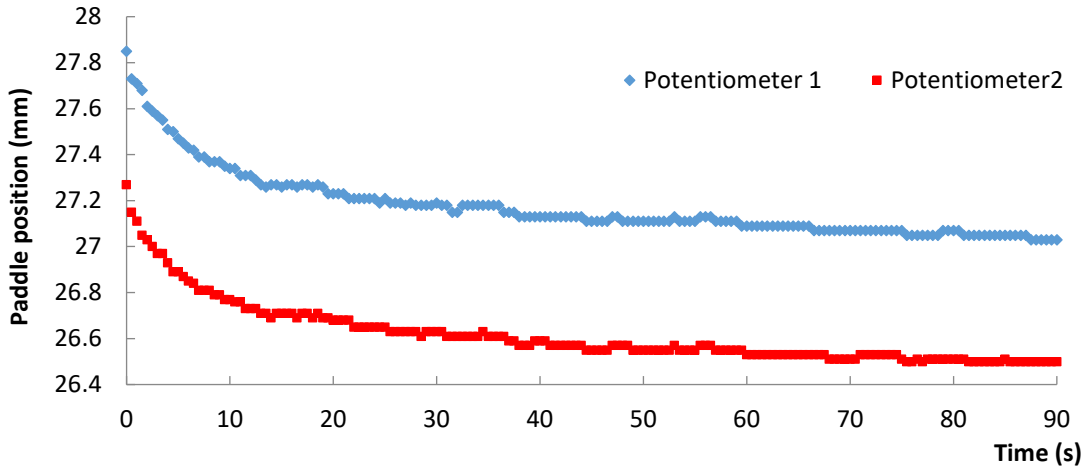

Figure 15. Paddle position against time for linear potentiometers at the anterior corners of the paddle

In theory, it would be ideal to place the linear potentiometers at the anterior corners and the centre of the paddle to obtain more data, but this was not possible due to the availability of only two potentiometers. Therefore, the two linear potentiometers were placed at the anterior corners of the paddle, and the readings were averaged.

Delay in data recording

In papers 1 and 2 the data recording was based on humans initiating the recording. This is because the reaction time required for the operator to recognise the cessation of compression force inevitably leads to a slight delay in recording (Avison, 2014). The time difference between the start of the data recording and the ceasing of compression force can affect the measured displacement. For example, if the start of the data recording is slightly delayed, the measured displacement may be smaller than the actual displacement. This is due to the change in paddle displacement being the highest in the

first few seconds. To minimise the delay in data recording, the operator immediately informed the person responsible for data recording once they ceased the compression. For future work an automated approach could be used to start the data recording process. For example, an infrared camera with custom software could monitor the application of compression force and activate the data recording process once the operator's hands left the hand wound. An alternative way to overcome the delay in data recording would be to start the data recording process before the end of the compression force application, because the clamping phase will start when the compression force reaches its maximum. This can be determined from the trace of the compression force.

The pros and cons of linear potentiometer

The rationale for using a linear potentiometer is that it can operate in adverse conditions, including high temperatures, vibration, and shock, which was necessary in this study because changes in compression force can be quite rapid and the measuring device must be able to withstand the sudden changes in motion. In addition, linear potentiometers have high sensitivity, which means even a small change in paddle motion can be detected. The limitation of using a linear potentiometer is that it only measures the displacement at a single point, thus necessitating a large number of linear potentiometers to be used to cover the paddle surface. The effect of measuring the paddle displacement at a single point is that the measured displacement may not represent the displacement at the paddle surface. One of the solutions to overcome this limitation is to use a laser displacement sensor to measure the paddle displacement over the whole paddle surface, however this technology was not commercially available at the time of the study. Another limitation of linear potentiometers is that they need to be in contact with the paddle to make the measurement. Therefore, the weight of the linear potentiometer itself may affect the paddle motion, especially if multiple linear potentiometers are used. Again, laser displacement sensors could be used to replace linear potentiometers for paddle displacement measurement. Given this technology is now commercially available, consideration should be given to its use for further work

(Keyence, 2019).

The laser technology

The main advantage of using laser displacement sensors is the non-contact nature of the laser sensor. This means the measurement can be made without touching the paddle and interfering with its motion. Another advantage of the laser displacement sensor is its high resolution. It can resolve measurements to less than 1 μm (Gupta, 2006), while the linear potentiometer can only resolve measurements to 0.01 mm (ATEK Sensor Technologies, 2018).

Despite all these advantages, laser technology was not used in this study because a suitable commercial system at a reasonable cost was not available when the research team first developed the potentiometer approach to measuring paddle motion in 2010. The Kinect (Microsoft Corp., Redmond, WA, US) has been widely used due to its low-cost, high accuracy, and repeatability (Galna et al., 2014; Adachi & Adachi, 2015; Otte et al., 2016; Mortazavi & Nadian-Ghomsheh, 2018).

The Kinect software development kit for Windows applications was released in 2012 (Microsoft, 2019). Since then, laser technology has become cheaper and more mainstream. Thus, future work could use laser technology to measure paddle displacement. Kinect is a motion sensing device developed by Microsoft for the Xbox 360 input device that uses infrared light for triangulation. Kinect can measure

displacement by projecting infrared light onto a surface. When the infrared light hits the surface, it rebounds and becomes distorted. Kinect then analyses the distorted infrared light patterns using the depth camera (Pöhlmann et al., 2014). The effect of using the Kinect in paddle displacement is that it can measure the displacement of the whole paddle surface instead of just at a single point. This can provide information to create a two-dimensional map in real time of the paddle displacement (Kamarudin et al., 2014).

Critical review on paper 3

Paper 3. Ma, W. K., Hogg, P., Kelly, J., & Millington, S. (2015). A method to investigate image blurring due to mammography machine compression paddle movement. *Radiography, 21*(1), 36-41.

The novelty of paper 3 is that it was the first study to investigate the image blur severity in different locations of the breast phantom. The findings of paper 3 are useful for the operator to identify possible areas of blurring. The following section will provide a critical review on paper 3.

Ball bearing segmentation

In paper 3, eleven metal ball bearings with 1.50 mm diameters were segmented from the background using the intensity thresholding method. Intensity thresholding is one of the most used methods for image segmentation and it separates the image into foreground and background (Russ and Neal, 2017). In intensity thresholding, pixels with an intensity less than or equal to the threshold turn into the background, while pixels with an intensity larger than the threshold turn into the foreground. Following segmentation using intensity thresholding, the diameter of the ball bearings was calculated from the area determined by the ImageJ. The limitation of this approach is that the area determined by ImageJ would be affected by the location of the ball bearing and the selection of the threshold value. Figure 16 shows the location of the eleven ball

bearings.

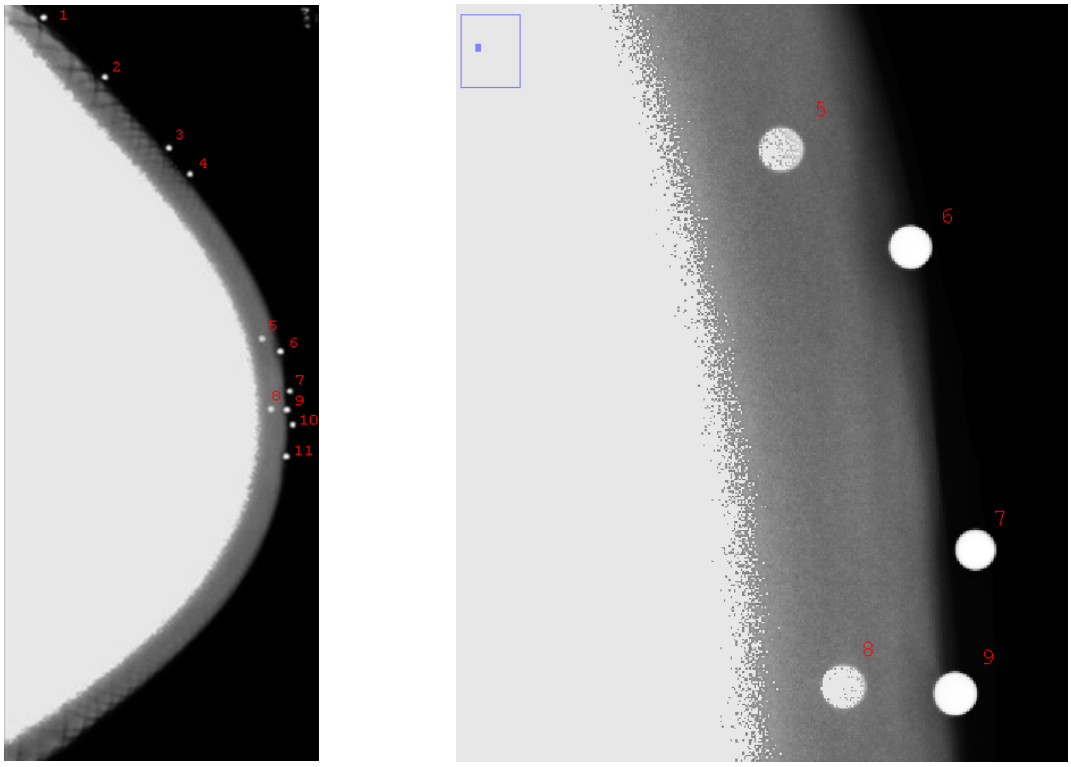

Figure 16. The location of eleven metal ball bearings with numbering; enlarged image shows ball bearings 5 and 8 has lower contrast. The white area within the image is the breast phantom

The effects of ball bearing location

As shown in Figure 16, ball bearings 5 and 8 had lower contrast compared with the other ball bearings. Because of scattering and absorption, less X-ray photons reached the detector when they passed through the breast phantom. The location of the ball bearings affected the regularity of the ball bearing after thresholding. As shown in Figure 17, ball bearings 5 and 8 became irregular after thresholding. Since the ball bearing diameter was calculated from the area detected by the ImageJ, if it became irregular after thresholding the calculated diameter would also be affected. The

regularity of the ball bearing can be measured quantitatively using circularity value. Circularity value is used as a shape descriptor and the equation (6) is shown below.

$$C = \frac{4\pi A}{P^2} \tag{6}$$

Where C is the circularity value, A is the area and P is the perimeter. The circularity value varies between 0 and 1. The larger the number, the higher the circularity. For instance, a value of 1.0 indicates a perfect circle whilst as the value approach 0.0 it indicates an elongated shape (Ferreira & Rasband, 2012).

Regarding the ball bearings on the surface of the breast phantom, their circularity values were higher than those covered by the phantom (ball bearings 5 and 8). Table 2 summaries how the circularity value, ball bearing diameter and the magnification varied in the different locations of the breast phantom.

Table 2 Circularity value, diameter, and magnification at threshold of 160

Ball number	Circularity value	Diameter (mm)	Magnification
1	0.93	1.70	1.14
2	0.95	1.65	1.10
3	0.92	1.62	1.08
4	0.92	1.64	1.10
5	0.91	1.83	1.21
6	0.95	1.75	1.17
7	0.94	1.64	1.09
8	0.91	1.80	1.20
9	0.93	1.77	1.18
10	0.93	1.63	1.09
11	0.94	1.76	1.17

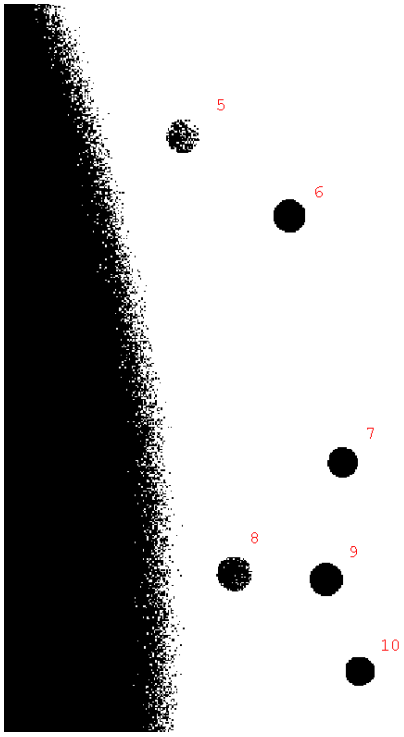

Figure 17. Ball bearings and phantom after thresholding

The circularity values for ball bearings 5 and 8 are smaller than the rest of the ball bearings because of thresholding. The differences in the calculated ball bearing diameters may have been caused by the non-uniform spherical shape of the breast phantom. The larger the distance between the ball bearing and the detector, the larger the magnification. For example, ball bearings 5 and 8 were located on the top of the breast phantom and therefore their distances to the detector are larger than other ball bearings, resulting in larger magnification. The ball bearings on the top of the phantom would have the maximum magnification (M_{max}), while the ball bearings at the bottom of the breast would have the minimum magnification (M_{min}).

$$M_{max} = \frac{SID}{SID-T-G} \quad (7)$$

$$M_{min} = \frac{SID}{SID-G} \quad (8)$$

$$G = SID - SOD - T \quad (9)$$

Where SID is the source to image distance, T is the compressed breast thickness, SOD is the source to object distance; and G is the gap between the support platform and the detector. SID, SOD and T were read from the DICOM header from which the value of G=25 mm could be calculated using equation (9). The range of magnification varied from 1.04 to 1.21. The magnification of the ball bearing diameters falls within magnification M_{min} and M_{max}. The implication is that the increase in ball bearings diameter could be a magnification effect because the measured sizes of all the ball bearings are entirely compatible with the magnification. This is due to their positioning within the breast phantom and that there is no excess size due to blurring. This magnification is a constant effect which affected the ball bearings diameter throughout the whole period.

The effects of threshold value

The calculated ball bearing diameter is not only affected by the location of the ball bearing but also the selection of threshold value. Figure 18 shows the relationship between the ball bearing area and the threshold value. The lower the threshold value, the larger the detected ball bearing area. It is possible that for a lower threshold value

some of the background is included and identified as part of the ball bearing area. The lower and upper limit for the threshold is 130 and 190, respectively.

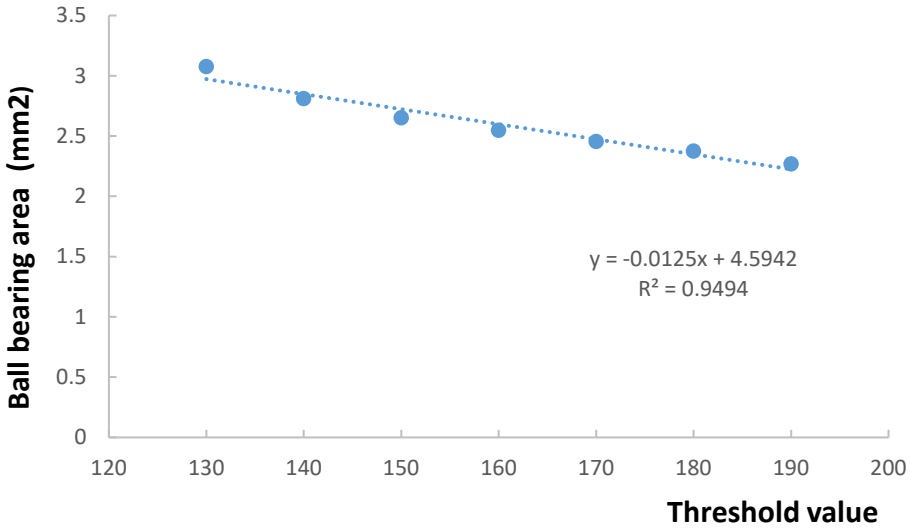

Figure 18. Ball bearing area against threshold value for ball bearing 8

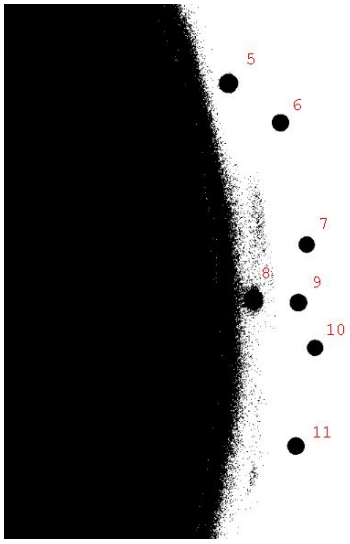

Figure 19. Ball bearing 8 cannot be distinguished from the background if the selected threshold value is too low

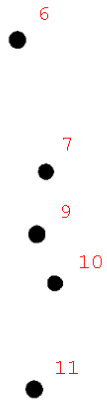

Figure 20. Ball bearings 5 and 8 disappear after thresholding if the selected threshold value is too high

As shown in Figures 19 and 20, when the selected threshold is below the lower limit, ball bearing 8 could not be distinguished from the background and, when the value is above the upper limit, ball bearings 5 and 8 disappeared after thresholding. As the threshold remains constant, only blurring would change the area of the bearing or its diameter. Thus, any induced errors would not vary between the ball bearings. In view of this, a fixed threshold of 160 was used in paper 3 throughout the analysis to ensure the area of the ball bearing would not be affected by the thresholding process.

Alternatively, a static image of the ball bearing could be used to verify the threshold. A new experiment was therefore carried out to acquire a static ball bearing image. Details of this can be referenced in appendix 2. In this experiment, no compression force was applied to the phantom and a 1.50 mm diameter metal ball-bearing was fixed at the bottom of it to ensure the magnification was reduced to the minimum. As shown in the previous section the ball bearing at the bottom of the phantom would have the minimum magnification (M_{min}) of 1.04. The expected size of the ball bearing should be 1.55 mm, which corresponds to an area of 1.90 mm^2. Figure 21 shows the relationship between the ball bearing area and the threshold value for the static ball bearing. A threshold of 240 gives an area of 1.90 mm^2 which corresponds to a diameter of 1.55 mm.

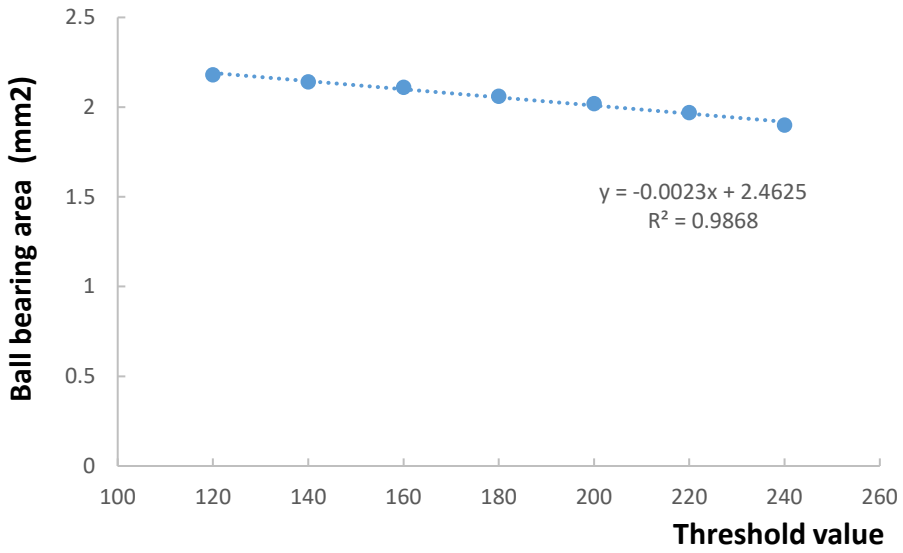

Figure 21. Ball bearing area against threshold value for the static ball bearing

The threshold value for the ball bearing was determined by subtracting the gray value of the Poly Methyl Methacrylate (PMMA) slab. As shown in Figure 22, the gray value of the PMMA slab was about 50 and therefore the threshold value for the ball bearing should have been 190. Table 3 shows the circularity value, ball bearing diameter and magnification at a threshold of 190. As shown in Table 3, the circularity value of ball bearing 5 and 8 were much lower than the rest of the ball bearings. This indicated that ball bearings 5 and 8 would become irregular after thresholding. As shown in Figure 23, the gray value across the breast phantom was not uniform because of the phantom's spherical shape. This means a threshold value of 190 may not be ideal for the ball bearings covered by the breast phantom. The implication is that it may require more than one threshold value to segment all eleven ball bearings.

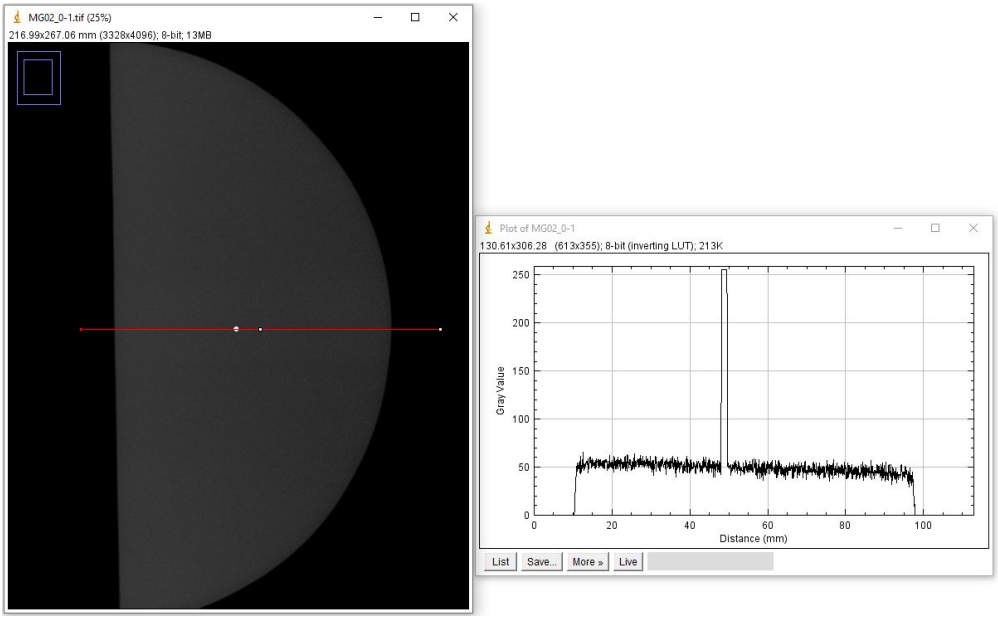

Figure 22. Line profile across the PMMA slab and the metal ball bearing

Table 3 Circularity value, diameter, and magnification at threshold of 190

Ball number	Circularity value	Diameter (mm)	Magnification
1	0.94	1.68	1.12
2	0.93	1.63	1.08
3	0.92	1.59	1.06
4	0.93	1.60	1.07
5	0.47	1.59	1.06
6	0.95	1.72	1.15
7	0.94	1.61	1.07
8	0.75	1.69	1.12
9	0.94	1.74	1.16
10	0.94	1.59	1.06
11	0.93	1.73	1.15

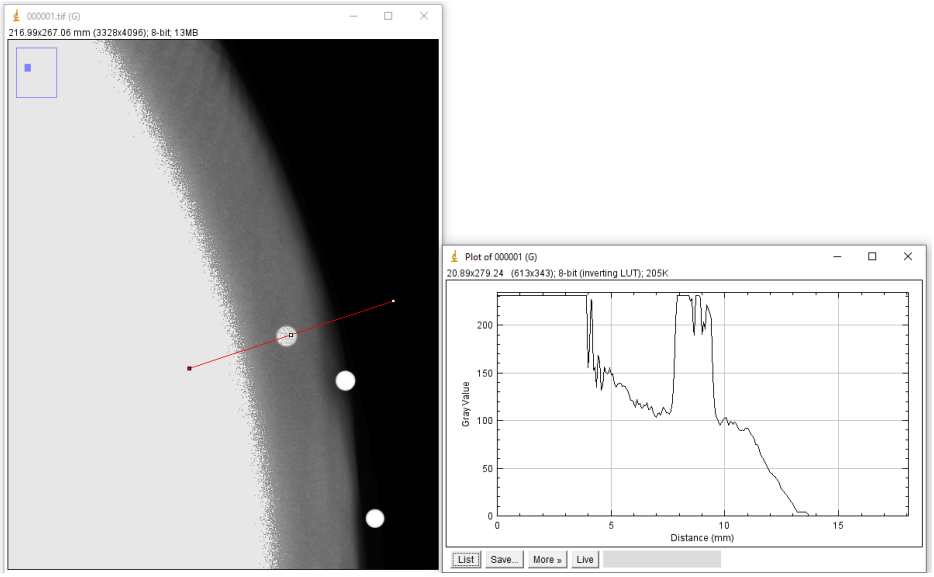

Figure 23. Line profile across the breast phantom and the metal ball bearing

Edge detection

The edge detection method can be used as an alternative approach to measure ball bearing diameter. As edges indicate sharp changes in the intensity, the ball bearings can be identified by the change in gray value between the boundary of the ball bearing and the background (Figure 24). As shown in Figure 25, the edges of the ball bearings and the breast phantom were highlighted after the application of edge detection. The advantage of this approach is that the detected ball bearing area would not be affected by the threshold. However, the edge detection method can be affected by noise. For example the background noise inside ball bearing 8 in Figure 25 may have been misinterpreted as part of the ball bearing. Median filter could be applied to the image before the edge detection process to reduce the background noise. Also, due to the smoothing effect of the operator used in the edge detection method, the natural edges in the output images are often thicker, leading to the overestimation of the detected ball bearing area (Tyagi 2018). Static images of the ball bearing can also be used to adjust the ball bearing area determined by the edge detection method.

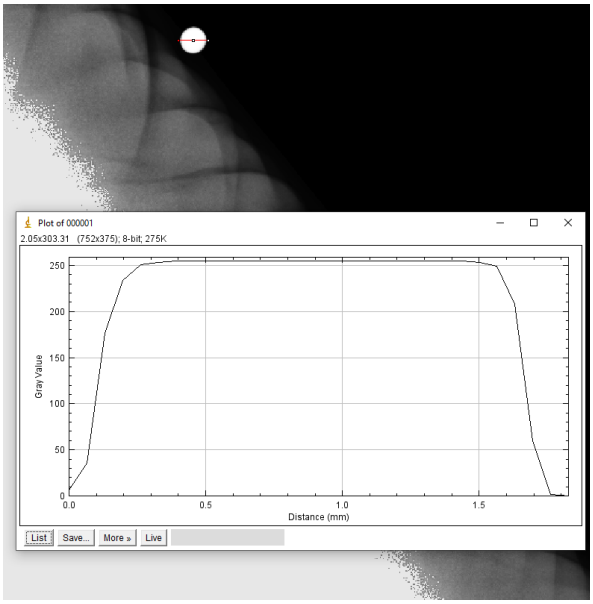

Figure 24. The profile plot of a ball bearing acquired from ImageJ

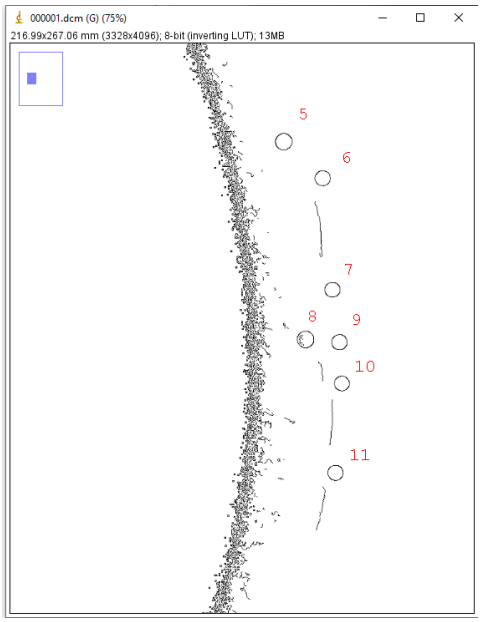

Figure 25. The edges of the ball bearings were highlighted after edge detection

The expected size of the ball bearing at the bottom of the phantom would be 1.55 mm which correspond to an area of 1.90 mm^2. The correction factor for the edge detection method was calculated by comparing the actual ball bearing area with the detected ball bearing area. The results are summarised in Table 4.

Table 4 Summary of the static ball bearing measurement

Area (mm^2)	Diameter (mm)	Correction factor
1.99	1.59	0.95

The correction factor can then be used to adjust the ball bearing diameter detected by the edge detection method. After the adjustment, the edge detection method is compared with the intensity thresholding method. If the work was repeated, then this approach may be advantageous to use. The advantages of the edge detection method over the intensity thresholding method will be discussed in the next section.

Intensity thresholding Vs edge detection methods

A paired t-test was used to test whether there is a significant difference in ball bearing diameters between the intensity thresholding and the edge detection methods. The results are summarised in Table 5. As shown in Table 5, there was a significant difference (p<0.05) in the ball bearing diameters between the two methods for all paddle/ compression force combinations. In fact, the differences in diameter for the ball bearings were about 0.01 mm, which is 0.6 %. Although the difference between the two methods is small, it is still statistically significant.

Table 5 *p*-values for intensity thresholding and edge detection methods

	80 N fixed paddle	80 N flexible paddle	150N fixed paddle	150 N flexible paddle
p-value	0.000	0.003	0.000	0.000

The ball bearing diameters calculated by the intensity thresholding and edge detection methods for fixed paddle and the corresponding compression force against time are shown in Figures 26 to 28. The rest of the paddle/compression force combinations can be found in appendix 3. The ball bearing diameter calculated by the intensity thresholding method had higher variability than the edge detection method. For example, ball bearing diameters for 5 and 8 calculated by the intensity thresholding method (Figure 26) fluctuate between 1.81-1.83 mm and 1.80-1.84 mm respectively, while the calculated ball bearing diameters for the edge detection method are relatively

stable (Figure 27). As shown in Figure 28, the compression force becomes stable after 80 s, but the ball bearing diameters for ball 5 and 8 calculated by the intensity thresholding method (Figure 26) still demonstrate fluctuations in diameter. This result suggests that the edge detection method is better than the intensity thresholding method in segmenting the ball bearings from the uneven background. For example ball bearings 5 and 8 appear to be covered by the phantom, which has a brighter background (Figure 29) than the rest of the ball bearings.

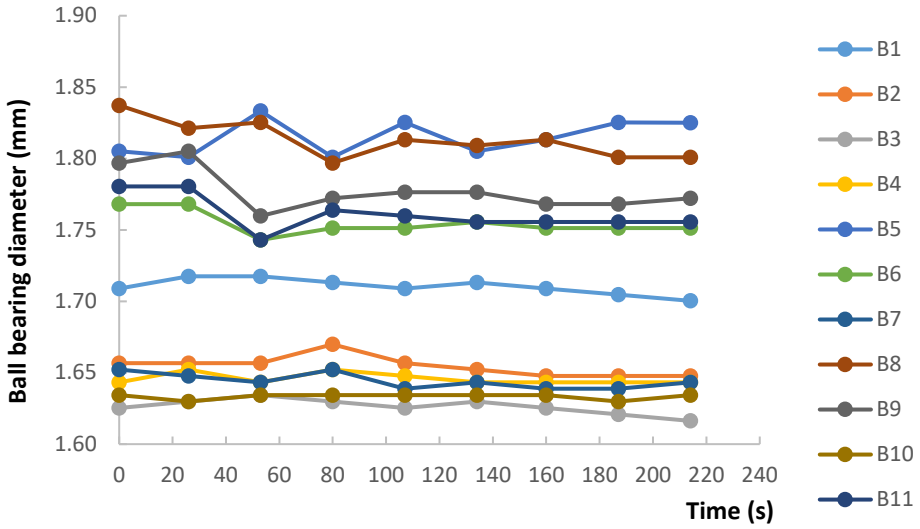

Figure 26. Ball-bearing diameters for fixed paddle with 80 N compression force calculated by intensity thresholding method

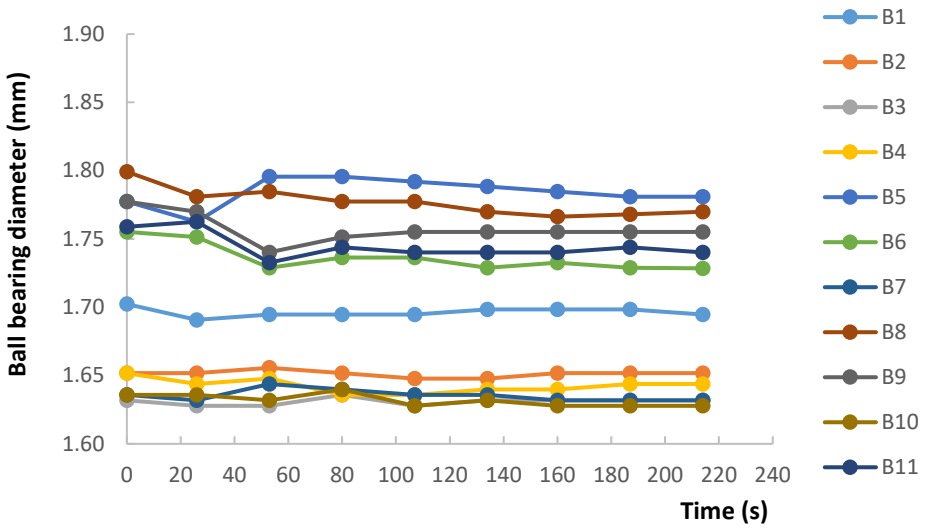

Figure 27. Ball-bearing diameters for fixed paddle with 80 N compression force calculated by edge detection method

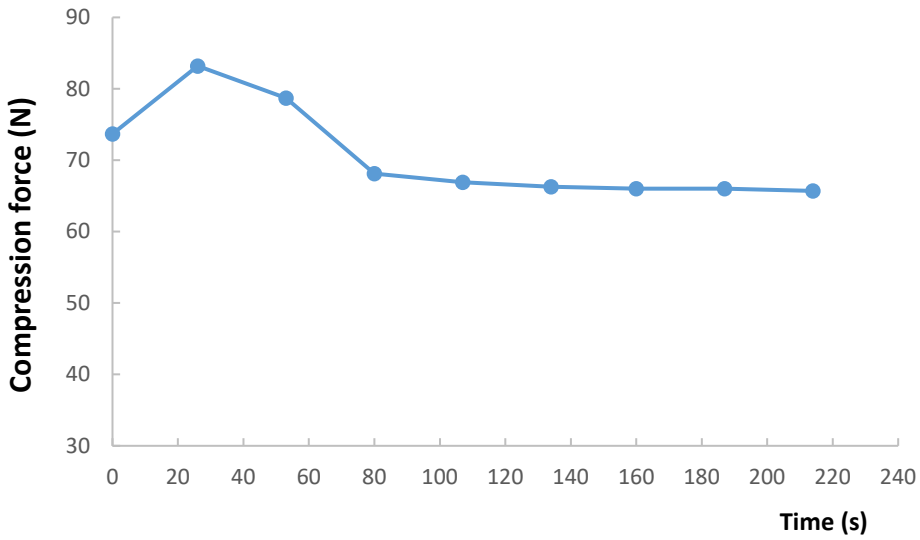

Figure 28. Compression force against time for fixed paddle

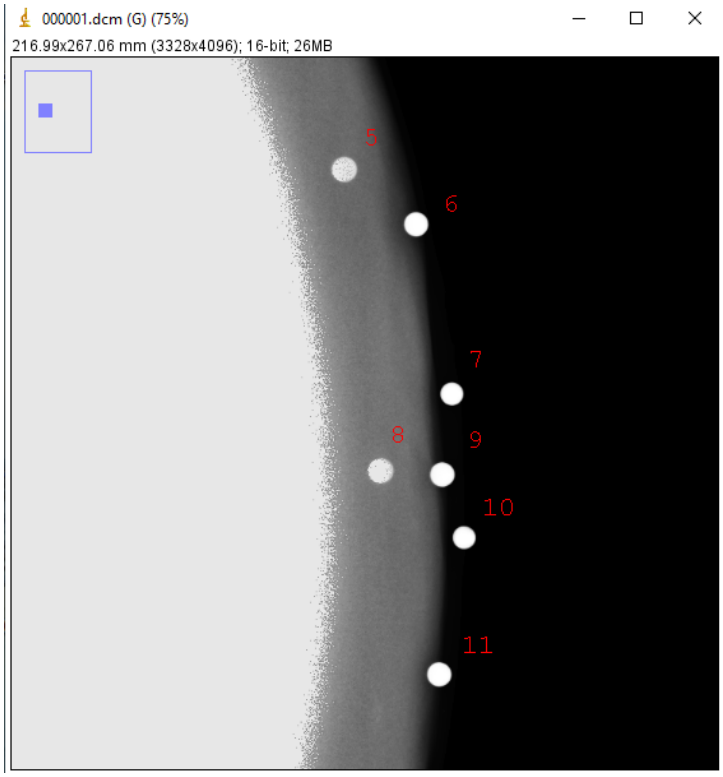

Figure 29. Ball bearings 5 and 8 has a brighter background than other ball bearings

Method to determine ball bearing motion

In paper 3, the ball bearing still seemed to move after 240 s when the expected motion should have stopped at 40 s. This may have been due to the method used to determine the ball bearing motion. In paper 3, the method used to determine the ball bearing motion was to compare the average ball bearing diameter with a fixed ball bearing diameter of 1.50 mm. The differences between the two values was considered as motion. As discussed earlier, the calculated ball bearing diameter can be affected by factors unrelated to motion, such as magnification. For example, ball bearing 5 was located on the top of the breast phantom and the increase in OID created magnification, therefore the differences between its diameter and the 1.50 mm ball bearing diameter was always larger than zero. Thus, the ball bearing motion should be determined by comparing the ball bearing diameters at different time intervals, rather than through comparison with a fixed diameter of 1.50 mm. A paired t-test was therefore used to compare the ball bearing diameters at different time intervals and the results are summarised in Table 6 to 9. The t-test results show that there was a significant difference ($p<0.05$) in ball bearing diameters in the 0 to 26 s time interval for the fixed paddle; the 0 to 27 s and the 27 to 53 s time intervals for the flexible paddle with 80 N compression force; and in the 164 to 190 s time interval for the fixed paddle with 150 N compression force. However, there was no significant difference ($p>0.05$) in ball bearing diameters for

flexible paddle with 150 N compression force.

The implication is that for both fixed and flexible paddles with 80 N compression force there was significant difference in ball bearing diameters in the early time period and after that the differences became statistically insignificant. The results indicated that that there could be blurring in the early time period.

Table 6 t-test results for fixed paddle with 80 N compression force

Time interval	0 to 26s	26 to 53s	53 to 80s	80 to 107s	107to 134s	134 to 160s	160 to 187s	187 to 214s
p-value	0.01	0.69	0.49	0.05	0.85	0.45	0.80	0.30

Table 7 t-test results for flexible paddle with 80 N compression force

Time interval	0 to 27s	27 to 53s	53 to 80s	80 to 107s	107 to 134s	134 to 161s	161 to 187s	187 to 214s	214 to 241s
p-value	0.04	0.02	0.64	0.30	0.40	0.41	0.06	0.61	0.64

Table 8 t-test results for fixed paddle with 150 N compression force

Time interval	0 to 30s	30 to 57s	57 to 83s	83 to 110s	110 to 137s	137 to 164s	164 to 190s	190 to 217s	217 to 244s
p-value	0.36	0.40	0.95	0.98	0.35	0.05	0.01	0.68	0.84

Table 9 t-test results for flexible paddle with 150 N compression force

Time interval	0 to 27s	27 to 54s	54 to 81s	81 to 107s	107 to 134s	134 to 161s	161 to 188s	188 to 215s	215 to 241s
p-value	0.90	0.28	0.79	0.84	0.64	0.12	0.71	0.33	0.21

Critical review on paper 4

Paper 4. Ma, W. K., Aspin, R., Kelly, J., Millington, S., & Hogg, P. (2015). What is the minimum amount of simulated breast movement required for visual detection of blurring? An exploratory investigation. *The British journal of radiology, 88*(1052), 20150126.

The novelty of paper 4 is that it was the first study to investigate the probability of blur detection for different motion simulation methods. The findings of paper 4 suggest that using probability to represent visual detection of blurring rather than a hard cut-off level. The following paragraph will provide a critical review on paper 4.

Observer Study

In paper 4, an observer study was used to determine the minimum amount of simulated motion required for the visual detection of blurring. Motion simulated images were used because of the practical difficulties in controlling mammographic machine motion with sub-millimetric precision. One of the limitations of using simulated images is that they might not fully represent actual blurred images. This is because image blur may fully or partly affect the image, whereas the simulation software used in this study fully blurred the images. Another limitation is that the motion simulation is present in the horizontal plane, while the paddle motion is in the vertical plane. This may not represent the real motion required for the visual detection of blurring.

The absence of vertical simulated motion meant that the effect of real motion may have been underestimated. Therefore, it is important to develop a validation study to determine whether the visual appearance of the simulated blurs is comparable with that of real blurs. A validation study for simulated blurring could be developed based on the study by Abdullah et al., (2017). In this validation study, the practitioners asked participants to review FFDM images, which included an equal amount of real blur, simulated blur, and unblurred images, in a randomised order. Unlike in the validation study by Abdullah et al. (2017), the practitioners should not be informed the presence of simulated blur images and then they would need to decide whether an image is blurred or not. This would avoid the practitioners' assumptions of the presence of image blur, even when they cannot identify any blur in the image.

A simple mathematical model can be used to estimate the effect of vertical paddle motion on horizontal breast motion. This is because breast tissues can be assumed be to nearly incompressible and their volume would remain constant after compression (Gefen & Dilmoney, 2007). Assuming the shape of the compressed breast can be represented by a half cylinder (equation 10), a thick breast with a large contact area would give more horizontal displacement than a thin breast with a small contact area. For example, for a thick breast with a 13 cm radius and 20 cm height, if the height decreases by 0.1 mm the radius also has to increase by 0.033 mm to keep the same

volume. For a thin breast with a 9 cm radius and 17 cm height, the radius would have to increase by 0.026 mm. In other words, 0.1 mm in vertical thickness reduction could result in a 0.033 mm horizontal breast tissue displacement for thick breasts, and a 0.026 mm horizontal breast tissue displacement for thin breasts.

$$V_c = \frac{1}{2}\pi r^2 h \tag{10}$$

Where V_c is the volume of the half cylinder, r is the radius, and h is the height.

Motion simulation models

In paper 4 three simulation models - Gaussian, hard-edge mask and soft-edge mask - were used to simulate motion blur for the images. The visually detected blurring level was affected by the profile curve for the simulation model. The profile curve was derived from the pixel walking application which was developed to model the motion of a pixel as the subject moves. Blur detection algorithms use depth of field in image to identify blur, but orthogonal images such as mammograms have no depth of field to assess the magnitude of the blur. This means the amount of blur in the processed image cannot be measured (Shi et al. 2015). Therefore, the image processing application was adapted to tune the convolution mask to ensure 1 mm of pixel motion represents 1 mm of breast tissue motion. Figures 30 and 31 shows the output of the application for the hard-edge mask and soft-edge mask methods. The left-hand panel shows the effect of

the pixel motion in terms of its spread over time while the right-hand panel shows the Gaussian function (black line) and the profile curve for the hard-edge/soft-edge mask method (green line). The Gaussian function shows a less rapid drop-off in intensity with a shorter tail of spread compared with the profile curve for the hard-edge/soft-edge mask method, while the profile curve for both hard-edge mask and soft-edge mask methods are similar in shape. This explain why when the same level of simulated motion is applied by the Gaussian method, a larger level of visual blur is produced than the soft-edge mask and hard-edge mask methods, while the difference in visual blur between the soft-edge mask and hard-edge mask methods is small.

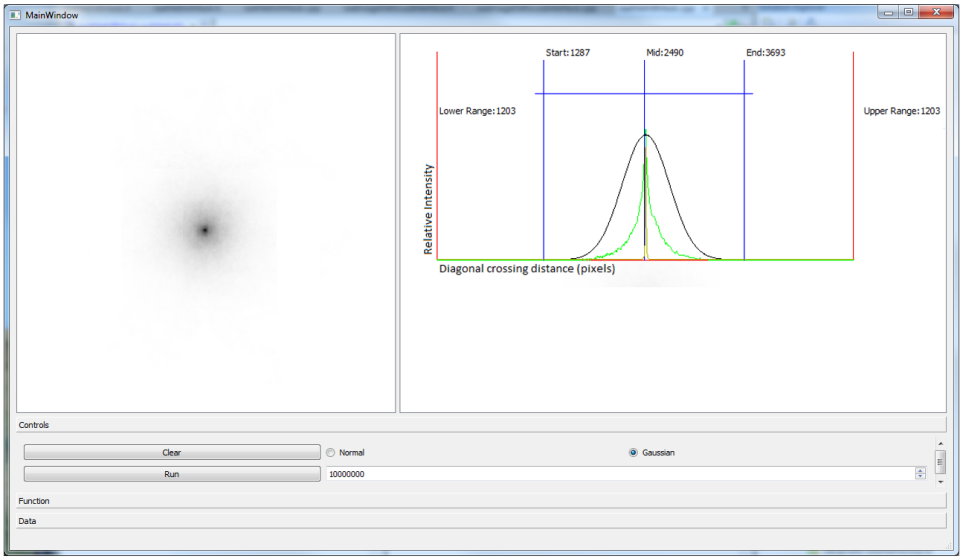

Figure 30. The left-hand panel shows the effect of the pixel motion for the hard-edge mask method the right-hand panel shows the profile curves for the hard-edge mask method (green line) and the Gaussian function (black line)

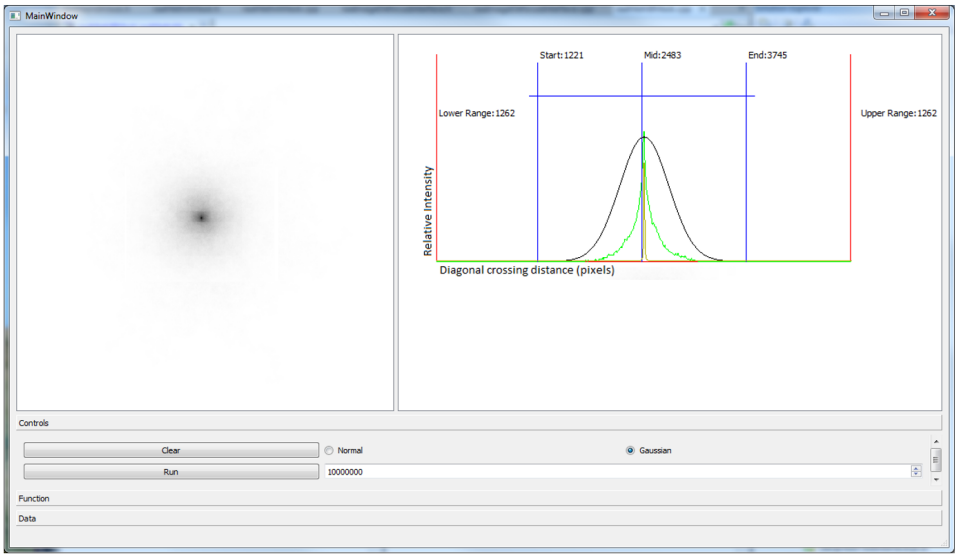

Figure 31. The left-hand panel shows the effect of the pixel motion for the soft-edge mask method the right-hand panel shows the profile curves for the soft-edge mask method (green line) and the Gaussian function (black line)

The Gaussian method is the standard approach for image blurring because it replicates the effect of putting a translucent film over an image and scattering light uniformly. However, the Gaussian method created too much blur for the simulated motion and its profile did not match simulated motion data.

Both hard-edge mask and soft-edge mask methods were developed based on a simple motion model which assumed a single point in the image would map to a single pixel at every point of its motion. The difference between the hard-edged mask and soft-edged mask methods is their assumption of pixel motion. The hard-edged mask method assumes a point under motion would move in exact pixel steps, while the soft-edged mask method assumes sub pixel-level motion between two captured pixels. The soft-

edged mask method is a more representative model as pixel motion is continuous rather than discrete. The study by Abdullah et al. (2017) shows that blurred images generated using the soft-edged mask method are visually comparable to real blur. In paper 4, three simulation models were used to determine the minimum amount of simulated breast motion required for the visual detection of blurring. As discussed, the soft-edged mask method best represented the physical process that caused the blurring effect and therefore should be chosen as the standard simulation approach for motion blurring. Therefore, the amount of simulated breast motion at which blurring can be detected visually is 0.7 mm.

Critical review on paper 5

Paper 5. Ma, W. K., Borgen, R., Kelly, J., Millington, S., Hilton, B., Aspin, R., ... & Hogg, P. (2017). Blurred digital mammography images: an analysis of technical recall and observer detection performance. *The British journal of radiology, 90*(1071), 20160271.

The novelty of paper 5 is that it was the first study to investigate the blurring detection rate for the 2.3 MP and 5 MP monitors. The findings of paper 5 suggest that monitors with resolutions lower than 2.3 MP are not suitable for the technical review of FFDM images. The following section will provide a critical review on paper 5.

To investigate whether a 12 MP monitor (RadiForce RX1270) is better than 2.3 MP (Multisync 243wm) and 5 MP monitors (Dome E5) for detecting image blur, factors such as observer eyes' resolution and interpolation needed to be considered.

Observer eyes' resolution

Observer eyes' resolution is measured based on angular size, which is the minimum separation between the two points that human eyes can resolve (Khurana et al., 2019). Figure 32 shows the angular size subtended by a fixed size object that was centered on a screen. By using trigonometry, the equation for angular size can be expressed as:

$$\theta = 2tan^{-1}\frac{O}{2d} \tag{11}$$

Where θ is the angular size, O is the object size, and d is the distance between object and the observer.

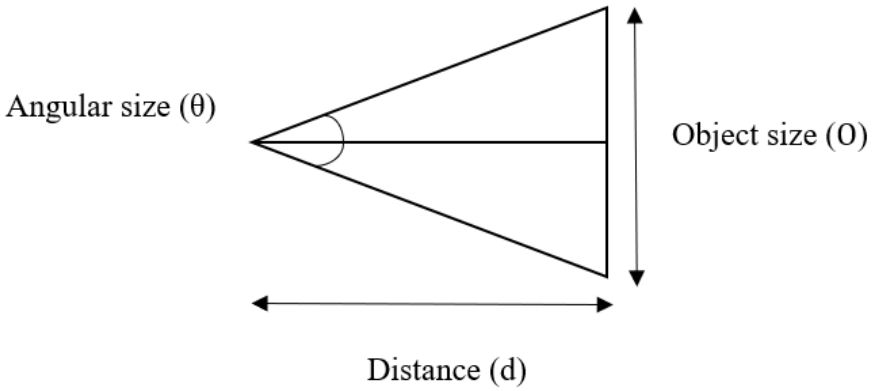

Figure 32.The geometry diagram for the angular size

For 20/20 vision the angular size that the observer can resolve is 1 arc minute, which is 0.017 degrees. Using this assumption, the observer eyes' resolution (O_{min}) in which the minimal size of an object that an observer can resolve can be calculated using equation (11), and the results are shown in Table 10. Pixel pitch is the distance from the center of a pixel to the center of the adjacent pixel (Salvaggio & Shagam, 2019). To determine whether an observer can be benefit from using higher resolution monitors, the pixel pitch of all three monitors is compared with observer eyes' resolution. The observer should be able to see the difference between the monitors if the value of O_{min} is smaller than the pixel pitch of the monitor.

Table 10 Pixel pitch and observer eyes' resolution for viewing distance of 30 cm and 75 cm

Monitor	Screen size (inch)	Resolution (MP)	Pixel pitch (mm)	O_{min} (mm) at 30 cm	O_{min} (mm) at 75 cm
Multisync	24	2.3 MP (1920 x 1200)	0.27	0.09	0.22
Dome	21.3	5 MP (2560 x 2048)	0.17		
RadiForce	30.9	12 MP (4200 x 2800)	0.16		

For a viewing distance of 30 cm, the observer eyes' resolution was better than the screen resolution for all three monitors and therefore an observer with 20/20 vision should be able to see the difference in the monitor. In other words, an image displayed on the 12 MP monitor will look sharper to an observer's eyes than an image displayed on 2.3 MP and 5 MP monitors.

For a viewing distance of 75 cm, the screen resolution for 5 MP and 12 MP monitors was better than the observer eyes' resolution which means the image displayed on the 5 MP monitor would appear to the observer as sharp as the image displayed in 12 MP monitor.

The observer benefit from using the 12 MP monitor for a viewing distance of 30 cm, as the observer does not reach the limits of eyesight. However, for a viewing distance of 75 cm the image displayed on the 12 MP monitor would appear to the observer as sharp as the image displayed in the 5 MP monitor. Nevertheless, an observer could still benefit from using the 12 MP monitor for blurring detection because of the lower loss in image

quality during interpolation. The following section will discuss how interpolation affects image quality.

Interpolation

Interpolation, also known as scaling, can change image quality which in turn affects blurring detection. If an image is displayed at a resolution different from the native resolution then interpolation (scaling of the image) needs to be performed (Mason et al., 2014). A 1.50 mm static metal ball bearing image (Figure 33) is used to illustrate how the displayed size and angular size of a physical object varies with or without interpolation when displayed in different resolution monitors.

Without interpolation

The display size of the ball bearing was calculated by multiplying the number of pixels forming the ball bearing and the pixel pitch of the monitor. The number of pixels forming the ball bearing was then measured by the ImageJ software using line profile measurement, which is 24 pixels (Figure 34). The static ball bearing image was assumed to be displayed in native resolution without interpolation. The angular size of the ball bearing was then calculated for viewing distances of 30 cm and 75 cm using equation (11) and the results are summarised in Table 11. As shown in Table 11, the display size and angular size of the ball bearing varies with the monitor resolution. The

lower the monitor resolution, the larger the display size and angular size of the ball bearing. For an observer with 20/20 vision, the angular size that the observer can resolve is 0.017°. Therefore, an observer could identify the ball bearing on all three monitors for viewing distances of 30 cm and 75 cm.

Table 11 Display size and angular size of the ball bearing for different resolution monitors without interpolation

Monitor	Resolution (pixels)	Pixel pitch (mm)	Displayed size (mm)	Angular size for 30 cm (degree)	Angular size for 75 cm (degree)
Multisync	2.3 MP (1920 x 1200)	0.27	6.46	1.23°	0.49°
Dome	5 MP (2560 x 2048)	0.17	3.96	0.76°	0.30°
RadiForce	12 MP (4200 x 2800)	0.16	3.73	0.71°	0.29°

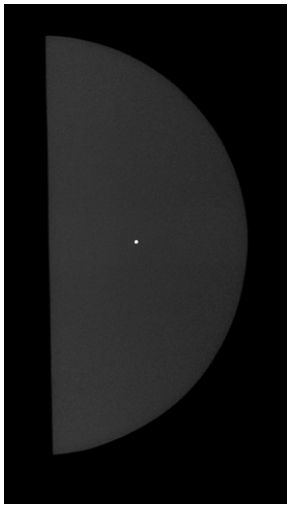

Figure 33.The white spot located on the center of the breast phantom is a 1.50 mm metal ball bearing

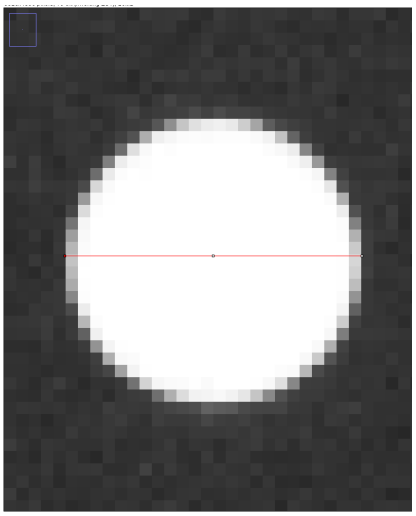

Figure 34.The image is zoom in until it reaches pixel level details

With interpolation

The resolution of a mammogram taken by a Hologic Selenia Dimensions mammography unit is 3328 x 4096 pixels (Hologic, 2020), which is higher than the screen resolution of all three monitors. Interpolation is required to fit the mammogram onto the monitor display. Table 12 summarises the scale factor, display size and angular size of the ball bearing after interpolation. As shown in Table 12, the lower the monitor resolution, the smaller the display size and angular size of the ball bearing. This trend is reversed with interpolation. As the angular size of the ball bearing is determined by its displayed size and distance from the observer, if the viewing distance is fixed the reduction in the displayed size for lower resolution monitors after interpolation will result in a decrease in the angular size of the ball bearing.

As shown in Table 12, the scale factor increased along with the monitor resolution which means the higher the monitor resolution, the lower the loss in image quality after interpolation. Deterioration in image quality is inevitable if an image is displayed at a resolution different from the native resolution. This is because, after interpolation, the number of pixels used to display the image decreases. For example, for 12 MP monitors, 20 pixels are used to display the ball bearing, while for 2.3 MP monitors only 9 pixels are used to display the ball bearing. The loss in the image quality is the highest for the 2.3 MP monitor which supports paper 5's conclusion that monitors with resolution less

than or equal to 2.3 MP are not suitable for the detection of blur. Among all three monitors, the 12 MP monitor has the lowest loss in image quality because the mammogram is almost displayed in full resolution. In full resolution each acquired pixel is displayed by a pixel on the monitor, meaning all the information in the acquisition is presented (Pisano et al., 2007). As the 12 MP monitor has the lowest loss in image quality after interpolation, this means the observer can be profit from using higher resolution monitors for blurring detecting.

Table 12 Display size and angular size of the ball bearing for different resolution monitors with interpolation

Monitor	Resolution (pixels)	Pixel pitch (mm)	Displayed size (mm)	Scale factor	Angular size for 30 cm (degree)	Angular size for 75 cm (degree)
Multisync	2.3 MP (1920 x 1200)	0.27	2.33	0.36	0.44°	0.18°
Dome E5	5 MP (2560 x 2048)	0.17	2.44	0.62	0.47°	0.19°
RadiForce	12MP (4200 x 2800)	0.16	3.14	0.84	0.60°	0.24°

Critical review on paper 6

Paper 6. Ma, W. K., Howard, D., & Hogg, P. (2017). Closed-loop control of compression paddle motion to reduce blurring in mammograms. *Medical physics, 44*(8), 4139-4147.

The novelty of paper 6 is that it was the first time a mathematical model for the breast, machine drive and compression paddle have been developed for simulation. The findings on paper 6 suggest that the settling time of breast side displacement can be significantly reduced by implementing a position feedback control system.

Breast compression model

In paper 6, a mathematical model was used to represent the behaviour of the breast and the compression system. Researchers have shown that the breast tissue demonstrates viscoelastic properties under compression (Insana et al., 2004; Carmichael et al., 2015). Therefore, the elastic characteristics of the breast are analogous to a spring, while the viscous characteristics of the breast are analogous to a damper. The breast compression system was represented by a spring-mass-damper model, which is a second-order system (Seeler, 2014). Figures 35 and 36 show how a spring-mass-damper model was used to represent the behaviour of the breast and the compression system. The paddle and breast transfer functions was then derived from the spring-mass-damper model and used in the simulation.

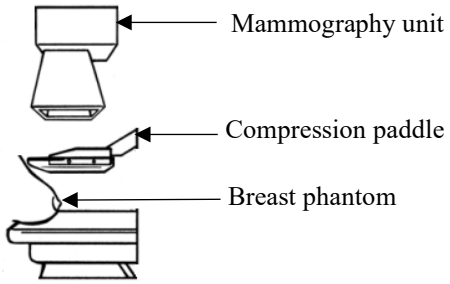

Figure 35. Spring-mass-damper system

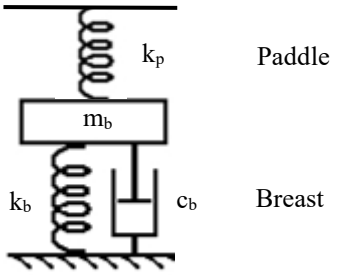

Figure 36. Breast compression system

The rationale for using a simulation is that it is too costly to build a real feedback control system. Simulation was therefore used as a first step to investigate the stability of such a system and to justify the creation of a prototype. The limitation of using a mathematical model for simulation is that the second-order system model used in paper 6 might not fully represent the real response of a breast and paddle under compression. Research by Sridhar and Insana (2007) showed that the response of breast tissue became nonlinear under large compression force. The effect of approximating the breast and paddle models with a second-order system model is that the simulated response may only be valid within a limited range of compression forces (Seeler, 2014). To overcome this limitation, a prototype for the feedback control system could be built to validate the simulation results and test the assumptions made based upon them.

Ramp input

One of the limitations of using step input is that it only tests the system's response to sudden changes in input, rather than continuous changes. As shown in Figure 37, the compression force decreases steadily during the clamping phase. Therefore it would

have been better to test the control system with a continuous function such as ramp input. A ramp function models the input that changes at a constant rate which can be used to test the control system's ability to follow a constantly changing input (Palm, 2013).

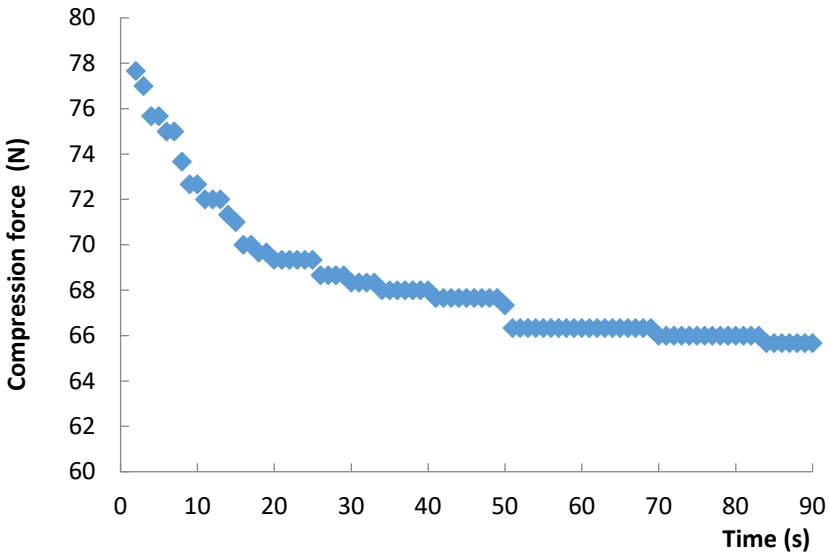

Figure 37. The compression force reading against time

The system response time for both step and ramp inputs are summarised in Table 13. In Table 13, there is no significant difference in rise and settling times between step and ramp inputs. This means the control system developed in paper 6 could also provide a reasonable response to the ramp input.

Table 13 PID controller step and ramp response performance for Selenia Dimensions and Lorad Selenia position feedback breast compression system for machine drive time constants (τ) of 0.1s, 0.2s and 0.4s

	Selenia Dimensions						Lorad Selenia					
	24x30 cm			18x24 cm			24x30 cm			18x24 cm		
	$\tau 1$= 0.1	$\tau 2$= 0.2	$\tau 3$= 0.4	$\tau 4$= 0.1	$\tau 5$= 0.2	$\tau 6$= 0.4	$\tau 1$= 0.1	$\tau 2$= 0.2	$\tau 3$= 0.4	$\tau 4$= 0.1	$\tau 5$= 0.2	$\tau 6$= 0.4
k_{prop}	91.96	51.39	25.99	100.77	49.66	27.11	42.78	33.13	22.26	98.20	51.55	28.41
k_{integ}	2.75	1.54	0.79	3.28	1.61	0.88	1.69	1.31	0.90	3.20	1.73	0.95
k_{deriv}	304.89	168.35	85.27	329.63	158.43	86.26	114.61	89.30	61.30	232.03	123.28	69.04
rise time (Step)	0.67	1.18	2.32	0.53	1.12	2.01	1.24	1.45	2.00	0.56	1.06	1.87
settling time (Step)	1.16	1.98	3.89	0.89	1.87	3.27	2.22	2.55	3.26	0.94	1.74	3.01
rise time (Ramp)	0.64	1.15	2.29	0.51	1.09	1.99	1.21	1.42	1.97	0.54	1.03	1.84
settling time (Ramp)	1.11	1.93	3.84	0.84	1.82	3.23	2.19	2.50	3.22	0.89	1.69	2.97

As the ramp input is similar to the compression force during clamping phase (Figure 37), it would have been better for the PID controller to be optimised with ramp input. The optimised PID gains and corresponding ramp responses are shown in Table 14. In Table 14, the rise and settling time for different paddles has been minimised by using relatively high proportional (k_{prop}) and derivative (k_{deriv})values and a relatively low integrator (k_{integ}) value. For a controller with small k_{integ}value, its ability to control the steady-state error is relatively low.

Table 14 Optimised PID controller gains and ramp response performance for Selenia Dimensions and Lorad Selenia position feedback breast compression system for machine drive time constants (τ) of 0.1s, 0.2s and 0.4s

	Selenia Dimensions						Lorad Selenia					
	24x30 cm			18x24 cm			24x30 cm			18x24 cm		
	$\tau 1$= 0.1	$\tau 2$= 0.2	$\tau 3$= 0.4	$\tau 4$= 0.1	$\tau 5$= 0.2	$\tau 6$= 0.4	$\tau 1$= 0.1	$\tau 2$= 0.2	$\tau 3$= 0.4	$\tau 4$= 0.1	$\tau 5$= 0.2	$\tau 6$= 0.4
k_{prop}	57.73	46.60	32.92	84.67	55.08	30.90	45.62	35.99	25.50	56.50	44.07	31.76
k_{integ}	2.99	1.84	1.73	3.98	2.79	1.87	2.11	1.87	1.18	2.53	3.20	0.96
k_{deriv}	227.13	160.32	129.39	280.72	219.87	116.35	124.12	109.91	74.33	143.93	119.52	82.58
rise time	0.76	1.09	1.5	0.56	0.79	1.5	0.85	1.01	1.41	0.78	0.98	1.56
settling time	1.37	1.82	2.38	0.93	1.27	2.36	1.45	1.74	2.55	1.37	1.66	2.47

The system response to the ramp input for different machine drive time constant (τ) is shown in Figures 38 and 39. In Figures 38 and 39, the system responses become parallel to the ramp input and the steady-state error for all τ values is constant but not zero. The smaller the τ value, the smaller the steady-state error. This could be explained by a faster motor response to the change in input. The steady-state error is related to the system type and this relation is summarised in Table 15. Since the paddle and breast control system was type 1, there was no steady-state error for step input. Instead, there was finite steady-state error for ramp input. Referring to Table 15, only type 2 systems can provide zero steady-state error for ramp input. Therefore, the controller would need to be modified to eliminate the steady-state error. The purpose of using the ramp input to test and optimise the control system was to ensure the PID controller could provide an optimal response to the steady change in the breast side paddle position.

Table 15 Type number and steady-state error

Input	Type 0	Type 1	Type 2
Unit step	$\frac{1}{1+C_p}$	0	0
Unit ramp	∞	$\frac{1}{C_v}$	0

Where C_p is the static position error coefficient and C_v is the static velocity error coefficient

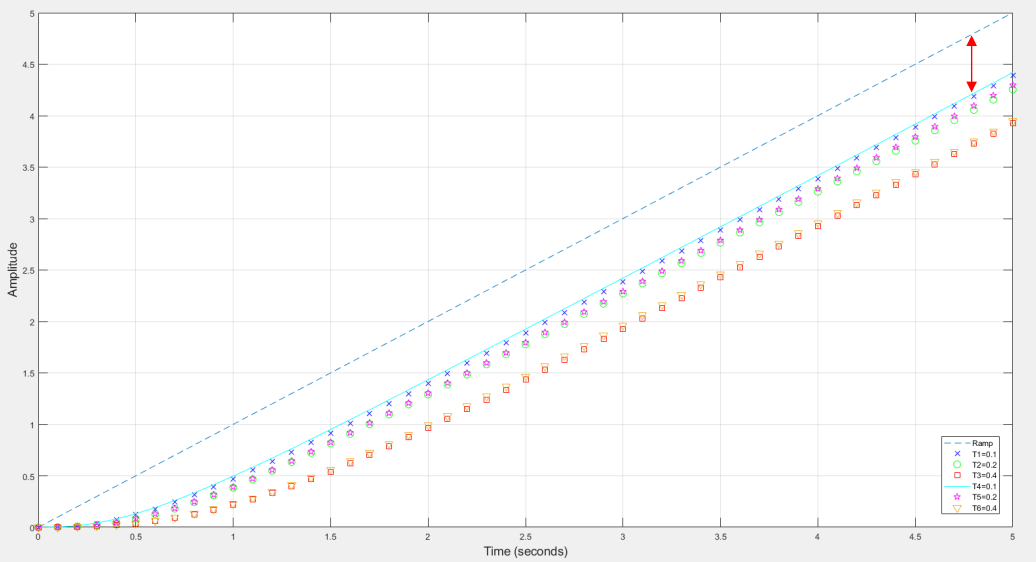

Figure 38. The ramp responses of the Selenia Dimensions position feedback breast compression system for machine drive time constants (τ) of 0.1s, 0.2s and 0.4s. The red arrow indicates the steady-state error.

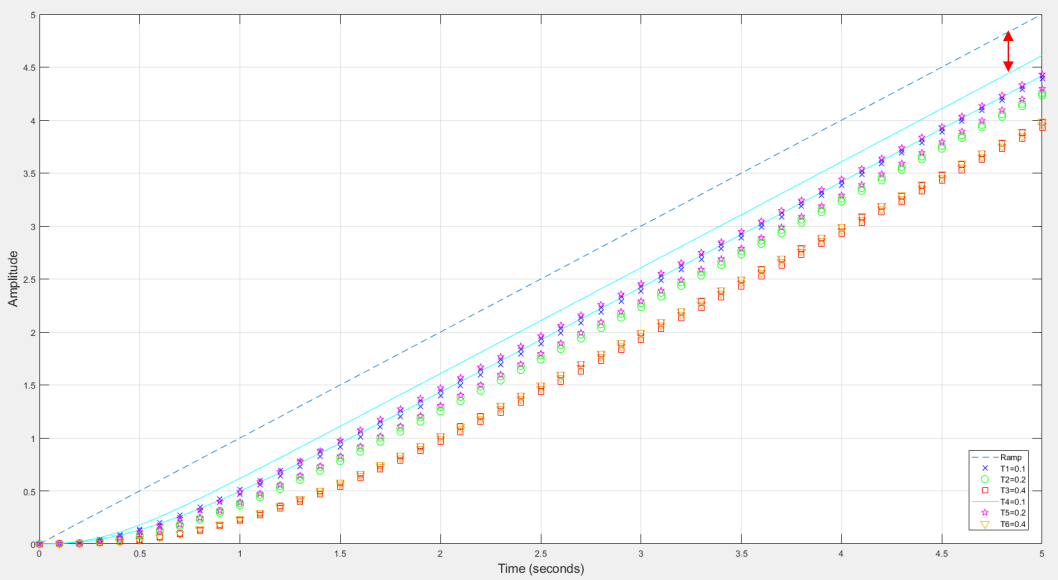

Figure 39. The ramp responses of the Lorad Selenia position feedback breast compression system for machine drive time constants (τ) of 0.1s, 0.2s and 0.4s.

The force overshoots

In paper 6, the position feedback control system was optimised to reduce paddle displacement settling time. There may be a possibility that the control system was optimised at the cost of force overshoot which may lead to an unexpectedly high force administered to the patient. In view of that, a paddle force equation was developed to determine the possibility of force overshoot when using this control model.

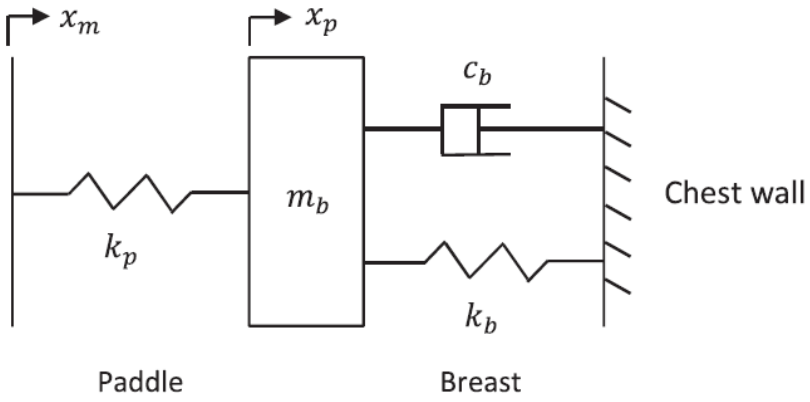

Figure 40. The lumped parameter model of the paddle and breast

Referring to Figure 40, the model lumps paddle mass (m_p) and breast mass are together as one combined mass (m_b). The boundary between paddle and breast is within the combined mass m_b, with m_p on the paddle side of the boundary, while the true breast mass is on the breast side of the boundary. The paddle force (F_P) applied to the breast would be:

$$F_P = k_p\left(x_m - x_p\right) - m_p\ddot{x}_p$$

Where F_P is the paddle force applied to the breast, k_p is the paddle spring constant, x_m and x_p are the machine side and breast side paddle position, m_p is the mass of the paddle and $\ddot{x}_p$ is the paddle acceleration.

To simplify the simulation, we assume the mass of the paddle (m_p) is negligible:

$$F_P = k_p \left(x_m - x_p\right) \tag{12}$$

F_P can be determined from the simulation using the signals x_m and x_p in the Simulink model, as shown in Figure 41. The resulting plot in Figures 42 and 43 show that force overshoot is possible for both step and ramp inputs. For step input F_P reach its maximum value almost instantaneously, the lower the machine drive time constant (τ), the higher the overshoot value (Figure 42). For ramp input F_P take a relatively short time to reach its maximum value, the order of magnitude is approximately 10 times smaller than the step input and requires a longer time to settle (Figure 43). In fact, the amount of force overshoot predicted by the mathematical model will be less than the real system as the force generated by the actuator is limited. If the controller sets the actuator to produce an output greater than its limit, the actuator output will become saturated. The implication of force overshoot for step input is that, if there is a sudden change in the breast side paddle position, the control system explained in Paper 6 would try to bring the paddle back to its new equilibrium position and this may administer an unexpectedly high force to the patient. To eliminate the possibility of force overshoot,

a feedback system in controlling the force instead of position can be used. The following section will discuss the design of a potential force control system.

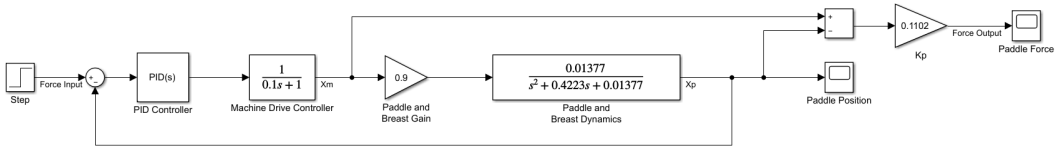

Figure 41. Simulink model for paddle force simulation

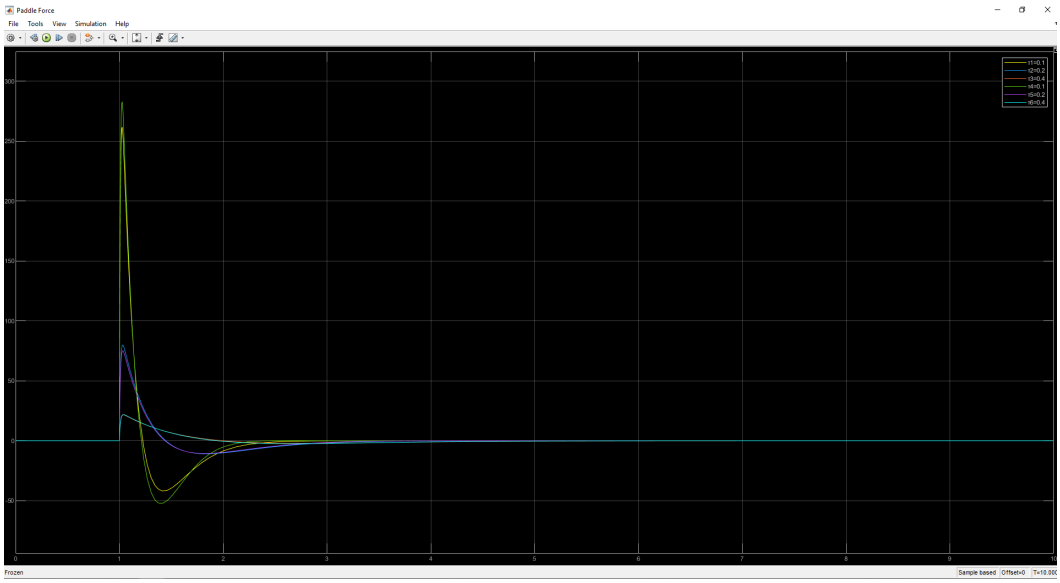

Figure 42. The scope output of paddle force against time for step input

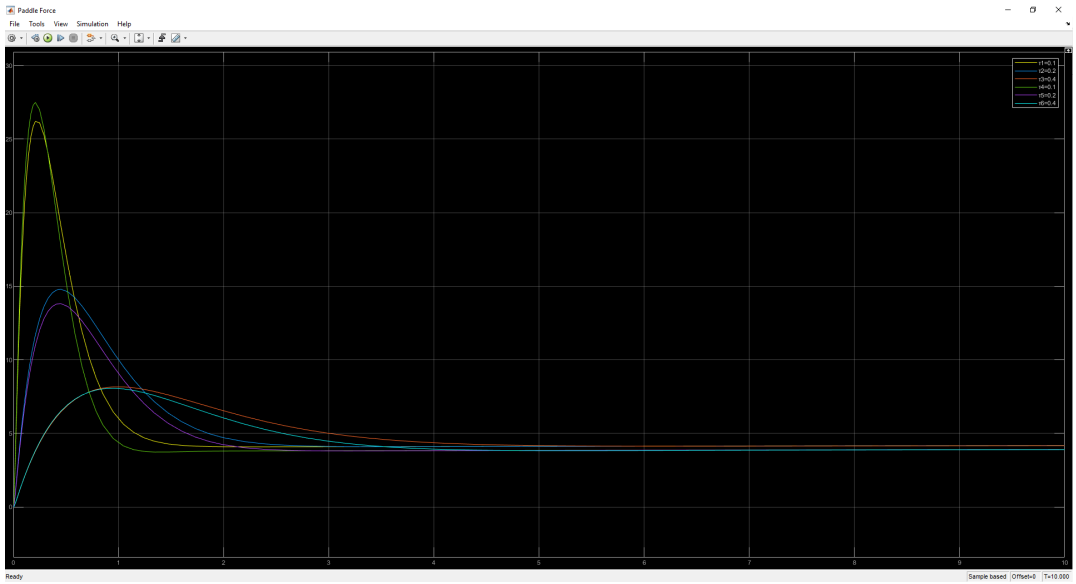

Figure 43. The scope output of paddle force against time for ramp input

Force control system

A force feedback control system can be developed by using F_P as feedback signal.

Rearranging equation 12 results in:

$$\frac{F_P}{x_m} = k_p(1 - DH) \tag{13}$$

Where $DH = \frac{x_p}{x_m}$ is the product of paddle and breast gain *D* as well as paddle and breast dynamics *H.* The force control system in Figure 45 was developed from the breast side position feedback system in Figure 44 and equation (13). The steady-state error in the force control system with ramp input was eliminated by adding an integrator in the forward loop to change the original system from type 1 to type 2.

The PID gains and corresponding ramp responses for the force control system after optimisation are shown in Table 16. In Table 16, the $k_{prop}$and k_{integ} values for the force control system appear much higher than the position feedback system and this implies a faster system response time and lower steady-state error.

The system response to the ramp input for different τ values is shown in Figures 46 and 47. In Figures 46 and 47, the system responses become equal to the ramp input and the steady-state error is zero for all τ values. This means the effect of the motor response on the change in input becomes negligible for the force control model. The settling time for the force control system would be higher than the estimated value because the limits on the actuator output limit the system response time. The advantage of using force

control instead of position control is that it can eliminate the possibility of force overshoot and hence increase patient comfort during the breast compression process. One of the applications of the force control system could be to implement pressure control for breast compression. If the paddle could provide the contact area in real time, then a force control system could be used to control its pressure. In other words, the pressure command would be multiplied by contact area to obtain the force command. This means the pressure standardised compression could be implemented by using this force control system and a customised paddle. On the other hand, the use of a force control system may increase paddle displacement during the clamping phase. As the breast tissue relaxes after its initial compression, the upwards resistance force of the breast decrease causes the paddle force to gradually drop during the clamping phase. If force feedback control is used to maintain a constant force during the clamping phase, then the paddle would have to move down further to maintain its force. This may increase the paddle displacement during the clamping phase.

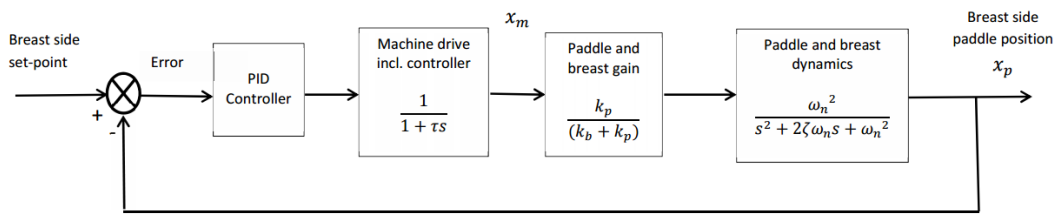

Figure 44. Block diagram of a position feedback system

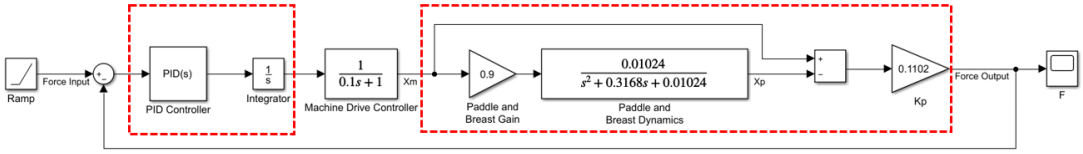

Figure 45. Simulink model of a force feedback system the red box highlighted the change in the original system

Table 16 PID controller gains and ramp response performance of the Selenia Dimensions and Lorad Selenia force feedback breast compression system for machine drive time constants (τ) of 0.1s, 0.2s and 0.4s

	Selenia Dimensions						Lorad Selenia					
	24x30 cm			18x24 cm			24x30 cm			18x24 cm		
	$\tau 1=$ 0.1	$\tau 2=$ 0.2	$\tau 3=$ 0.4	$\tau 4=$ 0.1	$\tau 5=$ 0.2	$\tau 6=$ 0.4	$\tau 1=$ 0.1	$\tau 2=$ 0.2	$\tau 3=$ 0.4	$\tau 4=$ 0.1	$\tau 5=$ 0.2	$\tau 6=$ 0.4
k_{prop}	537.22	494.16	438.32	562.93	537.03	452.82	604.01	627.32	487.31	565.31	539.14	454.37
k_{integ}	278.20	233.44	172.09	305.42	274.82	181.60	351.65	371.82	203.27	307.97	276.89	182.59
k_{deriv}	57.12	111.59	228.58	60.04	122.84	239.82	64.79	147.80	259.58	60.31	123.36	240.84
rise time	0.04	0.04	0.04	0.03	0.03	0.03	0.03	0.03	0.03	0.03	0.03	0.03
settling time	0.07	0.07	0.07	0.06	0.06	0.07	0.06	0.05	0.06	0.06	0.06	0.07

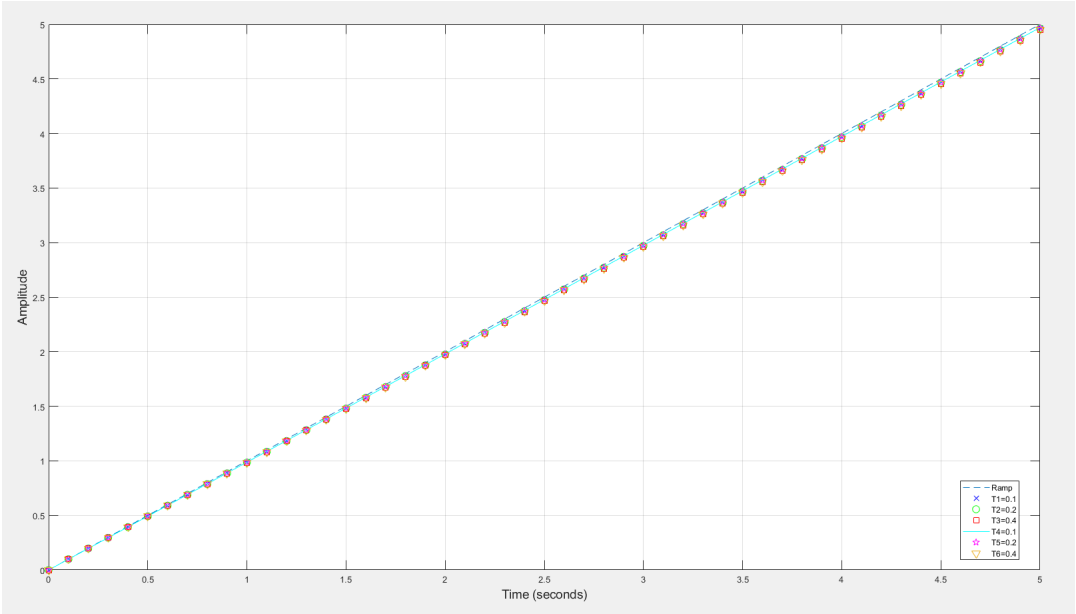

Figure 46. The ramp responses of the Selenia Dimensions force feedback breast compression system for machine drive time constants (τ) of 0.1s, 0.2s and 0.4s

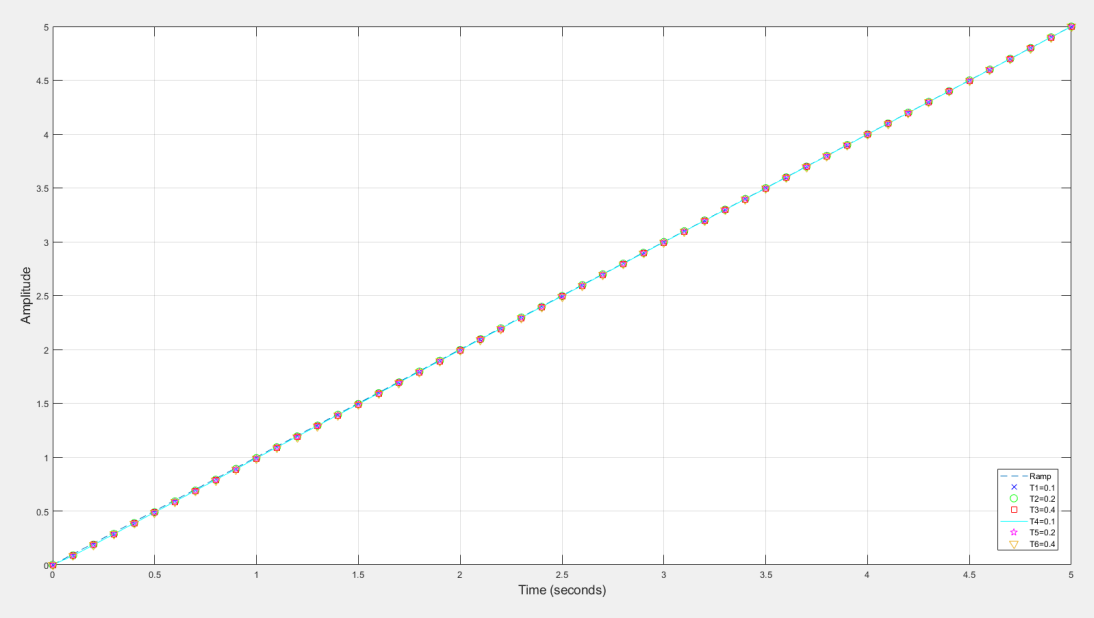

Figure 47. The ramp responses of the Lorad Selenia force feedback breast compression system for machine drive time constants (τ) of 0.1s, 0.2s and 0.4s

Contribution of the 6 journal papers to the field

Contribution of papers 1 and 2

Paper 1. Ma, W. K., Brettle, D., Howard, D., Kelly, J., Millington, S., & Hogg, P. (2014). Extra patient movement during mammographic imaging: an experimental study. *The British journal of radiology, 87*(1044), 20140241.

Paper 1 was the first publication to determine the amount of paddle motion during exposure and to detail the correlation between paddle displacement and the change in compression force. This paper is very novel, as it is the first time that a mathematical model has been used to represent paddle displacement. The mathematical model developed in paper 1 could be a useful tool for researchers to use in analysing and estimating paddle displacement in the clinical environment. This paper also provides recommendations for operators to employ to minimise the probability of blurring. For example, operators could also wait a few seconds after the compression force ceases to be applied, as the paddle displacement is the highest during in the first 10 s. This study had a direct effect on the work of Abdullah et al. (2017) in investigating simulated motion blur on lesion detection performance. They selected their maximum visual levels for blurring with reference to paper 1's findings that the extent of paddle motion in the vertical plane can reach as much as 1.5 mm. This critical review has identified that the paddle motion was misidentified as displacement therefore the amount of paddle motion in the vertical plane was overestimated. The influence of overestimation

in paddle motion on Abdullah's work is that they could have started with a smaller threshold level for the detection of blurring.

Paper 2. Ma, W. K., McEntee, M. F., Mercer, C., Kelly, J., Millington, S., & Hogg, P. (2016). Analysis of motion during the breast clamping phase of mammography. *The British journal of radiology, 89*(1059), 20150715.

Paper 2 was a continuation of the research findings of paper 1 and was the first multicentre study to measure paddle motion for 12 FFDM machines from three manufacturers during the breast clamping phase. This was also the first study to determine paddle tilt across the medial-lateral plane for a range of machine/paddle combinations, providing a reference for operators about the extent of paddle tilt for different manufacturers. It is important to minimise paddle tilting because the compression force applied on the paddle will not be evenly distributed. One side of the breast will be compressed more than the other if there is tilting. Uneven compression may cause under or overexposure on one side of the breast, and this uneven exposure could further affect the assessment of the breast mass density (Andolina & Lillé, 2011). The earlier critical review identified that the use of average paddle displacement to estimate the amount of motion would inevitably underestimate the worst case of the three runs of the experiment.

Contribution of paper 3

Paper 3. Ma, W. K., Hogg, P., Kelly, J., & Millington, S. (2015). A method to investigate image blurring due to mammography machine compression paddle movement. *Radiography, 21*(1), 36-41.

Paper 3 was the first published research paper to demonstrate that image blurring due to paddle motion can be detected in FFDM images. This paper is also very novel, as it was the first study to investigate whether paddle motion during image acquisition could cause image blur, and also the first to measure image blur severity. This research also determined the image blur severity in different locations of the breast, which is useful for operators or radiologists for identifying possible areas of blurring.

The earlier critical review identified that the ball bearings still seemed to move after 240 s which may be due to the method used to determine ball bearing motion. Metal ball bearings can still be used to indicate motion, however should be done by comparing the change in diameter at different time intervals instead of with a fixed diameter of 1.50 mm.

Contribution of paper 4

Paper 4. Ma, W. K., Aspin, R., Kelly, J., Millington, S., & Hogg, P. (2015). What is the minimum amount of simulated breast movement required for visual detection of blurring? An exploratory investigation. *The British journal of radiology, 88*(1052), 20150126.

Paper 4 was the first published research work to determine the minimum amount of simulated motion blur required for the visual detection of blurring. It was the first time that the concept of probability has been used to represent the visual detection of blurring. The clinical importance of this study is that it reminds the operators of the need to minimise patient motion during the image acquisition process. FFDM images are vulnerable to motion blur and even sub-millimetric motion would be visible. This study also had a direct effect on the work of Abdullah et al. (2017) in simulated motion blur on lesion detection performance. These authors selected their minimum visual levels for blurring with reference to the minimum amount of simulated motion blur required for the visual detection of the soft-edge mask estimation of blurring (0.7 mm), as determined in paper 4. The research outcomes of paper 4 may stimulate manufacturers or researchers to develop software for motion blur detection in mammography.

Recently, Hill et al. (2018) developed an algorithm to automate the detection of patient motion-related blur. They determined the spatial frequency range for their blur-detection method with reference to the minimum amount of simulated motion perceived by the human observers in paper 4. Paper 4 also helped to inspire the health care

company Volpara to develop a motion blur detection software (appendix 4) that provides an objective analysis to the operator in real time to support the retake decision (Hill et al., 2018). The motion detection software uses the motion severity score (scale: 0 to 100) to indicate the level of motion and produce a heatmap to show the blurring location and severity. Figure 48 shows the blur magnitude heatmap for a blurred mammogram that presents motion blur in the medial portion.

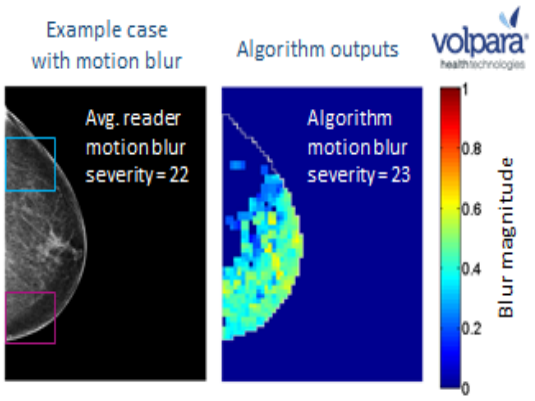

Figure 48. Blur magnitude heatmap for a mammography image with motion blur (Hill et al., 2018)

The earlier critical review identified that for the three motion simulation methods the soft-edged mask method is a more representative model of real blur compared with the hard-edge mask and Gaussian methods. Therefore, the minimum amount of simulated breast motion required for visual detection of blurring would be 0.7 mm.

Contribution of paper 5

Paper 5. Ma, W. K., Borgen, R., Kelly, J., Millington, S., Hilton, B., Aspin, R., ... & Hogg, P. (2017). Blurred digital mammography images: an analysis of technical recall and observer detection performance. *The British journal of radiology, 90*(1071), 20160271.

Paper 5 was the first publication to propose an observer standard for the visual detection of blurring. This paper was the first to use angular size calculations to determine the minimum amount of simulated motion blur required for the visual detection of blurring. Angular size is commonly used in vision sciences to describe how large an object appears from a given point of view (Legge & Bigelow, 2011; Changizi, 2010). This paper discussed research built on the study by Kinnear and Mercer (2016), which compared the detection of blurring on FFDM images on 1 MP and 5 MP monitors. This paper presented research that took the work done by Kinnear and Mercer (2016) further in various ways. Firstly, this study had a much larger number of observers (28 observers) than their study (6 observers). Secondly, five levels of simulated motion blur were used, which allowed for the investigation of observer performance at different blurring levels. Finally, the images were displayed and viewed in an ambient light-controlled room (<10 lux) to mimic normal image-reading conditions. The clinical importance of this study is that it demonstrated that monitors with resolutions lower than 2.3 MP are not suitable for the technical reviewing of FFDM images. This is because the number of blurred images missed by the observers for the 2.3 MP monitor was much higher than the

number for the 5 MP monitor, which might lead to a higher technical recall rate in clinical practice.

The earlier critical review identified that higher resolution FFDM needs to be scaled to fit the monitor display. The lower the monitor resolution, the higher the loss in image quality. This concurs with the conclusion that monitors with resolution lower than 2.3 MP are not suitable for the technical review of FFDM images.

Contribution of paper 6

Paper 6. Ma, W. K., Howard, D., & Hogg, P. (2017). Closed-loop control of compression paddle motion to reduce blurring in mammograms. *Medical physics, 44*(8), 4139-4147.

Paper 6 was the first published research work to demonstrate that paddle displacement settling time can be significantly reduced by implementing a position feedback system. This paper represents the first time that mathematical models for the compression paddle, machine drive, and breast were developed using paddle displacement data. These models were used in the simulation to demonstrate the performance of the proposed system.

The research outcomes of paper 6 may prompt manufacturers and control system experts to investigate the use of different control systems to optimise the response of paddle compression systems. In a recently granted US patent (US Patent No. US9855014B2, 2018) on the subject of compression paddles, inventors used a similar approach to paper 6. That is, they used an automatic feedback-driven method to control the paddle. In their design, strain sensors are employed on the edge of the paddle to measure and feed the applied compression force back to the motor controller, whilst also comparing the measured compression force against the target compression force. This is done to determine whether compression should stop or whether additional compression force is required.

The earlier critical review identified that force control systems can be used as an

alternative to position feedback systems to eliminate the possibility of force overshoot. Like the original system, paddle motion induced blur could be significantly reduced by implementing the force control system.

Conclusion

This critical review has revealed that the calculated displacements in paper 1 & 2 were misidentified as motion. This means that the amount of motion was initially overestimated. As shown in the hypothesis on paddle motion, the calculated paddle motion for the 18 x 24 cm fixed paddle was 0.15 mm during the time of the exposure (from 5 s to 7 s) which is much lower than the minimum amount of motion (0.7 mm) required for the visual detection of blurring. Therefore, the magnitude of motion caused by the paddle may not be visible to the observer. Therefore, there is not sufficient evidence to support the hypothesis that paddle motion causes image blur in FFDM.

In paper 3 the magnification of the ball bearing diameters falls within the calculated range of magnification ($1.04 \geq M \leq 1.21$). This indicates that the increase in ball bearings diameter may due to positioning within the breast phantom instead of paddle motion. Therefore, the increase in ball bearing diameter in FFDM images may not provide sufficient evidence to support the hypothesis that image blur is due to paddle motion. The implication is that the change in ball bearing diameter may not be useful to identify image blurring due to paddle motion.

In paper 4, motion was simulated in the horizontal plane (x-y), but paddle motion occurs is in the vertical plane (z). Therefore, a mathematical model was developed to determine the relationship between the vertical paddle motion and breast motion in the horizontal

plane. The ratio is approximately 1:0.3 which means the vertical thickness reduction will result in less horizontal breast displacement when the breast is compressed. As the ratio between the vertical paddle motion and the horizontal breast motion is not equal to 1, the amount of paddle motion required to cause visible image blurring has been underestimated.

In paper 5 the native resolution of the FFDM images is higher than the 2.3 MP, 5 MP and 12 MP monitors resolution so it has to be interpolated on the display. The lower the monitor resolution the higher the loss in the image quality after interpolation. For a viewing distance of 30 cm, an image displayed on the 12 MP monitor will look sharper than the 2.3 MP and 5 MP monitors to an observer with normal vision (20/20 vision). The observer can profit from using higher resolution monitors for blurring detecting as long as the viewing distance is suitable (30 cm).

In paper 6 a force control system was developed as an alternative way to control the paddle motion. Force overshoot was eliminated by using a feedback system to control the paddle force instead of paddle position. However, the use of the force control system may increase the paddle displacement during the clamping phase. As the breast tissue relaxes after the initial compression the paddle would have to move down to maintain a constant force during the clamping phase. Therefore, it is important to strike a balance between force overshoot and paddle displacement in designing the control system.

Future Work

Develop new phantom

The breast phantom used in this study would have degraded if the compression force was higher than 100 N. In future work, a more robust breast phantom could be made so that the effects of higher compression force on paddle motion can be investigated. In paper 1 the calibration graph developed from the breast phantom was used to relate the change in compression force to the change in displacement during the clamping phase. It could be that the calibration graph only applies to that breast phantom and may not be appropriate for application to all the patient breasts. Therefore, breast phantoms of different sizes and compositions could be produced to provide a wide range of calibration factors.

Compression force application

It was noticed that the way in which the operator applies the compression force may affect the starting position of the paddle. Therefore, further experiments could be carried out to measure the compression force and paddle displacement for breast phantoms of different sizes and compositions at different compression speeds. This could produce advice to the operator about what speed of compression would produce the least paddle motion during the clamping phase.

Variation in starting position

All three runs of the paddle displacement measurement showed large variation in their starting position. For future work, more than three repeats of the measurement could be carried out to investigate which is the worst-case starting position, and whether the speed of compression application would affect the starting position.

Effects of lighting and viewing time

In this study, the images were displayed and viewed in an ambient light-controlled room and the observers did not have a time limit for viewing each image. In the clinical environment, the operators would not have the same amount of time as the image readers involved in this study did. The level of light in the clinical rooms is also likely to be different from the light-controlled room in this study. Therefore, further studies should be conducted to investigate the effects of light and viewing time on the performance of operators regarding blurring detection.

Effects of regional blurring

In this study, the motion simulation software could only impose blurring globally (i.e. could only fully blur the entire image). In reality, real blurring may be either global or regional in nature. As the motion simulation software cannot introduce regional blurring, the effect of this on the observer performance in blurring detection is still unknown. For future work, the motion simulation software could be updated to introduce regional blurring to better reflect real blurring scenarios.

References

Abdullah, A. K., Kelly, J., Thompson, J. D., Mercer, C. E., Aspin, R., & Hogg, P. (2017). The impact of simulated motion blur on lesion detection performance in full-field digital mammography. *British Journal of Radiology*, *90*(1075), 1–7. doi.org/10.1259/bjr.20160871

Adachi, H., & Adachi, E. (2015). Using KINECT to measure joint movement for standing up and sitting down. In *2015 9th International Symposium on Medical Information and Communication Technology (ISMICT)* (pp. 68-72). IEEE.

Ali, R. M., England, A., McEntee, M. F., & Hogg, P. (2015). A method for calculating effective lifetime risk of radiation-induced cancer from screening mammography. *Radiography*,*21*(4), 298-303. doi.org/10.1016/j.radi.2015.07.008

Allisy-Roberts, P., Williams, J. (2007). *Farr's physics for medical imaging* (2nd ed.). Edinburgh: Saunders.

Altobelli, E., Rapacchietta, L., Angeletti, P. M., Barbante, L., Profeta, F. V., & Fagnano, R. (2017). Breast Cancer Screening Programmes across the WHO European Region: Differences among Countries Based on National Income Level. *International Journal of Environmental Research and Public Health*, *14*(4). doi.org/10.3390/ijerph14040452

Analoui, M., Bronzino, J. D., & Peterson, D. R. (Eds.). (2012). *Medical imaging: principles and practices*. London: CRC Press.

Andolina, V., & Lillé, S. (2011). *Mammographic imaging: a practical guide* (3rd ed.). Philadelphia: Lippincott Williams & Wilkins.

ATEK Sensor Techonologies (2018). Linear potenciometer LTP Series datasheet

Avison, P. (2014). *The world of physics* (2nd ed.). Oxford: Oxford University Press.

Bouwman, R. W., Diaz, O., Van Engen, R. E., Young, K. C., den Heeten, G. J., Broeders, M. J. M., ... & Dance, D. R. (2013). Phantoms for quality control procedures in digital breast tomosynthesis: dose assessment. *Physics in Medicine &*

Biology, 58(13), 4423.

Branderhorst, W., deGroot, J. E., Highnam, R., Chan, A., Böhm-Vélez, M., Broeders, M. J. M., …Grimbergen, C. A. (2015). Mammographic compression – A need for mechanical standardization. *European Journal of Radiology*, *84*(4), 596–602. doi.org/10.1016/J.EJRAD.2014.12.012

Brant, W. E., & Helms, C. A. (2012). *Fundamentals of diagnostic radiology* (4th ed.). Philadelphia: Lippincott Williams & Wilkins.

Bray, F., Ferlay, J., Soerjomataram, I., Siegel, R. L., Torre, L. A., & Jemal, A. (2018). Global cancer statistics 2018: GLOBOCAN estimates of incidence and mortality worldwide for 36 cancers in 185 countries. CA: *A Cancer Journal for Clinicians*. doi.org/10.3322/caac.21492

Bushberg, J. T., Seibert, J. A., Leidholdt, E. M., & Boone, J. M. (2011). *The essential physics of medical imaging* (3rd ed.). Philadelphia: Lippincott Williams & Wilkins.

Cardeñosa, G. (2006). *Clinical breast imaging: a patient focused teaching file*. Philadelphia: Lippincott Williams & Wilkins.

Carlton, R. R., & Adler, A. M. (2012). *Principles of radiographic imaging: an art and a science* (5th ed.). Boston: Cengage Learning.

Carmichael, B., Babahosseini, H., Mahmoodi, S. N., & Agah, M. (2015). The fractional viscoelastic response of human breast tissue cells. *Physical Biology*, *12*(4), 046001. doi.org/10.1088/1478-3975/12/4/046001

Carver, B., & Carver, E. (2012). *Medical imaging: techniques, reflection and evaluation* (2nd ed.). London: Churchill Livingstone.

Changizi, M. (2010). *The vision revolution: how the latest research overturns everything we thought we knew about human vision*. BenBella Books.

Cutter, M. A. G. (2018). *Thinking through breast cancer: a philosophical exploration of diagnosis, treatment, and survival.* Oxford: Oxford University Press.

Cynthia, E. L. D., Zhipeng, Z., Weston, B. G., & Ying, M. (2018*). Compression*

paddle for use in breast imaging. US Patent No. US9855014B2. Retrieved from https://patents.google.com/patent/US9855014B2/en

de Groot, J. E., Branderhorst, W., Grimbergen, C. A., den Heeten, G. J., & Broeders, M. J. (2015). Towards personalized compression in mammography: a comparison study between pressure-and force-standardization. *European journal of radiology, 84*(3), 384-391. doi.org/10.1016/j.ejrad.2014.12.005

de Groot, J. E., Broeders, M. J. M., Branderhorst, W., den Heeten, G. J., & Grimbergen, C. A. (2013). A novel approach to mammographic breast compression: improved standardization and reduced discomfort by controlling pressure instead of force. *Medical physics, 40*(8). 081901. doi.org/10.1118/1.4812418

deMunck, L., deBock, G. H., Otter, R., Reiding, D., Broeders, M. J., Willemse, P. H., & Siesling, S. (2016). Digital vs screen-film mammography in population-based breast cancer screening: performance indicators and tumour characteristics of screen-detected and interval cancers. *British Journal of Cancer*, *115*(5), 517–24. doi.org/10.1038/bjc.2016.226

denBoer, D., Dam-Vervloet, L. A. J., Boomsma, M. F., deBoer, E., vanDalen, J. A., & Poot, L. (2018). Clinical validation of a pressure-standardized compression mammography system. *European Journal of Radiology*, *105*, 251–254. doi.org/10.1016/J.EJRAD.2018.06.021

Dendy, P. P., & Heaton, B. (2012). *Physics for diagnostic radiology* (3rd ed.). London: CRC Press.

Ducheyne, P. (2017). *Comprehensive biomaterials II* (Vol. 1) (2nd ed.). London: Elsevier.

Ekpo, E. U., Alakhras, M., & Brennan, P. (2018). Errors in Mammography Cannot be Solved Through Technology Alone. *Asian Pacific Journal of Cancer Prevention*, *19*(2), 291–301. doi.org/10.22034/APJCP.2018.19.2.291

Fauber, T. L. (2013). *Radiographic imaging and exposure* (5th ed.). St Louis: Elsevier.

Ferreira, T., & Rasband, W. (2012). ImageJ user guide. *ImageJ/Fiji*, 1, 155-161.

Flower, M. A. (2012). *Webb's Physics of Medical Imaging* (2nd ed.). London: CRC Press.

Galna, B., Barry, G., Jackson, D., Mhiripiri, D., Olivier, P., & Rochester, L. (2014). Accuracy of the Microsoft Kinect sensor for measuring movement in people with Parkinson's disease. *Gait & posture, 39*(4), 1062-1068.

Gefen, A., & Dilmoney, B. (2007). Mechanics of the normal woman's breast. *Technology and Health Care*, *15*(4), 259-271.

Geiser, W. R., Haygood, T. M., Santiago, L., Stephens, T., Thames, D., & Whitman, G. J. (2011). Challenges in mammography: part 1, artifacts in digital mammography. *American Journal of Roentgenology, 197*(6), W1023-W1030.

Goodman, C. C., & Fuller, K. S. (2011). *Pathology for the physical therapist assistant*. Philadelphia: Saunders.

Gupta, B. D. (2006). *Fiber optic sensors: principles and applications*. Pitampura: New Indian Publishing Agency.

Hauge, I. H. R., Hogg, P., Szczepura, K., Connolly, P., McGill, G., & Mercer, C. (2012). The readout thickness versus the measured thickness for a range of screen film mammography and full-field digital mammography units. *Medical Physics*, *39*(1), 263–71. doi.org/10.1118/1.3663579

Hendee, W. R., & Ritenour, E. R. (2002). *Medical imaging physics* (4th ed.). New York: Wiley-Liss.

Hill, M. L., Whelehan, P., Vinnicombe, S. J., Tromans, C. E., Evans, A., Warwick, V. R., ... & Highnam, R. P. (2018). Development of an automated detection algorithm for patient motion blur in digital mammograms. In *14th International Workshop on Breast Imaging (IWBI 2018)* (Vol. 10718, p. 107180K). International Society for Optics and Photonics.

Hoff, S. R., Abrahamsen, A.-L., Samset, J. H., Vigeland, E., Klepp, O., & Hofvind, S. (2012). Breast Cancer: Missed Interval and Screening-detected Cancer at Full-Field Digital Mammography and Screen-Film Mammography— Results from a

Retrospective Review. *Radiology*, *264*(2), 378–386. doi.org/10.1148/radiol.12112074

Hologic (2020) Selenia dimensions with acquisition workstation 8000 http://www.hologic.ca/sites/default/files/product-files/Dimensions%20AWS%208000%20Datasheet%20%28DS-00193%29%20English%20Rev%20002%2011-13.pdf

Hogg, P., Kelly, J., & Mercer, C. (Eds.), (2015). *Digital mammography: a holistic approach*. London: Springer.

Hogg, P., Szczepura, K., Kelly, J., & Taylor, M. (2012). Blurred digital mammography images. *Radiography*, *18*(1), 55–56. doi.org/10.1016/j.radi.2011.11.008

Ikeda, D., & Miyake, K. K. (2016). *Breast imaging: the requisites* (3rd ed.). St Louis: Elsevier.

Insana, M. F., Pellot-Barakat, C., Sridhar, M., & Lindfors, K. K. (2004). Viscoelastic imaging of breast tumor microenvironment with ultrasound. *Journal of mammary gland biology and neoplasia, 9*(4), 393-404.

Johnston, J. N., & Fauber, T. L. (2015). *Essentials of radiographic physics and imaging* (2nd ed.). St Louis: Elsevier.

Kamarudin, K., Mamduh, S., Shakaff, A., & Zakaria, A. (2014). Performance Analysis of the Microsoft Kinect Sensor for 2D Simultaneous Localization and Mapping Techniques. *Sensors*, *14*(12), 23365–23387. doi.org/10.3390/s141223365

Kelly J, Hogg P, Szczepura K, McGeever G, Wilcock C, Tinston S, et al. (2011). *The blurring issue in mammography*. Seminar presented at the Mammographic Imaging Seminar, Salford, UK.

Kelly, J., & Hogg, P. (2018). The impact of image blurring in FFDM, *RAD Magazine*, 44, 517, 12-13.

Keyence. (2019). *CL-3000 Series Confocal Displacement Sensor Catalog*. Retrieved from https://www.keyence.com/products/measure/laser-1d/cl-3000/downloads/?mode=ca

Khurana, I., Khurana A., & Kowlgi, N. G. (2019). *Textbook of Medical Physiology* (3rd ed.). New Delhi: Elsevier India.

Kinnear, L., & Mercer, C. (2016). A study to compare the detection of visual blurring in 1 MP and 5 MP monitors within mammography clinical practice. *Imaging & Therapy Practice*, 23–28.

Kuppusamy, T. (2017). *Basic Radiological Physics* (2nd ed.). New Delhi: Jaypee Brothers Medical Publishers.

Lancaster, L. J., & Hasegawa, B. (2016). *Fundamental Mathematics and Physics of Medical Imaging*. London: CRC Press.

Legge, G. E., & Bigelow, C. A. (2011). Does print size matter for reading? A review of findings from vision science and typography. *Journal of vision, 11*(5), 8-8.

Linguraru, M. G., Brady, M., & Yam, M. (2001). Filtering h int Images for the Detection of Microcalcifications. In *International Conference on Medical Image Computing and Computer-Assisted Intervention* (pp. 629-636). Springer, Berlin, Heidelberg.

Mason A., Mukhopadhyay, S.C., Jayasundera K. P., & Bhattacharyya N., (2014). Sensing Technology: Current Status and Future Trends II. Springer

Marmot, M. G., Altman, D. G., Cameron, D. A., Dewar, J. A., Thompson, S. G., & Wilcox, M., (2013). The benefits and harms of breast cancer screening: an independent review. *British Journal of Cancer*, *108*(11), 2205–40. doi.org/10.1038/bjc.2013.177

McFedries, P. (2019). *Microsoft Excel 2019 Formulas and Functions*. Microsoft Press.

McGeever, G. C. (2012). *Deflection of a mammography paddle over a period of time* (Unpublished master's dissertation). University of Salford, Salford, United Kingdom.

Metrios. (2020). *Optical measurement on the shopfloor*. Retrieved from https://www.vicivision.co.uk/wp-content/uploads/2019/03/METRIOS_Optical-measuring-systems_ENG_HD.pdf

Microsoft. (2019). *Kinect for Windows SDK Beta*. Retrieved from https://www.microsoft.com/en-us/research/project/kinect-for-windows-sdk-beta.

Mortazavi, F., & Nadian-Ghomsheh, A. (2018). Stability of Kinect for range of motion analysis in static stretching exercises. *PloS one, 13*(7), e0200992.

Moss, S. M., Cuckle, H., Evans, A., Johns, L., Waller, M., & Bobrow, L. (2006). Effect of mammographic screening from age 40 years on breast cancer mortality at 10 years' follow-up: a randomised controlled trial. *The Lancet*, *368*(9552), 2053-2060. doi.org/10.1016/S0140-6736(06)69834-6

NHSBSP (2017a). *Guidance on collecting, monitoring and reporting technical recall and repeat examinations,* London: Public Health England.

NHSBSP (2017b). *Guidance for breast screening mammographers* (3rd ed.), London: Public Health England.

NHSBSP Equipment Report 0604. (2009). *Commissioning and routine testing of full field digital mammography systems.* Sheffield: NHS Cancer Screening Programmes.

Noone, A. M., Howlader, N., Krapcho, M., Miller, D., Brest, A., Yu, M., ... & Chen, H. S. (2018). SEER Cancer Statistics Review, 1975-2015, National Cancer Institute. Bethesda, MD.

Odom-Forren, J. (2017). *Drain's perianesthesia nursing: a critical care approach* (7th ed.). St Louis: Elsevier.

Otte, K., Kayser, B., Mansow-Model, S., Verrel, J., Paul, F., Brandt, A. U., & Schmitz-Hübsch, T. (2016). Accuracy and reliability of the kinect version 2 for clinical measurement of motor function. *PloS one*, *11*(11), e0166532. doi.org/10.1371/journal.pone.0166532.

Parikh, U., Chhor, C. M., & Mercado, C. L. (2018). Ductal carcinoma in situ: the whole truth. *American Journal of Roentgenology, 210*(2), 246-255.

Palm, W. (2013). *System Dynamics* (3rd ed.), New York: McGraw-Hill Education.

Pisano, E. D., Gatsonis, C., Hendrick, E., Yaffe, M., Baum, J. K., Acharyya, S., …Digital Mammographic Imaging Screening Trial (DMIST) Investigators Group. (2005). Diagnostic Performance of Digital versus Film Mammography for Breast-Cancer Screening. *New England Journal of Medicine*, *353*(17), 1773–1783. doi.org/10.1056/NEJMoa052911

Pisano, E. D., Zuley, M., Baum, J. K., & Marques, H. S. (2007). Issues to consider in converting to digital mammography. *Radiologic Clinics of North America*, *45*(5), 813-830.

Pisano, E. D., Hendrick, R. E., Yaffe, M. J., Baum, J. K., Acharyya, S., Cormack, J. B., ... & D'Orsi, C. J. (2008). Diagnostic accuracy of digital versus film mammography: exploratory analysis of selected population subgroups in DMIST. *Radiology, 246*(2), 376-383.

Popli, M. B., Teotia, R., Narang, M., & Krishna, H. (2014). Breast positioning during mammography: mistakes to be avoided. *Breast cancer: basic and clinical research*, *8*, BCBCR-S17617.

Pöhlmann, S. T., Hewes, J., Williamson, A. I., Sergeant, J. C., Hufton, A., Gandhi, A., ... & Astley, S. M. (2014). Breast volume measurement using a games console input device. In *International Workshop on Digital Mammography* (pp. 666-673). Springer, Cham. doi.org/10.1007/978-3-319-07887-8_92

Renart-Vicens, G., Puig-Vives, M., Albanell, J., Castañer, F., Ferrer, J., Carreras, M., …Marcos-Gragera, R. (2014). Evaluation of the interval cancer rate and its determinants on the Girona Health Region's early breast cancer detection program. *BMC Cancer*, *14*, 558. doi.org/10.1186/1471-2407-14-558

Rosen, E. L., Baker, J. A., & Soo, M. S. (2002). Malignant Lesions Initially Subjected to Short-term Mammographic Follow-up. *Radiology*, *223*(1), 221–228. doi.org/10.1148/radiol.2231011355

Rothschild, J., Lourenco, A. P., & Mainiero, M. B. (2013). Screening Mammography Recall Rate: Does Practice Site Matter? *Radiology*, *269*(2), 348–353. doi.org/10.1148/radiol.13121487

Rourke, J. O., Mercer, C. E. and Starr, L. (2014). *Programme Evaluation: Technical*

recall and image blur within a breast screening service. Paper presented at the Symposium Mammographicum, Bournemouth, UK.

Russ, J. C & Neal, F.B. (2017). *The Image Processing Handbook* (7th ed.). London: CRC Press

Salvaggio, N. & Shagam, J. (2019). *Basic photographic materials and processes*. New York: Routledge.

Sardanelli, F., Aase, H. S., Álvarez, M., Azavedo, E., Baarslag, H. J., Balleyguier, C., …Forrai, G. (2017). Position paper on screening for breast cancer by the European Society of Breast Imaging (EUSOBI) and 30 national breast radiology bodies from Austria, Belgium, Bosnia and Herzegovina, Bulgaria, Croatia, Czech Republic, Denmark, Estonia, Finland, France, Germany, Greece, Hungary, Iceland, Ireland, Italy, Israel, Lithuania, Moldova, The Netherlands, Norway, Poland, Portugal, Romania, Serbia, Slovakia, Spain, Sweden, Switzerland and Turkey. *European Radiology*, *27*(7), 2737–2743. doi.org/10.1007/s00330-016-4612-z

Seddon, D., Schofield, K., & Waite, C. (2000). Investigation into possible causes of blurring in mammograms. *Breast Cancer Research*, *2*(S2), A64. doi.org/10.1186/bcr253

Seeler, K. A. (2014). *System dynamics: An introduction for mechanical engineers.* New York: Springer.

Shah, B.A., & Mandava, S. (2013). *Breast Imaging: A Core Review*. Philadelphia: Lippincott Williams & Wilkins.

Shah, T. A., & Guraya, S. S. (2017). Breast cancer screening programs: Review of merits, demerits, and recent recommendations practiced across the world. *Journal of Microscopy and Ultrastructure*, *5*(2), 59–69. doi.org/10.1016/J.JMAU.2016.10.002

Shi, J., Xu, L., & Jia, J. (2015). Just noticeable defocus blur detection and estimation. In *Proceedings of the IEEE Conference on Computer Vision and Pattern Recognition* (pp. 657-665).

Sigmascreening. (2017). How does the Sensitive Sigma™ Paddle work? Retrieved from https://www.sigmascreening.com/products

Silverman, P. (2012). *Oncologic imaging: a multidisciplinary approach.* Philadelphia: Saunders.

Sridhar, M., & Insana, M. F. (2007). Ultrasonic measurements of breast viscoelasticity. *Medical Physics*, *34*(12), 4757–67. doi.org/10.1118/1.2805258

Sweeney, R.-J. I., Lewis, S. J., Hogg, P., & McEntee, M. F. (2017). A review of mammographic positioning image quality criteria for the craniocaudal projection. *The British Journal of Radiology*, *91*(1082), 20170611. doi.org/10.1259/bjr.20170611

Tyagi, V. (2018). *Understanding Digital Image Processing*. London: CRC Press.

Vinnicombe, S., Pinto Pereira, S. M., Mccormack, V. A., Shiel, S., Perry, N., & dos Santos Silva, I. M. (2009). Full-Field Digital versus Screen-Film Mammography: Comparison within the UK Breast Screening Program and Systematic Review of Published Data. *Radiology*, *251*(2), 347–358. doi.org/10.1148/radiol.2512081235

Welcsh, P. (Ed.) (2009). *The role of genetics in breast and reproductive cancers*. New York: Springer.

White, J. (2000). FDA Approves System for Digital Mammography. *Journal of the National Cancer Institute*, *92*(6), 442–442. doi.org/10.1093/jnci/92.6.442

Whitley, A. S. (2015). *Clark's positioning in radiography* (13th ed.). London: CRC Press.

World Cancer Research Fund International. (2018). Breast cancer statistics. Retrieved from https://www.wcrf.org/dietandcancer/cancer-trends/breast-cancer-statistics.

Appendices

Appendix 1: Contribution of work

Full reference for submitted work	Journal title, aims and scope	Detail of independent contribution
1. Ma WK, Brettle D, Howard D, Kelly J, Millington S, Hogg P. Extra patient movement during mammographic imaging: an experimental study. British Journal of Radiology 2014; 87: 20140241.	*British Journal of Radiology* is the international research journal of the British Institute of Radiology and is the oldest scientific journal in the field of radiology and related sciences. It covers the clinical and technical aspects of medical imaging, radiotherapy, oncology, medical physics, radiobiology and the underpinning sciences.	-Participated in paddle displacement data collection -Analysed dada and developed a theoretical model to analyse the paddle displacement -Carried out error analysis for the paddle measurement -Played a lead role in drafting the article, and approved the final draft
2. Ma WK, McEntee MF, Mercer C, Kelly J, Millington S, Hogg P. Analysis of motion during the breast clamping phase of mammography. British Journal of Radiology 2016; 89: 20150715	*British Journal of Radiology*; see above.	-Participated in paddle displacement data collection -Participated in the experimental design by choosing the paddle data recording period and brand of mammography unit included in the study -Performed statistical analysis to compare paddle motion between fixed and flexible paddles, small and large paddles -Played a lead role in drafting the article, and

		approved the final draft.
3. Ma WK, Hogg P, Kelly J, Millington S. A method to investigate image blurring due to mammography machine compression paddle movement. Radiography 2015; 21: 36–41.	*Radiography* is the official peer-reviewed journal of the Society and College of Radiographers and the European Federation of Radiographer Societies. It aims to promote evidence-based practice by disseminating high-quality clinical, scientific and educational research related to all aspects of diagnostic and therapeutic radiography.	-Participated in the experimental design by choosing the location of the ball bearing on the surface of the breast phantom and the compression forces used in the experiment -Performed statistical analysis to compare the change in ball-bearing diameter -Performed image segmentation of the metal ball bearing using ImageJ -Played a lead role in drafting the article, and approved the final draft
4. Ma WK, Aspin R, Kelly J, Millington S, Hogg P. What is the minimum amount of simulated breast movement required for visual detection of blurring? An exploratory investigation. British Journal of Radiology 2015; 88: 20150126.	*British Journal of Radiology*; see above.	-Participated in the experimental design by choosing the three simulation methods: gaussian, hard-edge and soft-edge mask estimation to simulate motion blurring -Gathering data from different observers and calculate the probability of blurring detection for each simulation method -Carried out statistical testing to determine the consistency between the observers -Played a lead role in drafting the article, and approved the final draft.

5. Ma WK, Borgen R, Kelly J, Millington S, Hilton B, Aspin R, Lança C, Hogg P. Blurred digital mammography images: an analysis of technical recall and observer detection performance. British Journal of Radiology 2017; 90: 20160271.	*British Journal of Radiology*; see above.	-Participated in the experimental design by choosing the levels of simulated blurring, monitor resolution and viewing distance -Performed statistical analysis to compare blurring detection rate between 2.3 and 5 MP monitors, and assess the interobserver variability -Performed angular size calculations to identify the minimum amount of blurring that can be detected by the observer -Played a lead role in drafting the article, and approved the final draft
6. Ma WK, Howard D, Hogg P. Closed-loop control of compression paddle motion to reduce blurring in mammograms. Medical Physics 2017; 44(8):4139–4147.	*Medical Physics* is the scientific journal of the American Association of Physicists in Medicine and is an official science journal of the Canadian Organization of Medical Physicists, the Canadian College of Physicists in Medicine, and the International Organization for Medical Physics. It publishes research concerned with the application of physics and mathematics to the solution of problems in medicine and human biology.	-Developed the mathematical model for the breast, machine drive and compression paddle for simulation -Designed the PID controller for the breast compression system -Carried out performance test for the PID controller in Mathworks Simulink -Played a lead role in drafting the article, and approved the final draft.

Statement of works

I confirm that WK Ma has complied with the ICMJE recommendations for being an author[1] for the following publications. Additionally he has taken the lead role (resulting in him becoming first author) for data collection, analysis, write up and revision and final proof checking prior to publication.

21st November 2017
Professor Peter Hogg
Research Dean
School of Health Sciences
University of Salford

1. Ma WK, Brettle D, Howard D, Kelly J, Millington S, Hogg P. Extra patient movement during mammographic imaging: an experimental study. British Journal of Radiology 2014; 87: 20140241.

2. Ma WK, McEntee MF, Mercer C, Kelly J, Millington S, Hogg P. Analysis of motion during the breast clamping phase of mammography. British Journal of Radiology 2016; 89: 20150715

3. Ma WK, Hogg P, Kelly J, Millington S. A method to investigate image blurring due to mammography machine compression paddle movement. Radiography 2015; 21: 36 – 41.

4. Ma WK, Aspin R, Kelly J, Millington S, Hogg P. What is the minimum amount of simulated breast movement required for visual detection of blurring? An exploratory investigation. British Journal of Radiology 2015; 88: 20150126.

5. Ma WK, Borgen R, Kelly J, Millington S, Hilton B, Aspin R, Lança C, Hogg P. Blurred digital mammography images: an analysis of technical recall and observer detection performance. British Journal of Radiology 2017; 90: 20160271.

6. Ma WK, Howard D, Hogg P. Closed-loop control of compression paddle motion to reduce blurring in mammograms. Medical Physics 2017; 44(8):4139-4147.

---

1 http://www.icmje.org/recommendations/browse/roles-and-responsibilities/defining-the-role-of-authors-and-contributors.html

Appendix 2: Experiment for static ball bearing

A Hologic Selenia Dimensions mammography machine calibrated to give compression force in Newtons (N) was used in this experiment. A custom-made breast phantom with 95mm radius and 53mm thickness which is composed of 32.5mm thickness Poly Methyl Methacrylate (PMMA) and 20.5 mm thickness polyethylene (PE) slabs were used to simulate the standard breast (Bouwman et al. 2013). A 1.50 mm hole was drilled into the bottom of the PMMA slab and a metal ball-bearing with 1.50 mm spherical diameter was inserted (Figure 49). The experimental setup is shown in Figure 50. Static ball bearing images were acquired using manual control mode without applying any compression force and exposed at 30 kVp, 120 mAs. Given the nature of metal ball bearings it is difficult to ensure they are completely still during exposure therefore in this experiment only craniocaudal (CC) view was taken to ensure the acquisition of static ball bearing image.

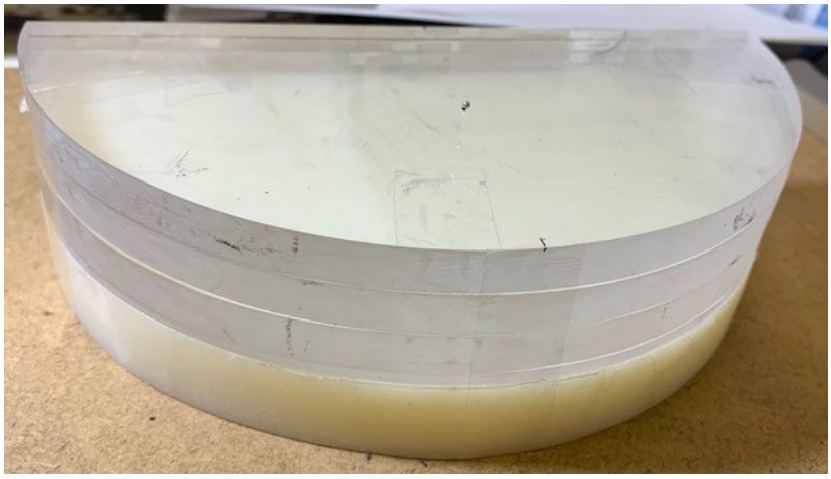

Figure 49. The makeup of the custom-made breast phantom

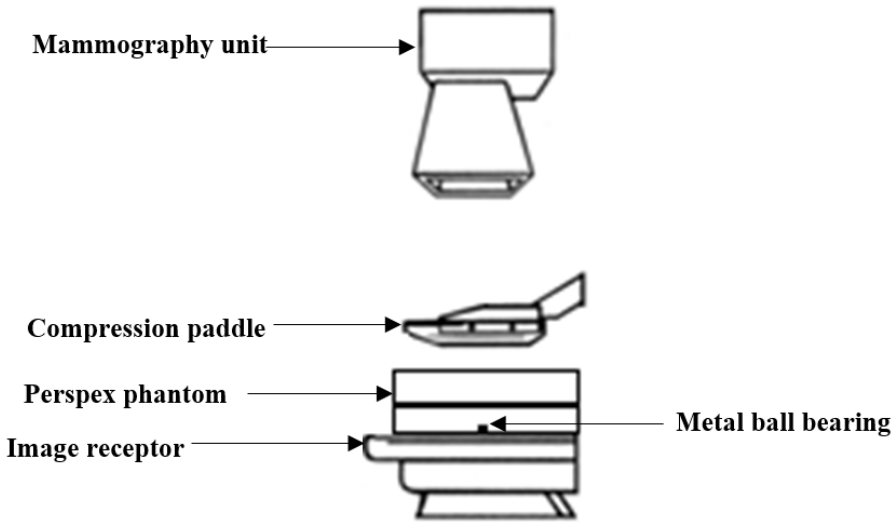

Figure 50. Schematic showing the experimental setup

Appendix 3: Compression force and ball-bearing diameters graphs for intensity thresholding and edge detection methods

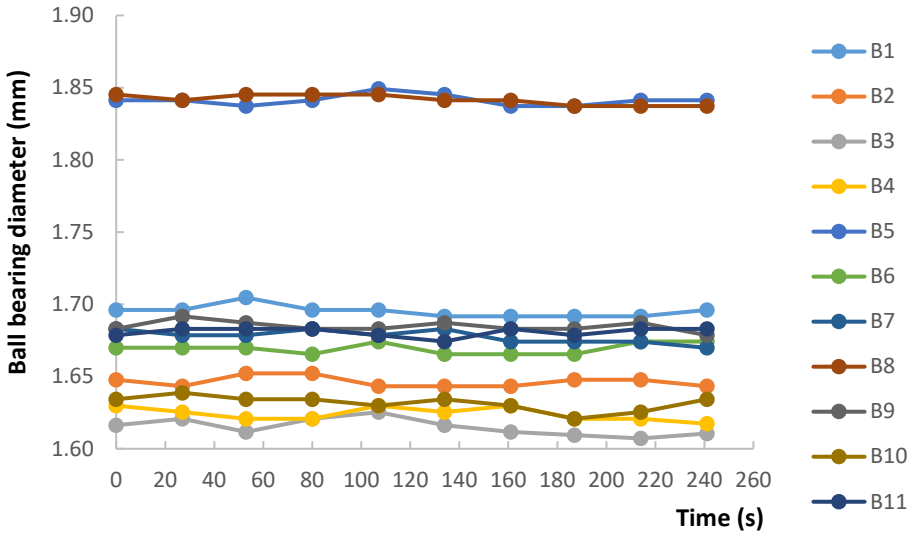

Figure 51. Ball-bearing diameters for flexible paddle with 80 N compression force calculated by intensity thresholding method

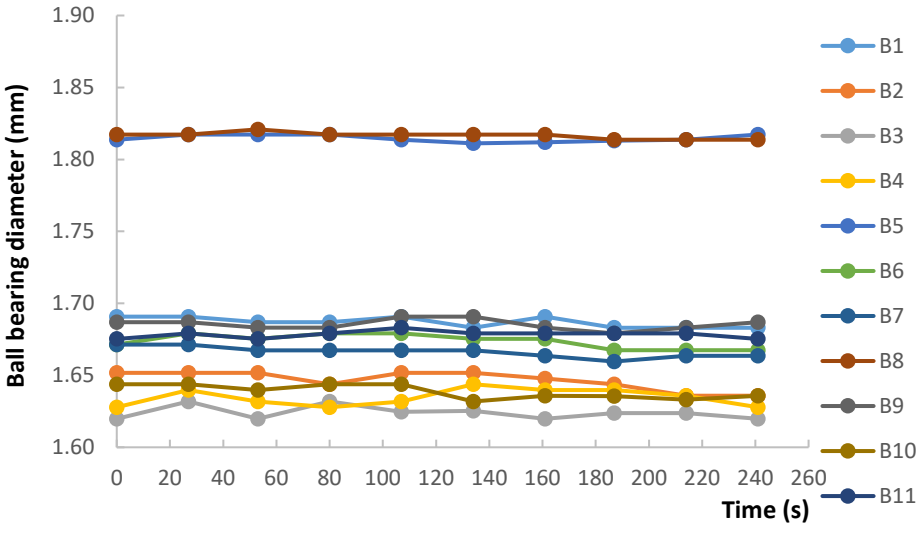

Figure 52. Ball-bearing diameters for flexible paddle with 80 N compression force calculated by edge detection method

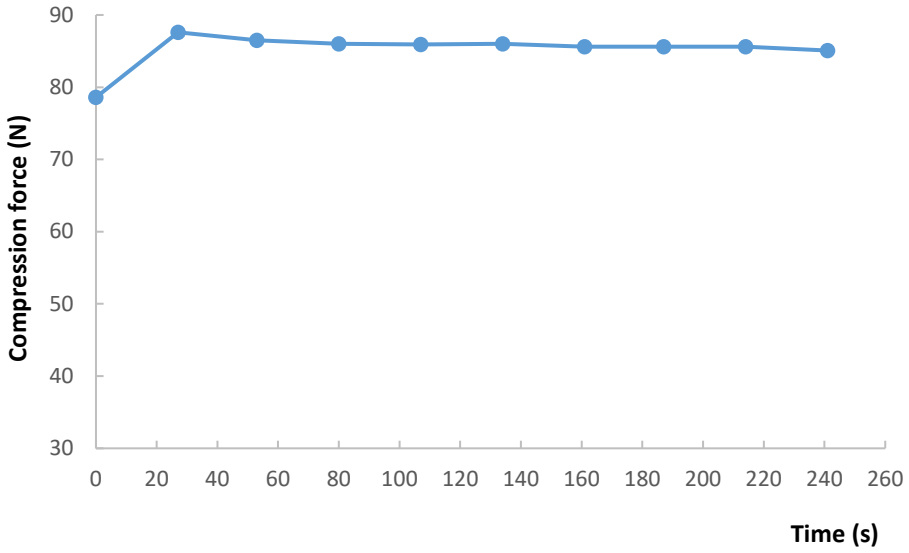

Figure 53. Compression force against time for flexible paddle with 80 N compression force

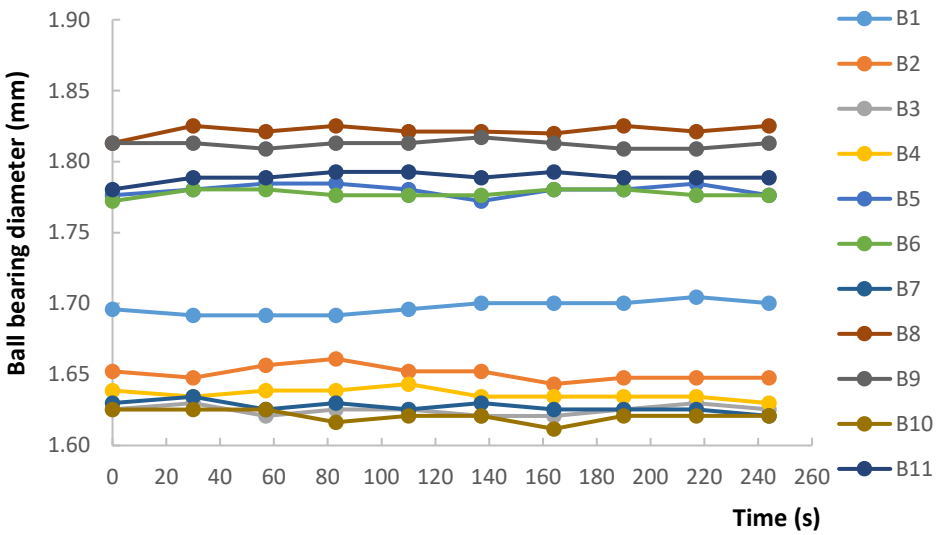

Figure 54. Ball-bearing diameters for fixed paddle with 150 N compression force calculated by intensity thresholding method

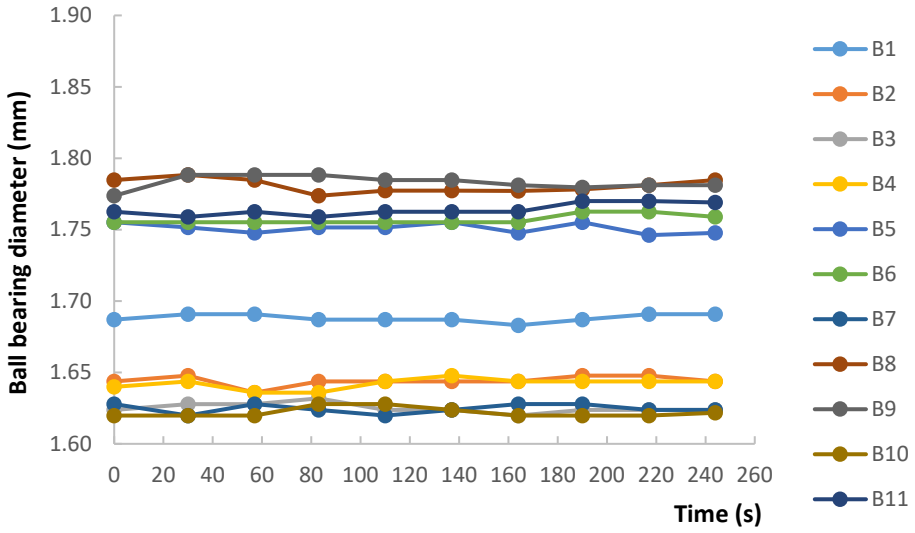

Figure 55. Ball-bearing diameters for fixed paddle with 150 N compression force calculated by edge detection method

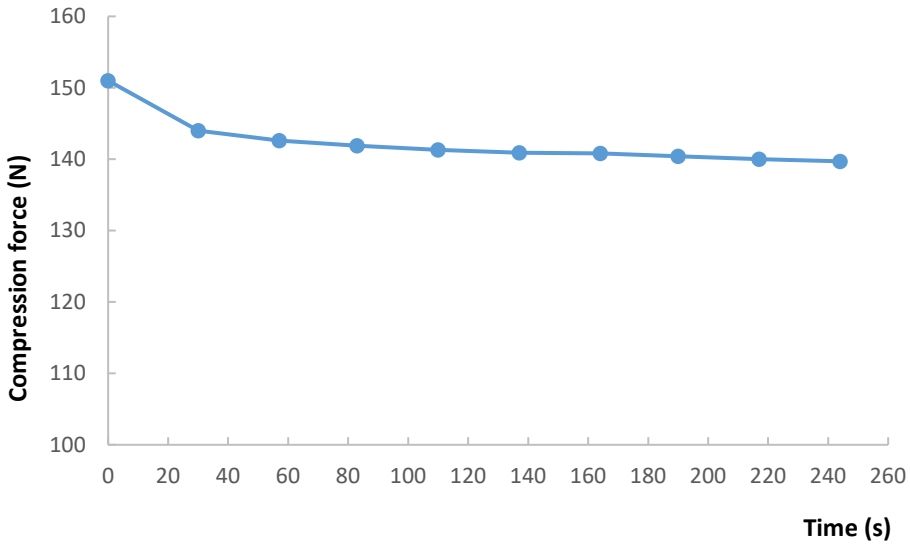

Figure 56. Compression force against time for fixed paddle with 150 N compression force

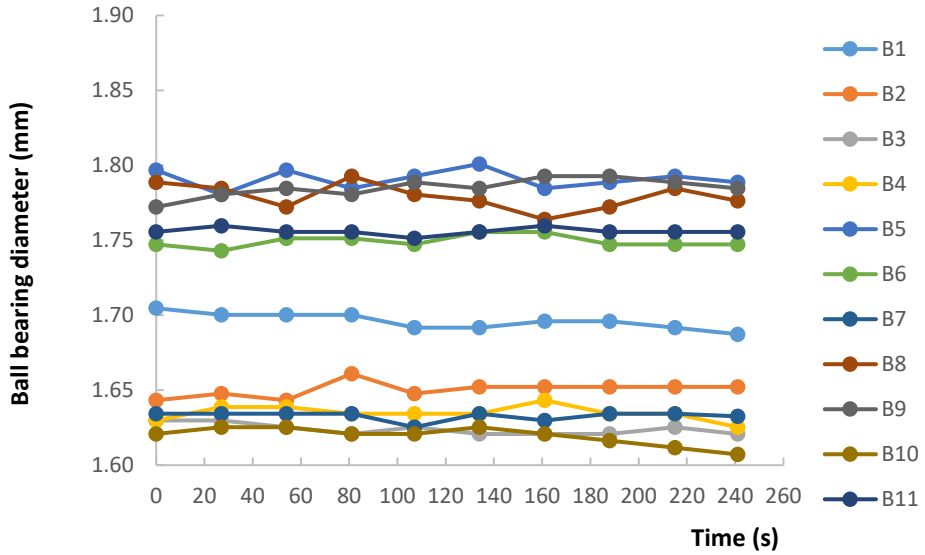

Figure 57. Ball-bearing diameters for flexible paddle with 150 N compression force calculated by intensity thresholding method

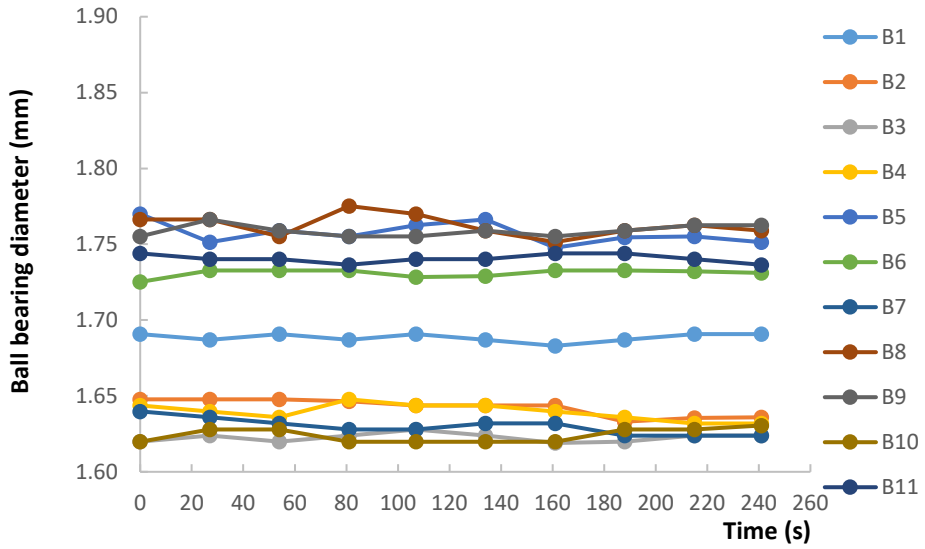

Figure 58. Ball-bearing diameters for flexible paddle with 150 N compression force calculated by edge detection method

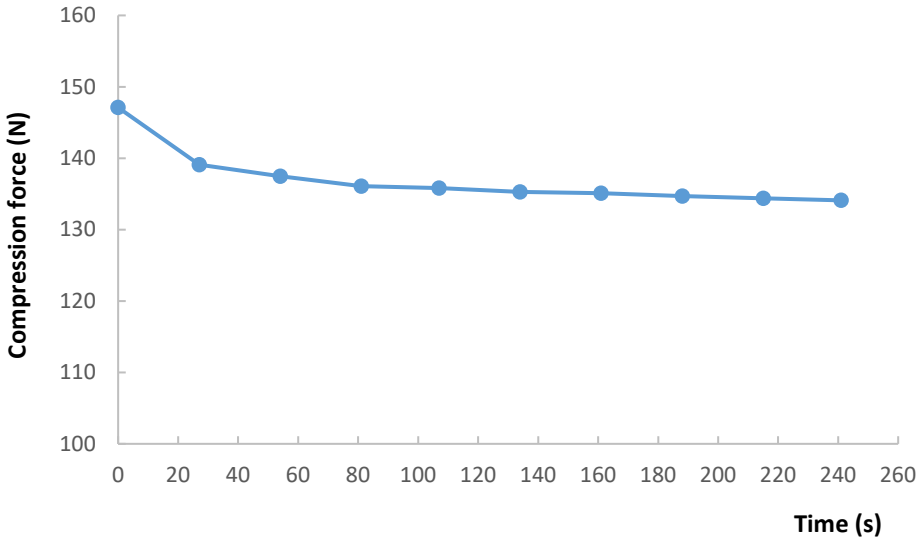

Figure 59. Compression force against time for flexible paddle with 150 N compression force

Appendix 4: News about Volpara's software

Volpara Solutions Introduces Two New Products at ECR

VolparaEnterprise Live! and VolparaRisk Software to be Shown at ECR for the First Time

volparasolutions

NEWS PROVIDED BY
Volpara Solutions →
Mar 01, 2018, 08:00 ET

VIENNA, March 1, 2018 /PRNewswire/ -- Volpara Solutions, Inc. announced the European introduction of two new products designed to help maintain consistent quality in breast screening and help identify women who may be at high risk of developing cancer, here at the European Congress of Radiology (ECR) meeting, February 28 – March 4, 2018. (Expo X1, 121). The company is introducing VolparaEnterprise Live!, a mammography quality control tool that provides the technologist with real-time, quality feedback at the gantry, and VolparaRisk software, which is designed to help identify high risk women based on factors other than family history who might otherwise be overlooked.

Designed to help acquire consistent, high quality mammograms, VolparaEnterprise Live! calculates the patient positioning score, dose, and compression pressure for each image. VolparaEnterprise Live! puts quality data in the technologists' hands before the patient leaves the room. This helps optimize productivity, reduce costs through the reduction of retakes, and increase staff effectiveness.

As the majority of breast cancer patients have no, or minimal, family history of breast cancer, reliance on traditional family history pathways does not capture all high-risk women. VolparaRisk software helps identify those women who may be at increased risk of developing breast cancer, irrespective of family history, and may benefit from a full risk assessment work-up. VolparaRisk software, available on the VolparaEnterprise Breast Imaging metrics platform,

applies data ranking once the Volpara clinical applications process the mammogram. Each mammogram is ranked according to the magnitude of the mammographic density relative to the woman's age and breast size. This helps identify additional women who may benefit from supplemental screening.

VolparaEnterprise software is the only solution currently available that provides comprehensive assessment of image quality on every mammography or tomosynthesis study, including patient positioning and compression, which are widely viewed as the causes of most clinical image deficiencies, and associated with delayed detection of breast cancer. It provides automated ConstantQuality™ performance monitoring through dynamic, interactive dashboards that drive technologist training and quality improvement programs.

Volpara will also showcase its new Volpara®Enterprise™ DDP software. The VolparaEnterprise Clinical Applications software package offers access to VolparaDensity, VolparaDose and VolparaPressure, in a SaaS subscription model for the first time. Volpara Solutions will showcase its entire suite of quantitative breast imaging tools, which allow for personalized measurements of volumetric breast density, patient dose, breast compression and other factors designed to help maintain accuracy and consistent quality in breast screening. VolparaEnterprise Clinical Applications provide quick, automated assessment of every mammography and tomosynthesis exam and produces a Volpara Scorecard for every patient. with the following data:

- VolparaDensity, the most clinically validated 3D Density solution, is in use at sites across the globe helping radiologists assess breast density more objectively and helping them better consider who might benefit from additional screening.
- VolparaDose helps understand the X-ray dose delivered to the patient, based on her specific breast density. VolparaDose is computed based on the patient's breast composition and provides a personalized dose measure because no two women are alike.
- VolparaPressure helps evaluate the effectiveness of the mammogram and to better understand the patient experience. VolparaPressure helps monitor and optimize pressure during mammography exams, which is important to decrease the discomfort experienced by women and to optimize screening outcomes.

Extra patient movement during mammographic imaging : an experimental study

Ma, WK, Brettle, D, Howard, D, Kelly, J, Millington, S and Hogg, P

http://dx.doi.org/10.1259/bjr.20140241

Full paper

Extra Patient Movement During Mammographic Imaging: An Experimental Study

ABSTRACT

Objectives: To determine if movement external to the patient occurring during mammography may be a source of image blur.

Methods: Four mammography machines with seven flexible and nine fixed paddles were evaluated. In the first stage, movement at the paddle was measured mechanically using two calibrated linear potentiometers. A deformable breast phantom was used to mimic a female breast. For each paddle, the movement in millimeters and change in compression force in Newton was recorded at 0.5 and 1 second intervals respectively for 40 seconds with the phantom in an initially compressed state under a load of 80N. In the second stage, clinical audit on 28 females was conducted on one mammography machine with the 18x24cm and 24x29cm flexible paddles.

Results: Movement at the paddle followed an exponential decay with a settling period of approximately 40 seconds. The compression force readings for both fixed and flexible paddles decreased exponentially with time while fixed paddles have a larger drop in compression force than flexible paddles. There is a linear relationship between movement at the paddle and change in compression force.

Conclusions: Movement measured at the paddle during an exposure can be represented by a second order system. The amount of extra-patient movement during the actual exposure can be estimated using the linear relationship between movement at the paddle and the change in compression force.

Advances in knowledge: This research provides a possible explanation to mammography image blurring caused by extra patient movement and proposes a theoretical model to analyze the movement.

Key words: mammography, breast compression, paddle motion, damping, blurring and thixotropic behavior

List of Figure Captions

INTRODUCTION

Since the introduction of full field digital mammography (FFDM), a number of breast imaging centers have identified blurred images through local audit. Individual centers have taken steps to reduce blurring through improving patient positioning, limiting the potential of patient movement and arresting patient respiration for the exposure duration, but blurring persists. Despite many centers anecdotally reporting the persistence of blurred images few reports have been published considering the isolation of the causal factors [1]. Persistent blurring was probably present on conventional film mammography but due to improvements in contrast resolution in FFDM and the ability to magnify images, it may have become more apparent [2,3]. Blurring may obscure significant breast pathology and can necessitate repeat imaging thus increasing the radiation dose received by patients and raising their anxiety. Figure 1 shows a left mediolateral oblique mammography image acquired on a Hologic Selenia Dimensions unit using a 18X24cm paddle. The image required repeating because it was not possible to determine whether pathology was present in the blurred areas. The repeat, sharp image demonstrated the presence of pathological features in this instance.

Figure 1. The image demonstrates significant blurring particularly around the junction of the mid to lower zone.

Despite reports of blurred images in UK National Health Service Breast Screening Programme (NHSBSP) quality assurance forums, there is currently a paucity of literature surrounding this topic and only two publications have been found regarding digital mammography image blurring [4,5]. Hogg et al reported a potential relationship between a perceived increase in blur and the use of FFDM systems and suggested this could be due to paddle motion or tissue relaxation [4]. They further suggested that blur was seen in up to 20% of screening mammograms even if deemed to be of adequate diagnostic quality. Choi et-al reported FFDM patient related motion to occur in only 0.4% of examinations and attributed this to longer exposure times. Motion artifacts were found to occur more commonly on linear grids rather than the crossed air type [5].

A number of hypotheses relating to causal factors for blur include inadequate compression, patient and paddle movement. In a multicentre study on paddle distortion Hauge et al. [6]

noticed that the paddle moved for a significant period of time after compression force had ceased being applied. Research by Kelly et al. [7] suggested that image blurring may be induced by compression paddle movement during the image acquisition process. This led to the hypothesis that during an exposure there is significant movement external to the control of the patient, called extra patient movement. The extra patient movement may be caused by the reduction in the compression force during the exposure, resulting in a change in compressed breast thickness and lead to the movement of the breast tissue. Another possibility is that the breast exhibits thixotropic behavior. This is supported by Geerligs et al. [8] who suggested that the adipose tissue undergoes structural changes when mechanical loading is applied. Therefore traditional strategies to reduce image blur, related to reducing controllable patient movement, called intra patient movement, may be inadequate. In light of that, a multicentre study was conducted to test our hypothesis and to propose a theoretical model to analyze and predict extra patient movement.

METHODS AND MATERIALS

This study was divided into two stages with the aim to determine the expected extra patient movement during exposure. In the first stage, a theoretical model of paddle movement was developed from the breast phantom study. In the second stage, a clinical audit was undertaken to assess compression force reduction in-vivo. The theoretical model developed in the first stage was then applied on the clinical audit data in the second stage to predict the average extra patient movement in the clinical environment.

Stage 1: Breast Phantom Study

Four mammography machines in three hospitals with seven fixed and nine flexible paddles (Table 1), calibrated to give compression force in Newtons (N), were included in this study.

Routine equipment quality assurance (QA) had been performed on the machines and the results complied with manufacturer specifications [9, 10]. Flexible paddles often have a spring-loaded system to allow compression force to be equally shared among the anterior and posterior parts of the paddle for more uniform compression (figure 2). However, the posterior part of many fixed paddles is fixed firmly to the supporting framework, which only allows movement in the anterior part when compressed (figure 3).

Table 1. List of mammography units and paddles used in this study

Hospital	Mammography unit	Paddle size and type	Number of Units Tested
A	Hologic Selenia Dimensions	18x24cm, fixed 18x24cm, flexible 24x29cm, fixed 24x29cm, flexible	2
B	Hologic Selenia Dimensions	18x24cm, fixed 18x24cm, flexible 24x29cm, fixed 24x29cm, flexible	1
C	Hologic Selenia Dimensions	18x24cm, fixed 18x24cm, flexible 24x29cm, fixed 24x29cm, flexible	1

Figure 2. Hologic Selenia 18x24cm flexible paddle

Figure 3. Hologic Selenia 18x24cm fixed paddle

Deformable breast phantom and compression force

A deformable female breast phantom (Trulife, Sheffield, United Kingdom) was used to investigate paddle movement. The phantom had similar compression characteristics to the human female breast, with a pre-compression thickness of 130mm. The phantom breast was encapsulated in a thin layer of latex and attached to a rigid supporting board via a semi-mobile mounting system (figure 4).

Figure 4. Deformable breast phantom mounted to rigid supporting board.

As shown in figure 4, the rigid supporting board was kept firmly against the paddle and detector using a ratchet strap. The ratchet strap prevented the breast slipping out of the paddle and detector region when compression force was applied. The strap therefore acted similarly to a human female leaning against the paddle and detector to prevent breast slippage when compression force was applied.

The semi-mobile mounting system allowed the breast phantom to have minor movement on the rigid supporting board, in a fashion similar to a real breast on the pectoralis major muscles [11]. The latex coating gave a level of rigidity to the phantom breast, similar to skin, which limited lateral and vertical motion. When compressed the breast phantom allowed the paddle to respond in a fashion similar to compressing real breast tissue. This meant that the distal end (chest wall)

of the paddle was slightly elevated when fixed paddles were used; as expected this elevation was more pronounced when flexible paddles were used.

For each paddle, the phantom was compressed to approximately 80N by applying the compression force slowly using the foot pedal initially and then hand winding to fine tune the compression force when the reading approached 80N. The 'machine given' compression force readings were recorded at 1 second intervals for 40 seconds after the compression force applied by the practitioner ceased. The schematic diagram for the experimental configuration is shown in figure 5.

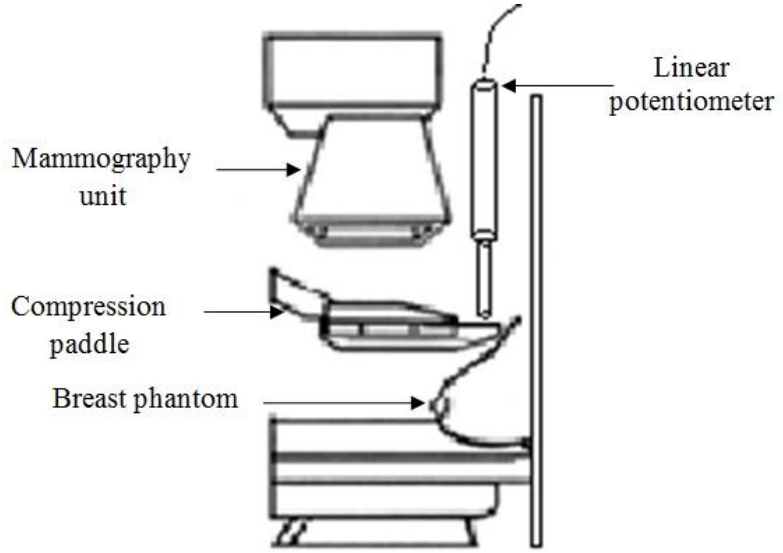

Figure 5. Schematic diagram showing the experimental configuration

Paddle movement

The paddle movement was measured mechanically using two calibrated linear potentiometers (CLS1321) (Indianapolis, USA) with a measurement range of 150mm and a non-linearity of 0.15%. The linear potentiometers were placed at the paddle corners adjacent to the chest wall to

measure movement in the vertical direction. For each paddle, the measurement was repeated three times to minimize experimental uncertainties; six potentiometer readings were therefore taken for each paddle. The rationale for locating the linear potentiometers at the paddle corners, adjacent to the chest wall, is based on the research findings from Hauge et al [6]. Hauge noticed that most of the paddle distortion was found at the chest wall side of the paddle, which suggests that most movement might occur in this region.

Data logging system

Paddle movement in millimeters (mm) was recorded at 0.5 second intervals for 40 seconds by a custom-made data logging system provided by Mass Measuring Ltd (Manchester, United Kingdom). A pilot study identified that movement stabilizes after approximately 30 seconds, on this basis it was decided to record readings for a period of 40 seconds; it was also considered that any clinical exposure will be much shorter than the threshold set so any potential clinical impact should be fully described in this time frame. A 16-bit analog to digital converter (ADC) was used in the data logging system. The data logging system serves three purposes: to calibrate the linear potentiometers before measurements are taken, to create a time log of the linear potentiometer readings, and to export the recorded potentiometer data into excel spread sheet format via a USB port for subsequent analysis.

Error analysis

Measurement Resolution

Because the ADC used in the data logging system is a 16 bit controller and the measurement range of the linear potentiometer is 150mm, the smallest division that can be measured by the linear potentiometer is 0.002mm. The uncertainty is assumed to be uniformly distributed [12].

The standard uncertainty can be found by dividing the half-width (0.001mm) by square root of 3, giving u_r = 0.0007mm.

Non-linearity

The linear potentiometer has a non-linearity of 0.15% (0.23mm). The uncertainty is assumed to be uniformly distributed [12]. The standard uncertainty can be found by dividing the half-width (0.23 mm) by square root of 3, giving u_n = 0.1 mm.

The combined standard uncertainty from all these factors

$u_t = \sqrt{{u_r}^2 + {u_n}^2}$, giving u_t = 0.1mm. For 95% level of confidence, the linear potentiometer standard uncertainty is ±0.2mm.

Data analysis

The potentiometer readings only indicate the relative position of the paddle at a specific time; the actual paddle movement was determined by subtracting the final position of the potentiometer at 40 seconds from the current position at time t_x. It was noticed that, on occasion, paddles tilt during the application of compression force and the paddle movement measured by one potentiometer can be different to the other. The term 'paddle tilt' used in this paper is defined as the inclination of the compression paddle in the frontal plane. To compensate for paddle tilt, the two potentiometer readings were averaged to provide a mean value for the paddle's movement in the vertical direction.

Stage 2: Clinical Audit

A relationship between paddle movement and the change in compression force was derived using the experimental phantom data from stage 1. Practical calibration factors were determined

from the paddle movement - change compression force relationship on a Hologic Selenia Dimensions machine with the 18X24cm and 24X24 flexible paddles. The calibration factors were then applied on the data from the clinical audit[i] in stage 2 to estimate the amount of paddle movement which might be present during the actual exposure of 28 female patients on the same mammography unit. Compression force at the start of each exposure and compression force at the end of each exposure were recorded for each patient.

[i] *Approval was granted by the hospital to carry out this audit.*

RESULTS

Stage 1: Phantom study

Paddle movement

Movement at the paddle for fixed and flexible paddles was plotted against time (figures 6 to 9). As can be seen in figures 6 to 9, the movement decreases exponentially without oscillation and fixed paddles have a shorter average settling time than flexible paddles. The error bars in figures 6 to 9 are the standard uncertainty of the measurement which is calculated in the error analysis section.

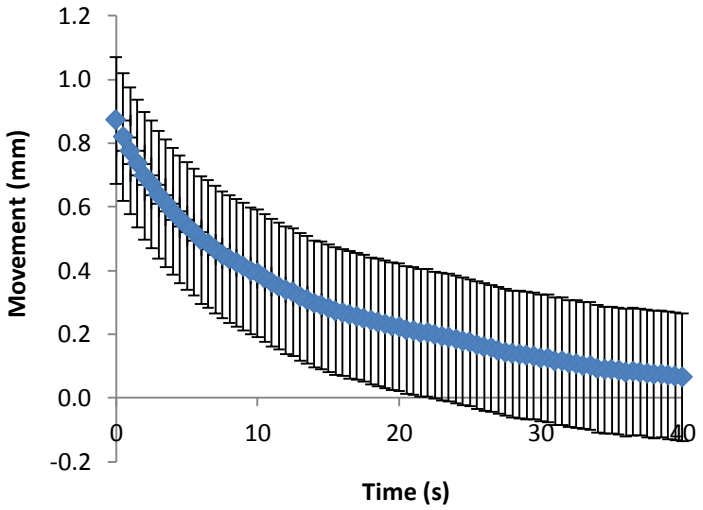

Figure 6. Movement-time curve for 18x24 cm fixed paddles. Error bars show the instrumentation error.

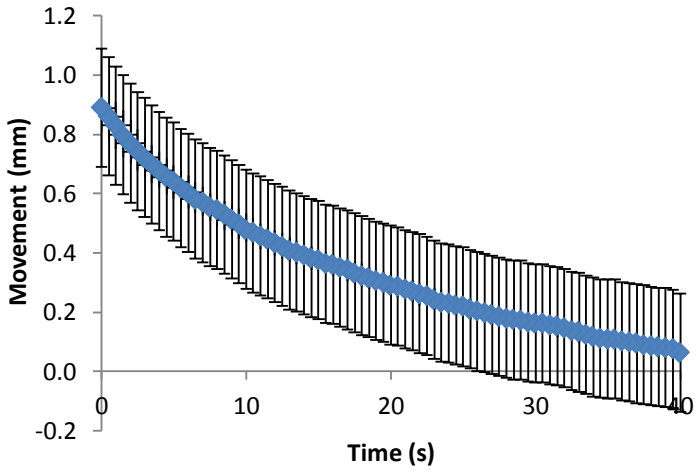

Figure 7. Movement-time curve for 18x24 cm flexible paddles. Error bars show the instrumentation error.

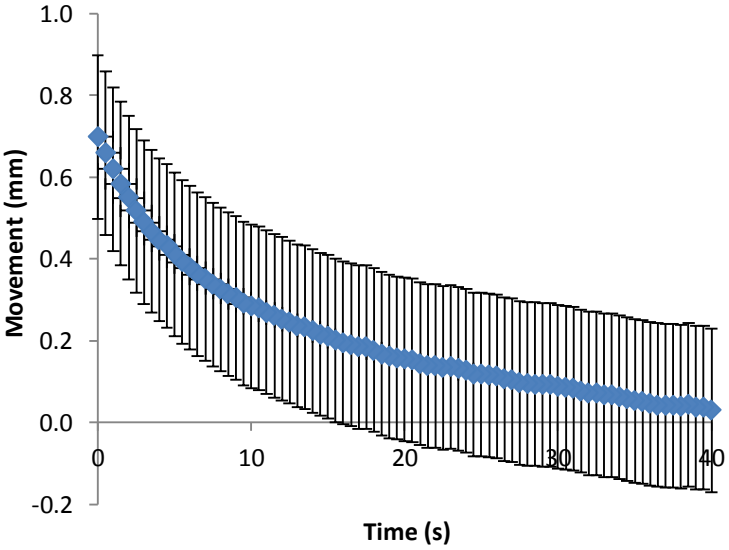

Figure 8. Movement-time curve for 24x29 cm fixed paddles. Error bars show the instrumentation error.

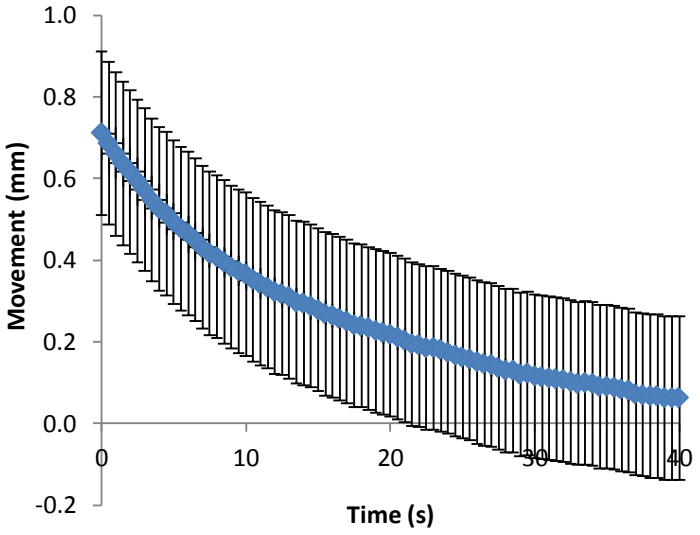

Figure 9. Movement-time curve for 24x29 cm flexible paddles. Error bars show the instrumentation error.

The average paddle movement for 18x24 cm fixed and flexible paddles in the first 10 seconds interval was 0.43mm and 0.38mm respectively which contributed to 59% and 48% of the total movement. The average paddle movement for 24x29cm fixed and flexible paddles in the first 10

seconds interval was 0.38mm and 0.32mm respectively which contributed to 61% and 54% of the total movement (Table 2). As can be seen in table 2 the rate of paddle movement for both fixed and flexible paddles is the highest in the first 10 seconds interval and drops significantly after the first 10 seconds interval.

Table 2: Average paddle movement and the rate of paddle movement over the 40 seconds measuring period mm,(mm/s)

	Time period (s)			
Paddle Type	0.5-10	10.5-20	20.5-30	30.5-40
18X24 cm fixed	0.43 (-0.044)	0.15 (-0.016)	0.09 (-0.010)	0.06 (-0.006)
18X24 cm flexible	0.38 (-0.038)	0.18 (-0.018)	0.13 (-0.013)	0.10 (-0.010)
24X29 cm fixed	0.38 (-0.037)	0.12 (-0.013)	0.06 (-0.007)	0.06 (-0.006)
24X29 cm flexible	0.32 (-0.034)	0.13 (-0.014)	0.09 (-0.010)	0.05 (-0.006)

Table 3 summarizes the maximum, minimum, average and standard deviation of paddle movement (over the settling period of 40 seconds) for the seven fixed and nine flexible paddles. The flexible paddles have slightly larger average movement than the fixed paddles.

Table 3. Summary of paddle movement across time.

Paddle size, paddle type	18x24cm, fixed	18x24cm, flexible	24x29cm, fixed	24x29cm, flexible
Maximum (mm)	1.41	0.96	0.86	0.85
Minimum (mm)	0.01	0.02	0.01	0.02
Average (mm)	0.28	0.34	0.21	0.26
Std Dev (mm)	0.25	0.22	0.18	0.18

The dynamics of mechanical systems and their controls can often be approximated to those of a second order system, for example a spring-mass-damper arrangement. In this case, the settling response of the movement at the paddle suggests second order dynamics that are damped, the standard solution for which is given by [13]:

$$x(t) = C_1 e^{\lambda_1 t} + C_2 e^{\lambda_2 t}$$

λ_1 and λ_2 are empirically identified constants that reflect the physical properties of the paddle and breast. C_1 and C_2 are empirically identified constants that depend on the initial conditions of the system at the start of the movement. The movement equations for fixed and flexible paddles were derived using iterative fitting, minimizing the residual sum of the squares (RSS) using Microsoft Excel (Redmond, Washington, USA). The RSS values for 18x24 cm and 24 x29cm fixed paddles were 0.0338 and 0.025, respectively; and for 18x24 cm and 24 x29cm flexible paddles were 0.0088 and 0.0071, respectively, which indicates only a small discrepancy between the experimental data and the proposed second order model. The general paddle movement equations for the 18x24 cm and 24x29cm fixed paddles are $x(t)_{18x24} = 0.392e^{-0.07t} + 0.392e^{-0.07t}$ and $x(t)_{24x29} = 0.313e^{-0.07t} + 0.313e^{-0.07t}$ respectively. The general paddle movement equations for the 18x24 cm and 24x29cm flexible paddles are $x(t)_{18x24} = 0.431e^{-0.06t} + 0.431e^{-0.06t}$ and $x(t)_{24x29} = 0.340e^{-0.06t} + 0.340e^{-0.06t}$ respectively. The damping ratio, ζ, and natural frequency, ω_n, for fixed paddles are 1 and 0.07 rad s^{-1}, respectively, and for flexible paddles are 1 and 0.06 rad s^{-1}, respectively.

Compression force

The 'machine given' compression force readings for both fixed and flexible paddles decreased exponentially with time (figures 10-13). The average drop in compression force for 18x24cm

fixed and flexible paddles in the first 10 seconds interval was 7N and 3N respectively which contributed to 64% and 75% of the total change in compression force. The average drop in compression force for 24x29cm fixed and flexible paddles in the first 10 seconds was 6 N and 3N respectively which contributed to 67% and 75% of the total change in compression force (Table 4). The rate of change of compression force in the first 10 seconds interval is the highest for both fixed and flexible paddles and drops significantly after the first 10 seconds interval.

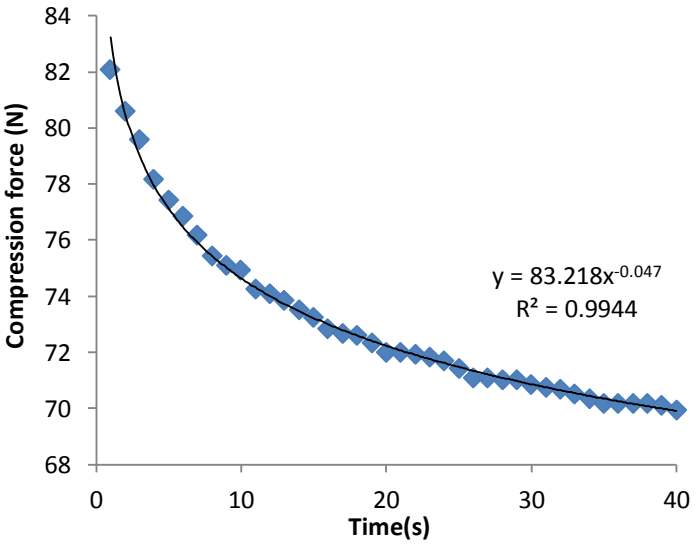

Figure 10: Compression force against time for 18X24 cm fixed paddles

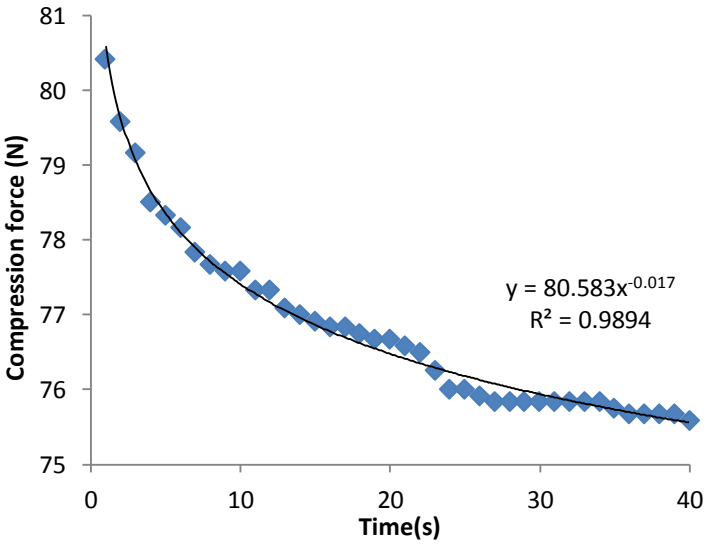

Figure 11: Compression force against time for 18X24 cm flexible paddles

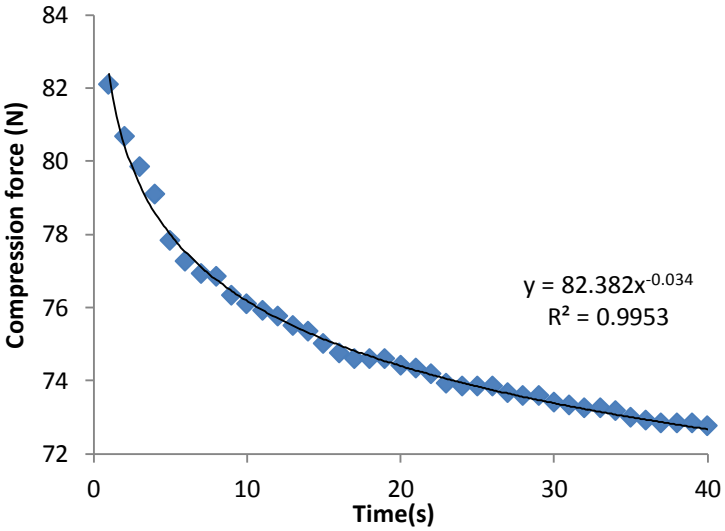

Figure 12: Compression force against time for 24X29cm fixed paddles

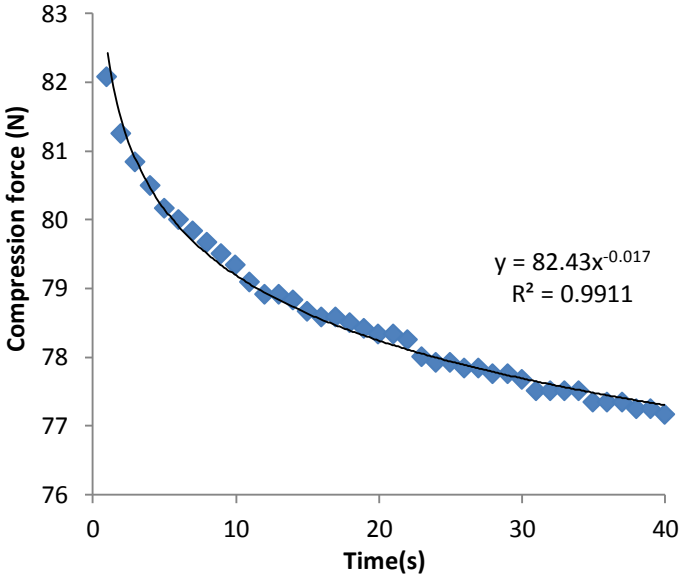

Figure 13: Compression force against time for 24X29cm flexible paddles

Table 4: Average compression force change and the rate of change over the 40 seconds measuring period N,(N/s)

	Time period (s)			
Paddle Type	1-10	11-20	21-30	31-40
18X24 cm fixed	7 (-0.7)	2 (-0.2)	1 (-0.1)	1 (-0.1)
18X24 cm flexible	3 (-0.3)	0 (0)	1 (-0.1)	0 (0)
24X29 cm fixed	6 (-0.6)	2 (-0.2)	1 (-0.1)	0 (0)
24X29 cm flexible	3 (-0.3)	1 (-0.1)	0 (0)	0 (0)

Table 5 summarizes the maximum, minimum, average and standard deviation of average compression force drop for the seven fixed and nine flexible paddles. The fixed paddles have a larger average compression force drop than the flexible paddles.

290 Table 5. Summary of compression force drop across time.

Paddle size, paddle type	18x24cm, fixed	18x24cm, flexible	24x29cm, fixed	24x29cm, flexible
Maximum (N)	18	7	11	7
Minimum (N)	6	3	8	4
Average (N)	12	5	9	5
Std Dev (N)	3.8	1.2	1.2	1.3

Compression force Vs Paddle movement

The change in compression force was determined by subtracting the initial compression force at time zero t_0 from the current compression force at time t_x. As seen in figures 14 and 15, a
295 proportional relationship between movement at the paddle and change in compression force was demonstrated. The calibration factors for the Hologic Selenia Dimensions unit with the 18X24cm and 24x29 cm flexible paddles were 0.1552 and 0.1304 respectively. This relationship between compression force and movement will depend on the elasticity of the breast. Our phantom has only one elasticity, unlike the female breasts which will have a range of elasticities
300 (k). Further work should bear this in mind.

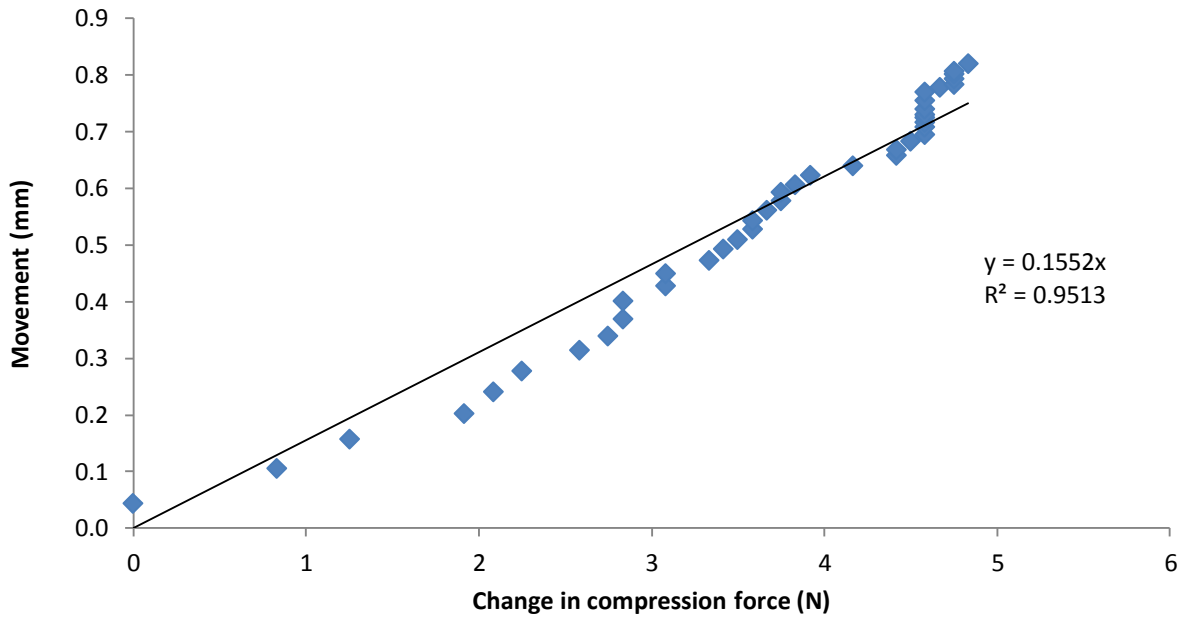

Figure 14. The relationship between paddle movement and change in compression force for 18X24cm flexible paddle.

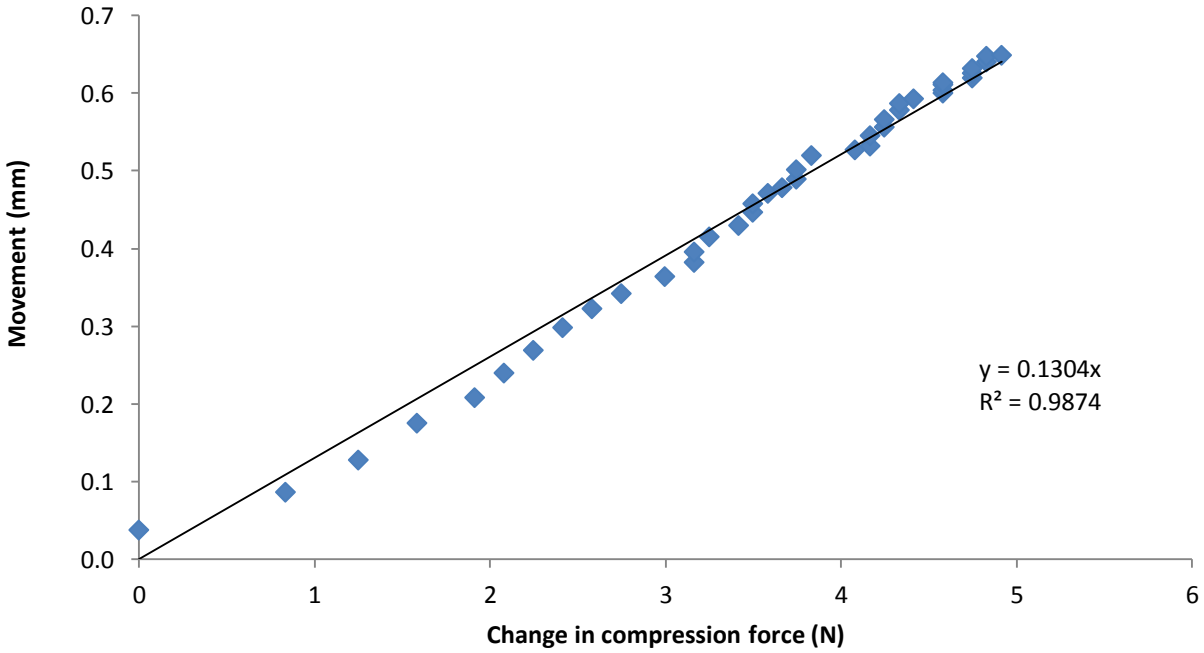

Figure 15. The relationship between paddle movement and change in compression force for 24X29cm flexible paddle.

Stage 2: Clinical Audit

Table 6 summarizes the maximum, minimum, average and standard deviation of change in compression force on the Hologic Selenia Dimensions unit used for the clinical audit using the 18X24cm and 24X29cm flexible paddles. Using the calibration factors derived from our phantom experiment the amount of movement that might be incurred during the exposure from the 28 females was predicted. The average movement for the 18X24cm and 24x29cm flexible paddles is 0.62mm and 0.61mm respectively.

Table 6. Summary of change in compression force at different time intervals

	Change in compression force (N)	
Paddle size (cm)	18x24	24x29
Time interval [ii]	t_1- t_2	t_1- t_2
Max	9	15
Min	1	1
Average	4	4.7
Std Dev	2.70	3.6

[ii] where t_1 – point at which compression force ceases to be applied, and t2 - point at which the exposure terminates

DISCUSSION

Study Limitations

Linear potentiometers

Although there may be a different rate of change between the two measurement points, the difference is not significant. As can be seen in figures 16 and 17 there is only a slight difference between the paddle movement measured by the two potentiometers for fixed (p=0.34) and flexible paddles (p=0.30) this may be due to paddle tilt during the application of compression which made the potentiometers to be at slightly different levels. Since the difference between the movements measured by the two potentiometers is insignificant we average the measurements from the two potentiometers to simply the interpretation and the presentation.

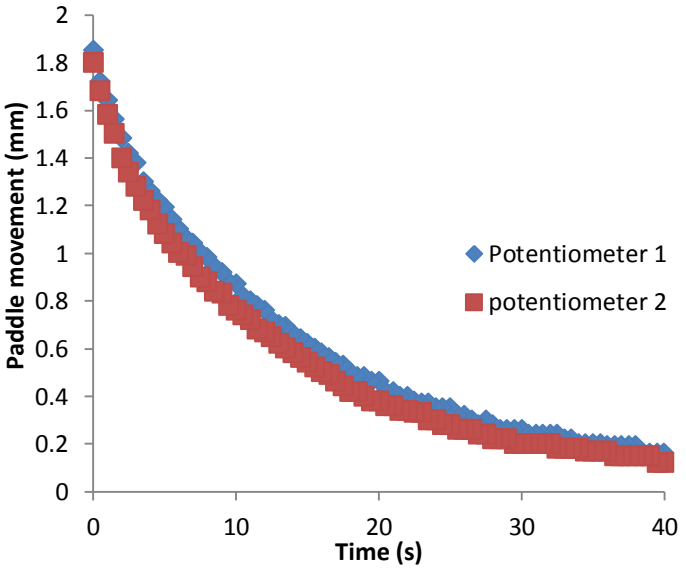

Figure 16.Paddle movement against time for a 18X24 cm fixed paddle

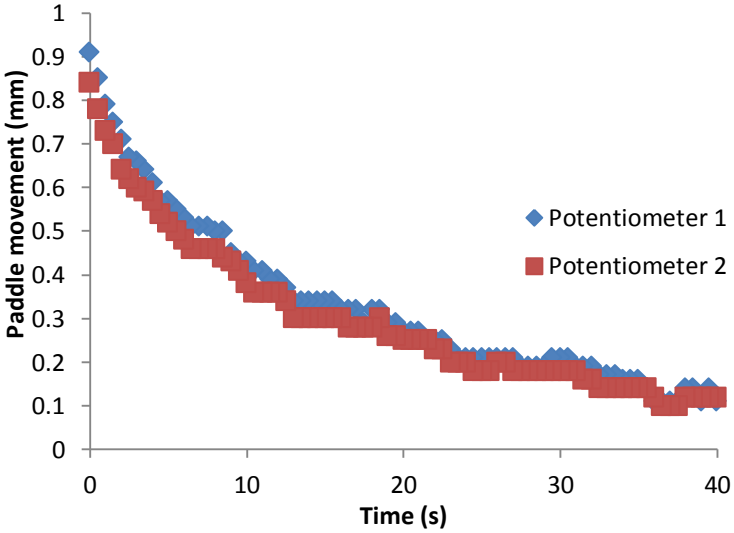

Figure 17.Paddle movement against time for a 18X24 cm flexible paddle

Compression force

As the compression force applied was not a rapid step input, the response of the breast and paddle can begin before the end of the hand winding period (start of measurement). Therefore, the recorded movement at the paddle after measurement begins may lead to an underestimation of the total movement. In extreme cases, if the winding is too slow, there would be no

exponential settling after measurement begins because it would have all happened during the hand winding period. Different design of compression systems among different brands of mammography units may play a significant role in paddle movement. In the human component of our study only Hologic Selenia Dimensions unit was used. Consequently we suggest the study should be repeated using a range of manufacturers to determine whether a similar effect will be seen.

Paddle movement

In this study, we only recorded movement of the paddle; we did not identify exactly where the movement occurred. But from the phantom experiment we have demonstrated there is significant movement that is independent of the patient when a compressible material is used. If the European guidelines are followed and passed there is no systematic issue with movement which indicates the breast response to compression is the dominant factor and should be further investigated [10]. The slightly less movement in the flexible paddles results may be attributed to more lateral retention of the soft tissue compared to fixed paddles; however this has not been verified and could be a focus of future work.

Breast phantom Vs Real breasts

Breasts vary in shape, size and composition. Our experiment only used one phantom and consequentially it did not simulate the range of female breasts. We hypothesize that different phantom designs and female breasts would demonstrate varying characteristics due to varying tissue composition and size. This is supported by the work of Geerligs et al [8] where the

mechanical properties of adipose tissue have been investigated. They reported that adipose tissue was viscoelastic with thixotropic behavior at large strains and anti-thixotropic at small strains. The material is thixotropic if the viscosity decreases with time at constant shear rate and if the viscosity increases with time at constant shear rate the material is anti-thixotropic. In thixotropic behavior structural changes occur due to mechanical loading and the longer the loading the more viscous the material becomes; anti-thixotropic materials increase viscosity over time. Further investigation of the thixotropic behavior of the breast, including glandular tissue, would be valuable in designing novel compression systems.

Perception in blurring

Paddle displacement

According to the European Guidelines for Quality Assurance in Breast Cancer Screening and Diagnosis [10], the acceptable exposure time limit for the standard breast thickness is 2 seconds. Using the general paddle movement equations developed from the breast phantom data, the estimated movement for the 2 seconds limit at the paddle 18 x 24 cm and 24 x 29 cm flexible paddles are 0.8±0.2mm and 0.6±0.2mm respectively. From our clinical audit the predicted movement during the exposure for 18 x 24 cm and 24 x 29 cm flexible paddles are 0.62mm and 0.61mm respectively which is quite close to the estimated value. Logically movement in the breast, along any vector that results in a lateral pixel movement of greater than 1 subtended pixel at the detector has the potential to produce blur. The impact of this will be dependent on the relative exposure time of the displaced pixel and the size of the feature of interest. Therefore considering a 6cm compressed breast with a feature of relevance at the point of greatest geometric magnification (1.1x), i.e. the upper breast, where 1 pixel detector movement is

unacceptable e.g. microcalcifications; a vector spatial movement in the breast of 90% of the detector pixel size could result in image blur. For a 0.1mm detector pixel size a 0.09mm spatial movement could therefore result in blur. This is dependent on the displaced element being exposed long enough to produce an appreciable resultant pixel contrast and therefore rate of change, rather than absolute, movement is the more important metric.

However, presently no published data exists to demonstrate how much movement needs to occur before image degradation (blurring) will be perceived and further research is needed. With this in mind we have already commenced two projects; one using a mathematical approach to generate images which have known amounts of simulated movement; the other was published using experimental approach to identify the image blurring due to paddle movement [14]

Key to reduce blurring

For both fixed and flexible paddles the rate of change of compression force (N/s) and rate of paddle movement, ie paddle velocity (mm/s), is the highest in the first 10 seconds. The rapid change in paddle movement is probably caused by the rapid change in compression force. One of the possible explanations could be the high rate of change of compression force (decreasing) causing the rapid drop in force acting on the paddle. The decrease in force would cause the reduction in the rate of change of the paddle movement, in other words deceleration in paddle velocity.

Motion blurring is caused by the rate of paddle movement during exposure, which is caused by the changing compression force. Since the changing compression force is the important factor for motion blurring, minimizing the rate of change of compression force is the key to reduce blurring.

Applications

Delayed exposure

It is known that larger breasts require longer exposures; therefore to minimize any impact of the extra patient movement the radiographer/technologist could apply compression force more slowly. If the risk of blur is strongly suspected, or a repeat due to blur is required, a wait of 15 seconds from the point at which compression force ceases to be applied, to the point at which the exposure is made, would allow the rate of change of the movement to reach a minimum.

Fixed paddle Vs Flexible paddles

Data from the phantom experiment shows that compared with flexible paddles, fixed paddles have a shorter settling time. This may be due to the higher decreasing rate of change of compression force or 'negative jerk' in fixed paddles ie the smaller the compression force on the phantom the shorter the time taken for the paddle to settle. Therefore to reduce the risk of blur it may be advantageous for the radiographer/technologist to use fixed paddles if possible.

System optimization

The settling time to reduce extra patient movement should ideally be as short as possible in order to reduce the possibility of inducing intra patient movement induced artifacts. In view of that, manufacturers should conduct further experiments and, if required, introduce design features that lead to shorter settling times. It might also be possible for manufacturers to include a feedback system between rate of change of compression and beginning the exposure or if thixotropic processes dominate consider how the compressive force is applied.

CONCLUSIONS

Using a breast phantom we have shown that there is extra patient movement at the compression paddle during mammographic exposures that can be approximated by a second order motion equation. In vivo movement with real patients has also been proposed to be proportional to the drop in compression force, using this derived relationship the actual motion can be estimated.

Conflict of interest statement

The authors have no conflict of interest.

ACKNOWLEDGMENTS

The authors would like to thank Mass Measuring Ltd for developing the data logging system used in this study and financial support from the Trustees of Symposium Mammographicum.

References

1. Hogg P, Kelly J, Millington S, Willcock C, McGeever G, Tinston S, et al. Paddle motion analysis: 2012. East of England Conference; 2012 December; Cambridge, UK: National Health Service Breast Screening Programme, 2012.

2. Bushberg JT, Seibert JA, Leidholdt EM, Boone JM. The Essential Physics of Medical Imaging. 3rd ed. New York: Williams & Wilkins; 2011.

3. Fischmann A, Siegmann KC, Wersebe A, Claussen CD, Müller-Schimpfle M. Comparison of full-field digital mammography and film-screen mammography: image quality and lesion detection. Br J Radiol 2005; 78: 312-315.

4. Hogg P, Szczepura K, Kelly J, Taylor J. Blurred digital mammography images. Radiography 2012; 18(1):55-56.

5. Choi JJ, Kim SH, Kang BJ, Choi BG, Song B, Jung Mammographic Artifacts on Full-Field Digital Mammography. J Digit Imaging. 2014 Apr;27(2):231-6.

6. Hauge I, Hogg P, Szczepura K, Connolly P, McGill G, and Mercer C. The readout thickness versus the measured thickness for a range of screen film mammography and full field digital mammography units, Med Phys 2012; 39(1):263–271.

7. Kelly J, Hogg P, Millington S, Sanderud A, Willcock C, McGeever G et al. Paddle Motion Analysis Preliminary Research: 2012. United Kingdom Radiological Congress; 2012 June 25-27; Manchester, UK: British Institute of Radiology, 2012.

8. Geerligs M, Peters G.W.M, Ackermans P.A.J, Oomens C.W.J, Baaijens F.P.T. Does subcutaneous adipose tissue behave as an (anti-)thixotropic material?. J Biomech 2010; 43, 1153-1159.

9. Moore A C, Dance D R, Evans D S, Lawinski C P, Pitcher E M, Rust A, et al. The Commissioning and Routine Testing of Mammographic X-Ray Systems: A Technical Quality Control Protocol. Report No. 89 York, UK: IPEM, 2005.

10. Perry N, Broeders M, Wolf C, Törnberg S, Holland R, Karsa L, et al. European guidelines for quality assurance in breast cancer screening and diagnosis. 4th ed. Luxembourg: European Communities, 2006.

11. Seeley R, Stephens T, Tate P. Anatomy and Physiology. 8th ed. New York, US: McGraw-Hill Science, 2007.

12. Bell S. Measurement Good Practice Guide No. 11: A Beginner's Guide to Uncertainty of Measurement. Issue 2. Middlesex, UK: National Physics Laboratory, 1999.

13. Zill G, Wright S. Advanced Engineering Mathematics. 5th ed. Boston, US: Jones & Bartlett Learning, 2012.

14. Ma WK, Hogg P, Kelly J, Millington S. A method to investigate image blurring due to mammography machine compression paddle movement. Radiography 2014; In Press.

Analysis of motion during the breast clamping phase of mammography

Ma, W, McEntee, M, Kelly, J, Millington, S, Mercer, CE and Hogg, P

http://dx.doi.org/10.1259/bjr.20150715

Full paper

Analysis of motion during the breast clamping phase of mammography

AUTHORS AND AFFIFIATIONS:

Wang Kei Ma
Directorate of Radiography, University of Salford, Salford, M6 6PU, United Kingdom

Mark F. McEntee
C43M, M Block Cumberland Campus, University of Sydney, Australia

Peter Hogg and Claire Mercer
Directorate of Radiography, University of Salford, Salford, M6 6PU, United Kingdom

Judith Kelly and Sara Millington
Department of Radiography, Countess of Chester Hospital, Chester, CH2 1UL, United Kingdom

Key words: compression, simulation, paddle motion

Full paper

Analysis of motion during the breast clamping phase of mammography

ABSTRACT

Objectives: To measure paddle motion during the clamping phase of a breast phantom for a range of machine/paddle combinations.

Methods: A deformable breast phantom was used to simulate a female breast. Twelve mammography machines from three manufacturers with twenty two flexible and twenty fixed paddles were evaluated. Vertical motion at the paddle was measured using two calibrated linear potentiometers. For each paddle, the motion in millimeters was recorded every 0.5 seconds for 40 seconds while the phantom was compressed with 80 N. Independent t-tests were used to determine differences in paddle motion between flexible and fixed, small and large, GE Senographe Essential and Hologic Selenia Dimensions paddles. Paddle tilt in the medial-lateral plane for each machine/paddle combination was calculated.

Results: All machine/paddle combinations demonstrate highest levels of motion during the first 10s of the clamping phase. Least motion is 0.17±0.05 mm/10s (n=20) and the most is 0.51±0.15 mm/10s (n=80). There is a statistical difference in paddle motion between fixed and flexible ($p<0.001$), GE Senographe Essential and Hologic Selenia Dimensions paddles ($p<0.001$). Paddle tilt in the medial-lateral plane is independent of time and varied from 0.04° to 0.69°.

Conclusions: All machine/paddle combinations exhibited motion and tilting and the extent varied with machine and paddle sizes and types.

Advances in knowledge: This research suggests that image blurring will likely be clinically insignificant 4 seconds or more after the clamping phase commences.

Key words: compression, simulation, paddle motion

Introduction:

Breast cancer is the most common cancer among females and the second most common cause of cancer death in the United Kingdom (UK) [1]. Mammographic screening is the key to early detection of breast cancer. In a randomized control trial of 282,777 women in Sweden there was a 24% reduction of breast cancer mortality compared to women without screening [2]. Screening can identify ductal carcinoma in situ (DCIS) which may never cause symptoms or death in a woman's lifetime. A study by Bleyer and Gilbert [3] estimated that 31% of breast cancers detected by screening in the United States are considered to be over diagnosis and according to the study by Biesheuvel et al [4] the over diagnosis rate can be as high as 54% for women aged between 50 and 59 years. Although over diagnosis might occur the benefit of screening is generally considered to outweigh the harm of over diagnosis. An independent review carried out by Marmot et al. [5] estimated that for 10,000 women aged 50 years who are invited to screening in the next 20 years, 129 would have been over diagnosed while 43 deaths from breast cancer would have been prevented. This suggests that one breast cancer death is prevented for every three over diagnosed cases.

Early detection of breast cancer relies on good image quality but factors such as image blurring, inadequate compression, incorrect exposure and skin folds can degrade image quality [6]. Repeat imaging for technical reasons such as these will increase radiation dose and possibly increase client anxiety [7].

Research studies to specifically evaluate image blurring rates within mammography services are limited. Within the UK screening service, the overall technical recall and repeat rates for each service should be below 3% with a target of 2% [8]. One study reviewed a units' recall and repeat rates and reported 0.86% of women were recalled due to image blur, constituting almost one third (29%) of the 3% maximum permissible rate for repeats [9]. A second study within the same unit reported over half of all their total clients recalled due to blurring with 1/20th repeated due to blurring [10]. A study within another unit reported that over 90% of their total technical recalls were due to blurred images [11]. Despite much anecdote within the UK National Health Breast Screening Programme, and others, about image blurring and the need for repeat imaging because of blurring this technical problem continues to be under-reported within the literature.

Groot et al. suggested that breast compression consists of a deformation phase for flattening and a clamping phase for immobilisation [12]. During the deformation phase, the breast is gradually flattened by the compression paddle by increasing the compression force. The clamping phase starts when the maximum compression force is reached. The deformation and clamping phases last approximately 7.5 and 12.8s respectively [12]. Groot et al. [12] in their study, which involved 117 women, observed that during the clamping phase, the compression force continues to change for a short period and it decreases substantially in the first few seconds after the clamping phase commences. This suggests paddle movement is likely to be occurring during mammography because of this change in compression force.

Ma et al. [13] proposed that paddle motion could be one source of image blurring. They found that the extent of paddle motion during a mammography exposure could be as much as 1.5 mm in the vertical plane. One of the limitations of the study by Ma et al. is that they only assessed mammography machines from one manufacturer, so their finding may be limited to the Hologic

Selenia Dimensions. Our current study extends the work of Ma et al. [13] to examine paddle motion during the clamping phase of a deformable breast phantom for a wider range of machine/paddle combinations.

Method:

The present study used the same approach as that described by Ma et al. [13]. A deformable breast phantom, made of silicone (medium 360 cm^3, Bodicool Triangle, Trulife, Sheffield, United Kingdom) was mounted on a wooden board to simulate the chest wall. A line was marked onto the centre of the phantom to ensure it was aligned to the centre of the paddle prior to applying compression. For each combination of FFDM machines and paddles the phantom was compressed to 80 N. In previous work [14] we found that the phantom integrity would be preserved only if the compression force does not exceed 100N. 80N was selected to preserve phantom integrity and it is within the range of compression forces used by mammography practitioners [15, 16, 17].

Motion at the paddle in the vertical plane was measured mechanically by two calibrated linear potentiometers (CLS1321) (Indianapolis, USA), placed at the corners of the compression paddle near the phantom chest wall (figures 1 and 2). For each paddle the measurement was repeated three times and averaged to minimise random error; the same team performed the experiment on all the paddle/machine combinations to ensure consistency in setup and measurements. Previous research into paddle motion [13] demonstrated that the time required for the paddle motion to stabilise was approximately 30 seconds; therefore data were recorded for a period of 40 s at 0.5 s intervals.

Vertical paddle motion for 10 seconds time periods after the clamping phase commenced was calculated. The first 10 seconds after the clamping phase commenced was chosen for comparing machines and paddles. The rationale of choosing this time period is that the average exposure time and clamping phases lasts 1 and 12.8 s respectively [12] therefore 11.8 seconds after the clamp started is the average time-window during which blurring is likely. Vertical paddle motion at 2, 4, 8, 16 and 32 seconds after commencement of the clamping phase was also calculated to demonstrate how paddle instantaneous motion (the tangent slope to the potentiometer-recordings) varies with time.

Paddle tilt across the medial-lateral plane for each combination of FFDM machines and paddles was calculated using trigonometric function by considering the difference between the two potentiometer readings (tilt level) and the paddle width.

Twelve FFDM machines from three manufactures (Hologic, General Electric and Siemens) which met QA testing specifications [18] were used, and a range of paddle sizes were used: 18x24 cm, 24x29 cm and 24x30 cm. This resulted in 42 FFDM machine / paddle combinations, with 22 flexible and 20 fixed paddles (table 1). Since the 24x29 cm and 24x30 cm paddles are very similar in size, for practical purposes the 24x29 cm and 24x30 cm paddles are combined into “large” paddle group, while the 18x24 cm paddles are combined into “small” paddle group. Three independent t-tests were conducted to determine whether there is a significant difference in paddle motion between fixed and flexible paddles, small and large paddles, GE Senographe Essential and Hologic Selenia Dimensions paddles. The reason Hologic Lorad Selenia and Siemens Mammomat Inspiration paddles were not included in the t-test is because the sample size for the Hologic Lorad Selenia and Siemens Mammomat Inspiration paddles are too small, compared with GE Senographe Essential and Hologic Selenia Dimensions paddles (see table1).

The statistical comparison was performed in the first 10 seconds of the clamping phase rather than on the entire dataset (0-40 seconds) because the first 10 seconds is the time period of interest where the probability of blurring is highest.

Results:

Vertical paddle motion for 18x24 cm (small), 24x29 cm and 24x30 cm (large) during the first, second, third and fourth ten second time periods are shown in tables 2 and 3, respectively. As can be seen all machine/paddle combinations have the greatest motion in the first 10 seconds of clamping phase commencement with a trend of decreasing motion towards 40 seconds. Vertical paddle motion for 18x24 cm (small), 24x29 cm and 24x30 cm (large) at 2, 4, 8, 16 and 32 seconds after clamping commencement are shown in tables 4 and 5. For small and large paddles, the vertical paddle motion has the highest value in the first 2s of clamping and it decreases gradually 4s after clamping phase commencement.

For small paddles, the GE Senographe Essential flexible paddle has the lowest mean motion (0.21±0.06 mm/10s, n=120) in the first 10 seconds after clamping commencement while the Hologic Selenia Dimensions fixed paddle has the largest mean motion (0.51±0.15 mm/10s, n=80) (table 2). For large paddles, the Hologic Lorad Selenia flexible paddle has the lowest mean motion (0.17±0.05 mm/10s, n=20) in the first 10 seconds after clamping commencement while the Hologic Selenia Dimensions fixed paddle has the largest mean motion (0.42±0.13, mm/10s, n=80) (table 3).

There is a statistical difference in paddle motion between fixed ($\bar{x}$=0.24, SD= 0.15, n=400) and flexible paddles ($\bar{x}$=0.20, SD= 0.10, n=440); t (838) =5.11, p<0.001, GE Senographe Essential ($\bar{x}$=0.19, SD= 0.11, n=420) and Hologic Selenia Dimensions paddles ($\bar{x}$=0.26, SD= 0.15, n=320); t (738) =8.15, p<0.001. However, there is no statistical difference in paddle motion between small ($\bar{x}$=0.21, SD= 0.14, n=460) and large paddles ($\bar{x}$=0.22, SD= 0.12, n=380); t (838) =0.865, p=0.387.

The mean paddle tilt in the medial-lateral plane for small (18x24 cm) and large (24x29 cm and 24x30 cm) paddles is shown in figures 3 and 4. As can be seen, all machine/paddle combinations demonstrate tilt is independent of time. The 18x24 cm Hologic Lorad Selenia flexible paddle has the smallest tilt (0.04°) (figure 3), while the 24x30 cm Siemens Mammomat Inspiration flexible paddle has the largest tilt (0.69°) (figure 4).

Discussion:

Research into the perception of motion in FFDM images, using computer-based simulation to mimic blurring, demonstrated that simulated motion as low as 0.4 mm in the horizontal plane can be detected visually [19]. Further work is needed to determine what relationship exists between vertical motion and reactionary horizontal displacement in female breast tissue. Studies show that harmonious breast height (H) to width (W) ratio (H/W) should be between 0.7 and 1.3 [20]. Given the female breast deforms rather than squashes when compressed the vertical thickness

reduction will result in horizontal breast tissue displacement and the ratio could therefore vary between 0.7 and 1.3.

All paddles demonstrated motion. Most of this motion occurred in the first 10 seconds of clamping. According to the study by Groot et al. [12], the average exposure time and clamping phases last 1 and 12.8s respectively. If the exposure is made when the paddle is moving then image blurring could occur. Although paddle motion decreases with time, it would be impractical to wait tens of seconds before making the exposure for reasons such as patient movement and discomfort [21, 22].

Our research, suggests the Hologic Selenia Dimensions with 18x24 cm fixed paddle (0.51±0.15 mm/10s, n=80) has the highest potential to create blurring during imaging, while the Hologic Lorad Selenia with 24x29cm flexible paddle (0.17±0.05 mm/10s, n=20) has the lowest potential.

One of the practical solutions to minimise the probability of image blurring is to use the fixed paddle with caution, as our findings show there is a significant difference ($p<0.001$) in motion for fixed and flexible paddles. Fixed paddles have slightly higher motion ($\bar{x}=0.24$, SD= 0.15, n=400) compared with flexible paddles ($\bar{x}=0.20$, SD= 0.10, n=440), suggesting that the fixed paddles might incur more motion artifacts. Extra caution could therefore be exercised by radiographers when positioning patients using fixed paddles because of this. An additional preventative measure could include waiting an additional few seconds prior to making an exposure thereby allowing any paddle motion to have ceased by the time the exposure commences. Tables 4 and 5 suggest that motion will be clinically insignificant or not visually apparent, 4 seconds or more after the clamping phase commences as all motion values are likely to below 0.4mm for typical exposure times [19]. However, caution should be exercised as this

prediction is based upon a data generated from a phantom breast and motion in the vertical plane from Ma et al's work [19]. Further research is therefore needed using human female breast alongside measures of horizontal displacement.

The presence of tilting in the medial-lateral plane among paddles suggests that the compression force applied on the paddle may not be evenly distributed which could mean one side of the breast may be compressed more compared with the other side. A limitation of this study is the breast phantom used cannot fully represent the compression characteristics of the female breast. Our silicone breast phantom exhibits a purely elastic compression characteristic, whereas the female breast exhibits a visco-elastic compression characteristic [23]. If the compression speed is too fast for the viscous effect to occur during the deformation phase, the paddle motion measured in the clamping phase would be influenced by the female breast's viscosity. Consequently the female breast is likely to continue to flatten during the clamping phase, while the purely elastic phantom may not. Therefore, phantom measurements would give an underestimation of paddle and therefore breast motion if the compression speed is fast.

In this study we only sampled two points on the paddle surface to measure the paddle motion, as at the time of conducting the study, limited affordable technology existed to map the entire surface. This has now changed – for example technology like Kinect (Microsoft, Washington, USA) would allow monitoring of the whole paddle surface over time which would allow for assessment of regional differences in motion across the paddle surface [24].

The clinical impact of mammography image blurring needs further investigation. For instance, an analysis of lesion detection performance using free response operating characteristic with blurred and non blurred images would give an indication as to whether cancer / non-cancer

localisation and observer confidence in decision making would be impaired during blurred image conditions.

Presently, compression paddle QA guidelines (e.g. European Guidelines for Quality Assurance in Breast Cancer Screening and Diagnosis [25]) only indicate a compression force test and compression plate alignment. There is no manufacturer guidance or QA standards regarding assessment of paddle motion, particularly using a deformable object / phantom in an attempt to mimic clinical demands. Our work suggests that new QA tests / guidelines be developed to assess paddle motion using a suitable deformable object prior to a paddle being used in practice.

Conclusions:

All machine / paddle combinations exhibited motion and tilt and the extent varies with machine, paddle sizes and paddle types. Most motion occurred within the first 10 seconds of clamping and after 4 seconds paddle motion will likely be clinically insignificant. Paddle tilt in the medial-lateral plane is independent of time under compression. Our findings may have implications for practice, including the need for a new QA motion test and the need for radiographers to possibly take additional precautions when using fixed paddles in order to minimise the potential of paddle motion and image blurring.

Conflict of interest statement:

The authors have no conflict of interest.

References:

1. Cancer Statistics Registrations, England (Series MB1) No. 43; UK Statistics Authority; 2012

2. Nyström L et al. Breast cancer screening with mammography: overview of Swedish randomised trials. Lancet1993; 341(8851):973-8. DOI: 10.1016/0140-6736(93)91067-V

3. Bleyer A , Welch H G. Effect of three decades of screening mammography on breast-cancer incidence. N Engl J Med 2012; 367:1998-2005.DOI: 10.1056/NEJMoa1206809

4. Biesheuvel C, Barratt A, Howard K, Houssami N, Irwig L. Effects of study methods and biases on estimates of invasive breast cancer overdetection with mammography screening: a systematic review. Lancet Oncol 2007;8:1129-38

5. Marmot MG, Altman DG, Cameron DA, Dewar JA, Thompson SG, Wilcox M. The benefits and harms of breast cancer screening: an independent review. Lancet 2012; 380(9855):1778–1786. DOI: 10.1016/S0140-6736(12)61611-0

6. Guidelines for quality assurance in mammography screening. 3rd ed. Dublin, Ireland: The National Cancer Screening Service Board, 2008.

7. Hogg P, Kelly J, Claire E, eds. Digital mammography: a holistic approach. 1st ed. London, UK: Springer; 2015.

8. NHS Cancer Screening Programmes. Consolidated guidance on standards for the NHS Breast Screening Programme. NHSBSP Publication No 60 (Version 2), UK: Sheffield, 2005.

9. Julie R, Claire E, Laura S. Programme evaluation: Technical recall and image blur within a breast screening service. Symposium Mammographicum 2014, UK: Bournemouth, 2014.

10. Kinnear L, Mercer C. The detection of visual blurring in 1MP and 5MP monitors within mammography clinical practice. Imaging and therapy Practice, IN PRESS

11. Seddon D, Schofield K A, Waite C A. Investigation into possible caused of blurring in mammograms. Breast Cancer Res. 2000; 2(suppl2): A64. DOI: 10.1186/bcr253

12. Groot J E de, Broeders M J M, Grimbergen CA, Heeten G J den. Pain-preventing strategies in mammography: an observational study of simultaneously recorded pain and breast mechanics throughout the entire breast compression cycle. BMC Women's Health 2015; 15:26. DOI:10.1186/s12905-015-0185-2

13. Ma WK, Brettle D, Howard D, Kelly J, Millington S, Hogg P. Extra Patient Movement During Mammographic Imaging: An Experimental Study. Br J Radiol 2014; 87: 20140241. doi: 10.1259/bjr.20140241

14. Hauge I, Hogg P, Szczepura K, Connolly P, McGill G, Mercer C. The readout thickness versus the measured thickness for a range of screen film mammography and full field digital mammography units, Med Phys 2012; 39(1):263–271.

15 Mercer C, Szczepura K, Kelly J, Millington S, Denton E, Borgend R et al. A 6-year study of mammographic compression force: Practitioner variability within and between screening sites. Radiography 2014; 21 (1):68 – 73. DOI: 10.1016/j.radi.2014.07.004

16. Hogg P, Taylor M, Szczepura K, Mercer CE, Denton E. Pressure and breast thickness in mammography—an exploratory calibration study. Br J Radiol 2013; 86:20120222. DOI: 10.1259/bjr.20120222

17. Mercer C, Hogg P, Lawson R, Diffey J, Denton ERE. Practitioner compression force variability in mammography: a preliminary study. Br J Radiol 2013; 86:20110596. DOI: 10.1259/bjr.20110596

18. Moore A C, Dance D R, Evans D S, Lawinski C P, Pitcher E M, Rust A, et al. The Commissioning and Routine Testing of Mammographic X-Ray Systems: A Technical Quality Control Protocol. Report No. 89 York, UK: IPEM, 2005.

19. Ma WK, Aspin R, Kelly J, S. Millington, Hogg P. What is the minimum amount of simulated breast movement required for visual detection of blurring? An exploratory investigation. Br J Radiol 2015; 88: 20150126. DOI: 10.1259/bjr.20150126

20. Shiffman A, eds. Breast Augmentation: Principles and Practice 1st ed., London, UK: Springer; 2009

21. Poulos A, Rickard M, Compression in mammography and the perception of discomfort, Australian Radiol., 1997, 41(3): 247-52.

22. Sapir R, Patlas M, Strano SD, Hadas-Halpern I, Cherny NI. Does mammography hurt?, J Pain Symptom Manage, 2003 25(1): 53-63.

23. Geerligs M, Peters G.W.M, Ackermans P.A.J, Oomens C.W.J, Baaijens F.P.T. Does subcutaneous adipose tissue behave as an (anti-)thixotropic material?. J Biomech 2010; 43, 1153-1159.

24. Pohlmann ST L, Hewes J, Williamson A I, Sergeant J C, Hufton A, Gandhi A et al. Breast Volume Measurement Using a Games Console Input Device, Breast Imaging: Lecture notes in Computer Science 8539: International Workshop on Breast Imaging; Gifu, Japan. Switzerland: Springer International, 2014: 666-673.

25. Perry N, Broeders M, Wolf C, Törnberg S, Holland R, Karsa L. European guidelines for quality assurance in breast cancer screening and diagnosis. 4th ed. Luxembourg: European Communities, 2006.

List of Figure Captions

Figure 1: The two calibrated linear potentiometers (indicated by two arrows) were located near the phantom chest wall.

Figure 2: Schematic diagram showing the location of the linear potentiometers

Figure 3: Paddle tilt against time for small paddles (18x24 cm)

Figure 4: Paddle tilt against time for large paddles (24x29 cm and 24x30 cm)

Figure 1

Click here to download Figure Figure 1 revised.jpg

Figure 2

Click here to download Figure Figure 2 revised.jpg

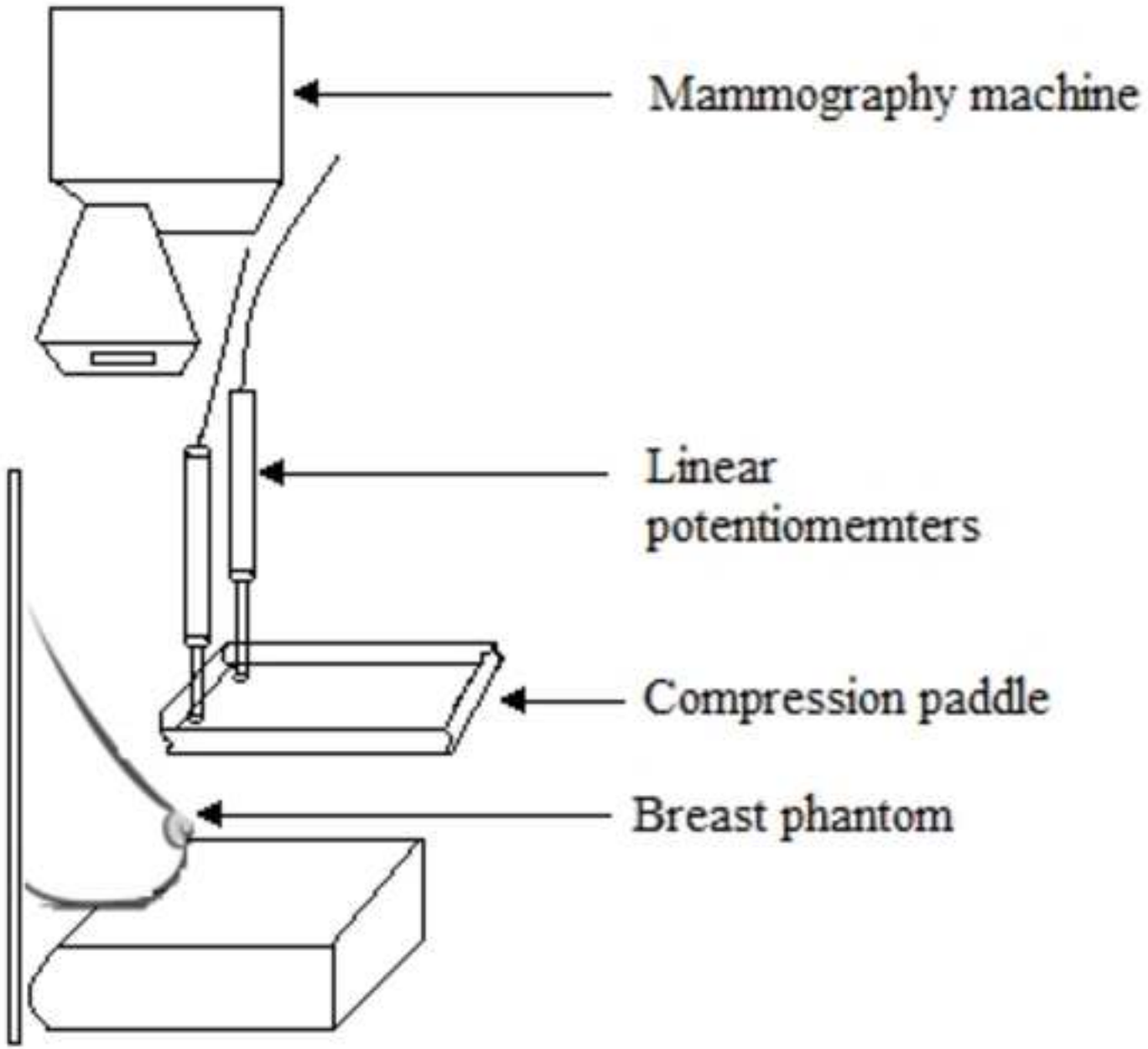

Figure 3

Click here to download Figure Figure 3 revised.jpg

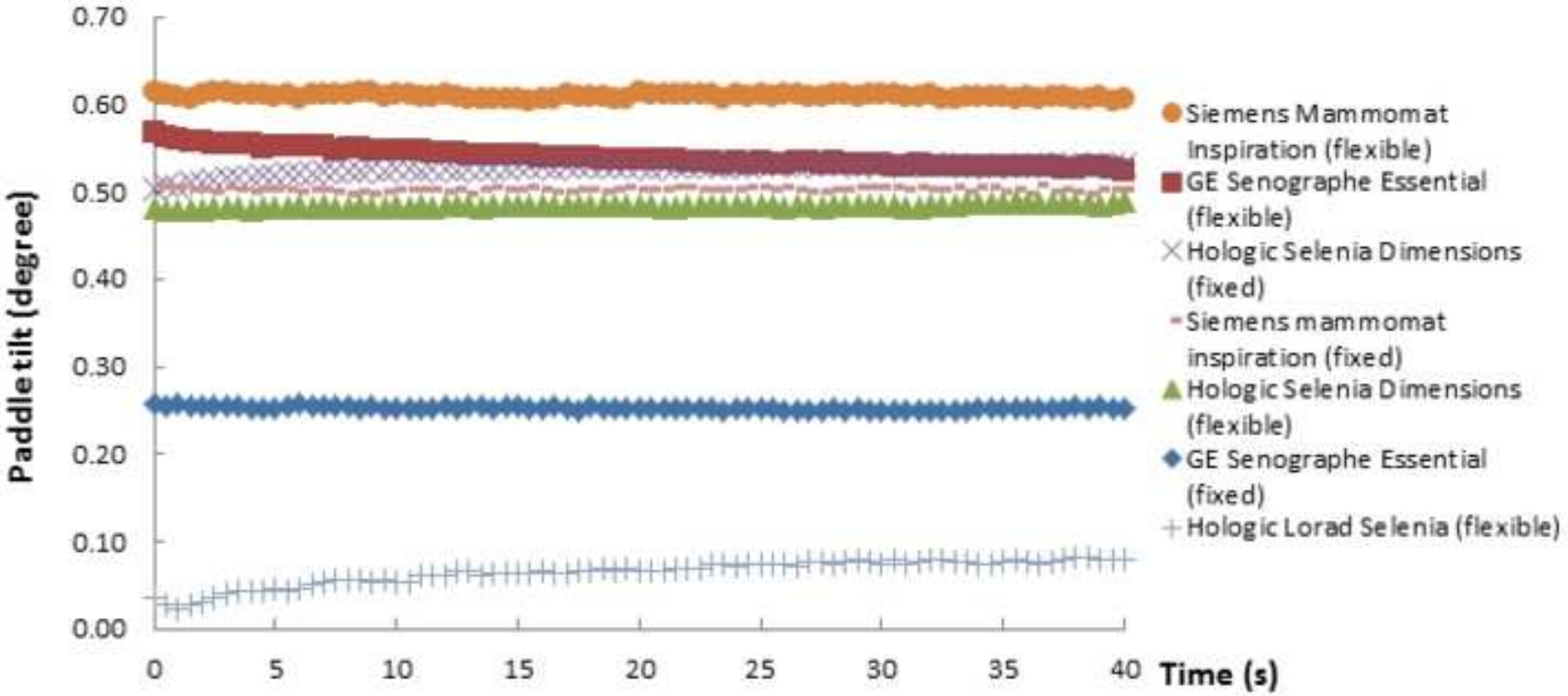

Figure 4

Click here to download Figure Figure 4 revised.jpg

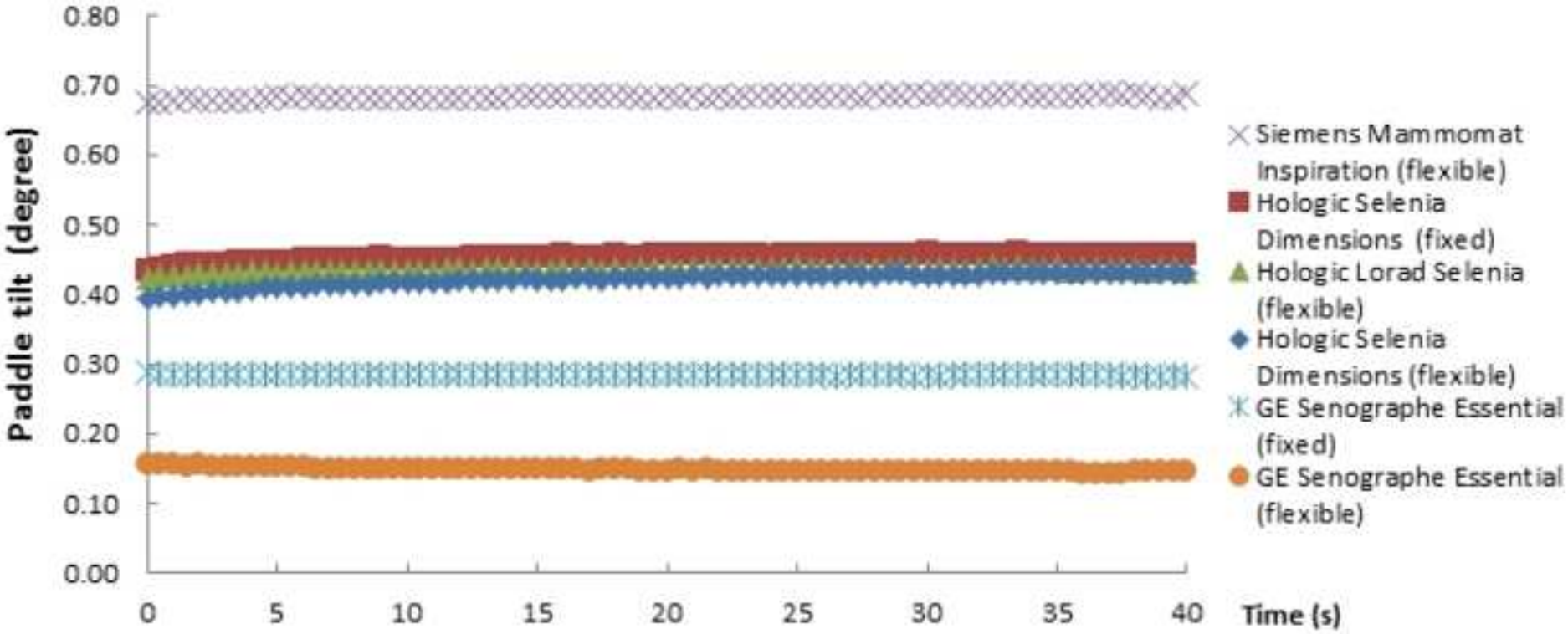

Table1: Mammography machines and paddles used in this study

Mammography machine	**Flexible paddle (small)**	**Fixed paddle (small)**	**Flexible paddle (large)**	**Fixed paddle (large)**	**Total**
GE Senographe Essential	6	6	4	5	21
Hologic Selenia Dimensions	4	4	4	4	16
Hologic Lorad Selenia	1	0	1	0	2
Siemens mammomat inspiration	1	1	1	0	3
Total	12	11	10	9	42

Table 2

Table 2: Vertical paddle motion for small paddles (18x24 cm) during the first, second, third and fourth section of 10 seconds time periods after the clamping commencement. Where $\bar{x}$ is the mean; SD is the standard deviation and n is the number of observations. Flexible paddles are in grey

Time period (s) / Paddle type	0-10	10-20	20-30	30-40	0-40
	Average paddle motion ($\bar{x}$± SD, n) (mm/10s)				
GE Senographe Essential (flexible)	0.21±0.06, 120	0.08±0.03, 120	0.04±0.01, 120	0.03±0.01, 120	0.36±0.09, 480
Hologic Lorad Selenia (flexible)	0.26±0.07, 20	0.05±0.01, 20	0.03±0.01, 20	0.03±0.01, 20	0.37±0.08, 80
GE Senographe Essential (fixed)	0.26±0.07, 120	0.06±0.02, 120	0.05±0.01, 120	0.02±0.01, 120	0.39±0.09, 480
Siemens Mammomat Inspiration (fixed)	0.28±0.08, 20	0.13±0.04, 20	0.08±0.02, 20	0.05±0.02, 20	0.54±0.14, 80
Siemens Mammomat Inspiration (flexible)	0.35±0.11, 20	0.13±0.03, 20	0.10±0.02, 20	0.05±0.01, 20	0.63±0.16, 80
Hologic Selenia Dimensions (flexible)	0.39±0.12, 80	0.18±0.05, 80	0.12±0.04, 80	0.10±0.03, 80	0.79±0.22, 320
Hologic Selenia Dimensions (fixed)	0.51±0.15, 80	0.18±0.05, 80	0.11±0.03, 80	0.07±0.02, 80	0.87±0.22, 320

Table 3: Vertical paddle motion for large paddles (24x29 cm and 24x30 cm) during the first, second, third and fourth 10 second time periods after the clamping commencement. Where $\bar{x}$ is the mean; SD is the standard deviation and n is the number of observations. Flexible paddles are in grey

Time period (s) / Paddle type	0-10	10-20	20-30	30-40	0-40
	Average paddle motion ($\bar{x}$± SD, n) (mm/10 s)				
Hologic Lorad Selenia (flexible)	0.17±0.05, 20	0.06±0.02, 20	0.03±0.01, 20	0.01±0.01, 20	0.27±0.07, 80
GE Senographe Essential (flexible)	0.30±0.09, 80	0.06±0.02, 80	0.05±0.02, 80	0.04±0.01, 80	0.45±0.10, 320
GE Senographe Essential (fixed)	0.31±0.09, 100	0.08±0.02, 100	0.04±0.01, 100	0.03±0.01, 100	0.46±0.10, 400
Siemens Mammomat Inspiration (flexible)	0.33±0.10, 20	0.12±0.04, 20	0.09±0.03, 20	0.04±0.01, 20	0.58±0.15, 80
Hologic Selenia Dimensions (flexible)	0.35±0.11, 80	0.15 ±0.04, 80	0.10±0.03, 80	0.05± 0.02, 80	0.65±0.17, 320
Hologic Selenia Dimensions (fixed)	0.42±0.13, 80	0.13 ±0.04, 80	0.07±0.02, 80	0.06±0.02, 80	0.68±0.16, 320

Table 4

Table 4: Vertical paddle motion for small paddles (18x24 cm) at 2, 4, 8, 16, and 32 seconds after clamping commencement. Flexible paddles are in grey.

Second after clamping / Paddle type	2	4	8	16	32
	Paddle motion (mm/s)				
GE Senographe Essential (flexible)	0.15	0.06	0.02	0.01	<0.01
Hologic Lorad Selenia (flexible)	0.12	0.04	0.02	0.004	<0.01
GE Senographe Essential (fixed)	0.14	0.05	0.02	<0.01	<0.01
Siemens Mammomat Inspiration (fixed)	0.22	0.09	0.04	0.01	<0.01
Siemens Mammomat Inspiration (flexible)	0.25	0.11	0.04	0.01	<0.01
Hologic Selenia Dimensions (flexible)	0.35	0.15	0.06	0.02	<0.01
Hologic Selenia Dimensions (fixed)	0.34	0.14	0.05	0.01	<0.01

Table 5

Table 5: Vertical paddle motion for large paddles (24x29 cm and 24x30 cm) at 2, 4, 8, 16, and 32 seconds after clamping commencement . Flexible paddles are in grey.

Second after clamping / Paddle type	2	4	8	16	32
	Paddle motion (mm/s)				
Hologic Lorad Selenia (flexible)	0.09	0.04	0.01	<0.01	<0.01
GE Senographe Essential (flexible)	0.16	0.06	0.02	0.01	<0.01
GE Senographe Essential (fixed)	0.16	0.06	0.02	0.01	<0.01
Siemens Mammomat Inspiration (flexible)	0.23	0.10	0.03	0.01	<0.01
Hologic Selenia Dimensions (flexible)	0.28	0.12	0.04	0.01	<0.01
Hologic Selenia Dimensions (fixed)	0.26	0.10	0.04	0.01	<0.01

A method to investigate image blurring due to mammography machine compression paddle movement

Wang, MK, Hogg, P, Kelly, J and Millington, S

http://dx.doi.org/10.1016/j.radi.2014.06.004

Radiography 21 (2015) 36–41

Contents lists available at ScienceDirect

Radiography

journal homepage: www.elsevier.com/locate/radi

A method to investigate image blurring due to mammography machine compression paddle movement

Wang Kei Ma [a, *], Peter Hogg [a], Judith Kelly [b], Sara Millington [b]

[a] Department of Radiography, University of Salford, Salford M6 6PU, United Kingdom
[b] Department of Radiography, Countess of Chester Hospital, Chester CH2 1UL, United Kingdom

ARTICLE INFO

Article history:
Received 3 March 2014
Received in revised form
19 May 2014
Accepted 3 June 2014
Available online 22 June 2014

Keywords:
Blurring
Mammography
Compression

ABSTRACT

Background: Compression paddles can move during mammography exposures. Speculation suggests that this movement can cause image blurring. No research has been published to demonstrate whether such movement could cause image blurring.
Aim: Develop a method to determine whether paddle movement can cause image blurring
Method: A Hologic Selenia Dimensions mammography machine calibrated to give compression force in Newtons (N) with 24 × 30 cm fixed and flexible paddles was used. Eleven metal ball-bearings with 1.50 mm diameter were inserted onto the surface of a deformable breast phantom. The ball-bearings were placed at various points, from nipple to chest wall. The phantom was compressed using the foot pedal then hand wound to 80 N and also 150 N respectively to represent low and high compression forces used in clinical mammography. Under these conditions, images were created by exposing the phantom/ball-bearings. Image blurring was determined by measuring the change in ball-bearing diameter (distortion) using computer software.
Results: Ball-bearing diameters increased, illustrating the effect of compression paddle motion on the images. The change in ball-bearing diameter is the highest around the nipple region for both fixed (1.688 ± 0.013 mm at 80 N, 1.694 ± 0.005 mm at 150 N) and flexible (1.714 ± 0.003 mm at 80 N, 1.661 ± 0.005 mm at 150 N) paddles.
Conclusion: The increase in ball-bearing diameter suggests that image blurring due to paddle movement can be identified on images of ball-bearings adhered to the surface of a deformable breast phantom. Increase in diameter could be used as an indicator of movement severity.

Introduction

Mammographic images seem to have become more susceptible to blurring since the introduction of full field digital mammography (FFDM). The superior contrast resolution of FFDM, compared to film/screen systems, could make blurring more visible.[1,2] Previous work suggests that image blurring may be induced by poor positioning technique, patient movement, patient respiration and suboptimal compression.[3,4] A number of breast imaging centres have identified blurred images and have taken steps to minimise these factors. However, blurring still persists, and few reports have been published about this phenomena.[5,6] Research by Kelly et al.[7] suggests that image blurring may be induced by compression paddle movement during the image acquisition process. In a multicenter phantom study, Hauge et al.[8] noticed that compression paddles continue to move slightly after compression force had ceased being applied. Measurements made during a different phantom-based multicentre study by Ma et al.[9] also suggests that movement at the paddle can occur in the 'compressed state'. Ma went onto explain that this movement followed an exponential decay. According to Geerligs et al.[10] the movement at the paddle is probably caused by the thixotropic behaviour of the breast, which is the structural changes of the adipose tissue due to mechanical loading.

This study outlines a method to determine whether image blurring due to paddle motion can be detected on FFDM mammography images.

* Corresponding author.
E-mail addresses: carnby2000@gmail.com (W.K. Ma), P.Hogg@salford.ac.uk (P. Hogg), judith.kelly2@nhs.net (J. Kelly), saramillington@nhs.net (S. Millington).

http://dx.doi.org/10.1016/j.radi.2014.06.004
1078-8174/

Method

Equipment setup

A Hologic Selenia Dimensions 2-D FFDM unit (*Hologic Incorporated, Bedford, MA, USA*) calibrated to give a compression force in Newtons (N) was used in this study. FFDM system resolution was 15.33 pixels per mm. Routine equipment quality assurance (QA) had been performed on the machine and the results complied with manufacturer specifications.[11] It would be un-ethical to expose the patients repeatedly in order to investigate the effect of paddle motion on image quality. Consequently, a deformable breast phantom was used to simulate clinical imaging conditions. The phantom, originally described by Hauge,[8] comprised of a prosthetic breast insert (*Trulife, Sheffield, United Kingdom*), this was attached in a semi-mobile fashion to a rigid backboard, thereby representing the chest wall and the minor motion associated with the breast sitting on the pectoral muscle. A thin latex coating was applied to the surface of the prosthesis, allowing it to be fixed to the backboard in a fashion similar to Skin. Hauge demonstrated similar compression characteristics to human female breast tissue for this construction.

Eleven metal ball-bearings, with 1.50 mm spherical diameter, were adhered onto the phantom surface using adhesive tape. The ball-bearings were positioned at various points, from nipple to chest wall, Figs. 1 and 2. The phantom was compressed to approximately 80 N and then 150 N to represent low and high compression forces used in clinical mammography. The experimental setup is shown, Fig. 3. Four sets of images (40 in total) were acquired by using fixed and flexible 24 × 30 cm paddles at 80 N and 150 N compression. The images were acquired after compression was applied in order to study how ball-bearing diameters vary at various points in time after compression force application had ceased. The time interval between the acquired images is 26 s (ie T_1

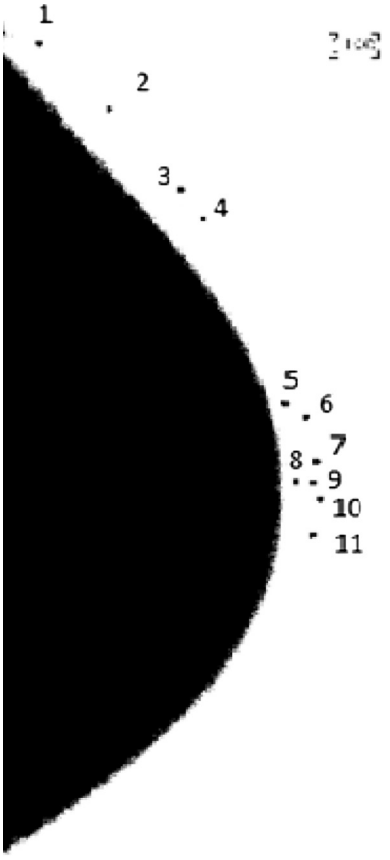

Figure 2. Schematic diagram showing the relative location of the eleven metal ball-bearings using numbering system.

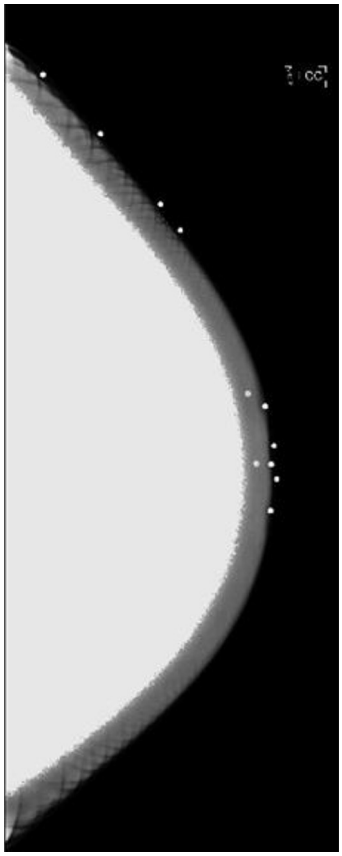

Figure 1. Mammogram showing the adhesion location of the eleven metal ball-bearings on the phantom surface.

Figure 3. The experiment setup showing the breast phantom mounted semi-mobile onto a rigid supporting board.

Table 1
Summary of the acquisition conditions of the images.

Paddle size and type	Compression force (N)	Time interval (s)	Number of images
24 × 30 cm, Fixed paddle	80	26	10
24 × 30 cm, Flexible paddle	80	26	10
24 × 30 cm, Fixed paddle	150	26	10
24 × 30 cm, Flexible paddle	150	26	10

and T_2 were 26 s apart); this was the shortest time before the mammography machine would permit the next exposure to be made (Table 1).

Image analysis

Motion blur occurs when an object moves during exposure and if motion blur exists the object would appear to be smeared or distorted in one or more directions.[12] Therefore, an approach to assessing the presence of image blurring can be determined by measuring the change in ball-bearing diameter using computer software ImageJ.[13] Within ImageJ, the 40 images were converted into binary image format and contoured to include all the metal ball-bearings. The outline of the ball-bearings was drawn automatically and their areas were calculated using a plug-in called Analyze Particles within ImageJ, Fig. 4. The diameters of the ball-bearings were than calculated using the areas determined by ImageJ (The diameter mentioned here is not in the horizontal nor vertical planes it is a theoretical diameter calculated by the area of the ball using the equation of the circle ie Area $= \pi \times r^2$). A *t*-test was used to determine whether any significant difference in ball-bearing diameter existed. A difference was considered significant at $\alpha = 0.05$. Skewness of the data was calculated in order to measure symmetry. If the data is normally distributed its skewness values should be zero. If the skewness value is negative it indicates the data are skewed to left and positive value indicate the data are skewed to right.[14]

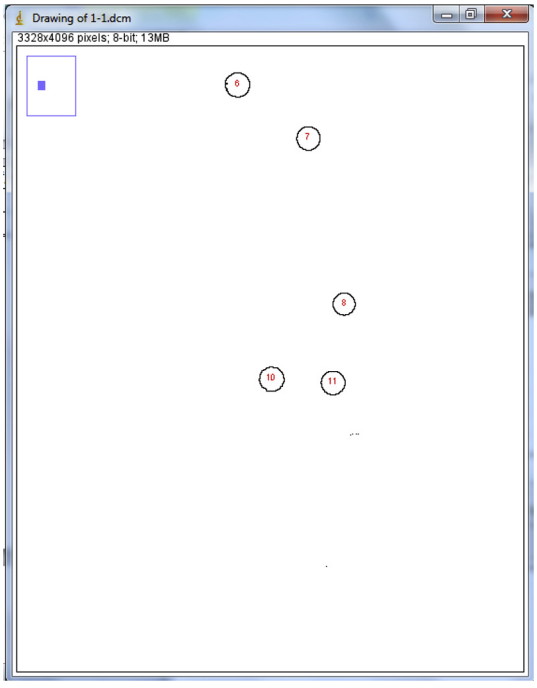

Figure 4. The ball-bearings are numbered and outlined by ImageJ.

Results

Ball-bearing diameters, skewness values and their percentage change for different compression paddle/compression force combinations are shown in Tables 2–5. In this study all the data has skewness values between −1 and 1 ($-1 \leq x \leq 1$), which indicates they do not deviate significantly from the normal distribution, where the mean and standard deviation of the ball-bearing diameter were not distorted by extreme values.

All ball-bearing locations demonstrated a unidirectional diameter increase. The oval appearance of the ball-bearing is consistent with movement having occurred during the image acquisition phase.

The change in ball-bearing diameter was at its peak around the nipple region for both fixed (1.688 ± 0.013 mm at 80 N, 1.694 ± 0.005 mm at 150 N) and flexible (1.714 ± 0.003 mm at 80 N, 1.661 ± 0.005 mm at 150 N) paddles. Given the oval appearance of the ball-bearings, this is suggestive of maximal motion around the nipple region.

The *t*-test was used to test the change in ball-bearing diameter with time. The results are summarised in Tables 6 and 7. At 80 N compression, there is a significant difference ($p < 0.05$) in ball-bearing diameters in the fixed paddle excepting at T_3 ($p = 0.0975$, $t = 1.8282$) and T_8 ($p = 0.1784$, $t = 1.4472$). At 80 N compression, there is significant difference ($p < 0.05$) in ball-bearing diameters in the flexible paddle at T_2 ($p = 0.0041$, $t = 3.7083$) and T_8 ($p = 0.0411$, $t = -2.3440$). At 150 N compression, there is no significant difference ($p > 0.05$) in ball-bearing diameters for both fixed and flexible paddles.

Discussion

This research is the first to investigate whether compression paddle movement during the image acquisition process could account for image blurring. The method used in this study identified that image blurring is likely to be caused by paddle motion which can be detected on FFDM mammography images. The image blurring was detected by mathematical techniques using ImageJ however whether the human eye can discern such level of motion would need further investigation.

A limitation of our study relates to the restricted number of points in time when exposures could be made after compression force had ceased to be applied. Previous research into paddle movement shows that approximately 60% of motion occurs within the first 10 s. It is likely that the highest amount of motion artifact would be induced in this period.[9] However the mammography machine in this study only permitted repeat imaging after an average time of 29.5 s. Ideally more exposures per unit time would be preferable, from the point after which compression forces ceases to be applied. This would permit many more images to be available for analysis. Future work should consider this.

The findings of our study and those of related research[9] suggest that movement at the paddle during exposure can occur. Motion is minor, typically being 1 mm or less,[9] consequently the perceptual significance of this needs investigating. In light of this, a motion simulation study will be conducted using mammogram image data. In this study a bespoke computer program has been written to degrade mammogram image data to simulate different amounts of motion. The degraded images will be reviewed by experienced practitioners to determine the limits at which the human visual system can detect sub-millimetre motion.

Conclusion

Using a phantom and mathematical techniques, the increase in ball-bearing diameters suggests that blurring due to paddle

Table 2
Ball-bearing diameters for fixed paddle with 80 N compression force.

Ball-bearing no.	1	2	3	4	5	6	7	8	9	10	11
Diameter ± SD (mm)	1.593 ± 0.005	1.541 ± 0.006	1.514 ± 0.005	1.531 ± 0.007	1.687 ± 0.012	1.634 ± 0.008	1.531 ± 0.005	1.688 ± 0.013	1.654 ± 0.013	1.519 ± 0.003	1.640 ± 0.011
Skewness	−0.8	0.4	−0.5	0.1	0.3	0.7	0.5	0.5	1.0	−0.7	0.7
Change in diameter (%)	6.2	2.7	0.9	2.1	12.5	8.9	2.1	12.5	10.3	1.3	9.3

Table 3
Ball-bearing diameters for flexible paddle with 80 N compression force.

Ball-bearing no.	1	2	3	4	5	6	7	8	9	10	11
Diameter ± SD (mm)	1.579 ± 0.004	1.533 ± 0.003	1.502 ± 0.006	1.512 ± 0.004	1.714 ± 0.004	1.554 ± 0.004	1.563 ± 0.003	1.714 ± 0.003	1.569 ± 0.004	1.520 ± 0.005	1.564 ± 0.003
Skewness	0.8	−0.3	0.2	−0.4	0.5	0.1	0.3	−0.3	0.1	−0.5	−0.4
Change in diameter (%)	5.3	2.2	0.1	0.8	14.3	3.6	4.2	14.3	4.6	1.3	4.3

Table 4
Ball-bearing diameters for fixed paddles with 150 N compression force.

Ball-bearing no.	1	2	3	4	5	6	7	8	9	10	11
Diameter ± SD (mm)	1.580 ± 0.005	1.538 ± 0.004	1.513 ± 0.003	1.523 ± 0.004	1.656 ± 0.004	1.655 ± 0.003	1.514 ± 0.004	1.694 ± 0.005	1.686 ± 0.002	1.509 ± 0.004	1.665 ± 0.004
Skewness	−0.5	0.9	−0.3	0	−0.6	−0.4	0.7	−0.9	−0.4	−0.3	−1
Change in diameter (%)	5.3	2.5	0.9	1.5	10.4	10.3	0.9	12.9	12.4	0.6	11.0

Table 5
Ball-bearing diameters for flexible paddles with 150 N compression force.

Ball-bearing no.	1	2	3	4	5	6	7	8	9	10	11
Diameter ± SD (mm)	1.579 ± 0.005	1.537 ± 0.004	1.511 ± 0.003	1.522 ± 0.005	1.667 ± 0.006	1.629 ± 0.003	1.521 ± 0.004	1.656 ± 0.008	1.661 ± 0.005	1.507 ± 0.005	1.635 ± 0.003
Skewness	−0.4	0.9	0.5	−0.2	0.1	0	−0.2	−0.3	−0.9	−0.8	0.8
Change in diameter (%)	5.3	2.5	0.7	1.5	11.1	8.6	1.4	10.4	10.7	0.5	9.0

Table 6
Significance of ball-bearing movement over time for fixed and flexible paddles with 80 N compression force;* indicate *p*-value smaller than 0.05.

Time interval (s)	T_1	T_2	T_3	T_4	T_5	T_6	T_7	T_8
p-Value (Fixed)	0.0003*	0.0002*	0.0975	0.0062*	0.0128*	0.0035*	0.0419*	0.1784
t-Value (Fixed)	5.3404	5.7045	1.8282	3.4480	3.0229	3.7927	2.3317	1.4472
p-Value (Flexible)	0.1711	0.0041*	0.1295	0.0796	0.0657	0.5614	0.7866	0.0411*
t-Value (Flexible)	1.4745	3.7083	1.6521	1.9514	2.0661	0.6008	−0.2781	−2.3440

Table 7
Significance of ball-bearing movement over time for fixed and flexible paddles with 150 N compression force;* indicate *p*-value smaller than 0.05.

Time interval (s)	T_1	T_2	T_3	T_4	T_5	T_6	T_7	T_8
p-Value (Fixed)	0.9853	0.2873	0.6004	0.2397	0.1403	0.5145	0.4764	0.1156
t-Value (Fixed)	0.0189	1.1239	0.5410	1.2502	1.6017	−0.6757	−0.7398	1.7231
p-Value (Flexible)	0.2553	0.1474	0.1550	0.0603	0.3985	0.1383	0.4483	0.2882
t-Value (Flexible)	1.2067	1.5702	1.5382	2.1177	0.8820	1.6108	0.7892	1.1217

movement can be identified on FFDM images. Further work is needs undertaking to determine whether such movement would have any visual impact on image quality or lesion visibility.

Acknowledgements

The authors would like to thank John Thompson, University Hospitals of Morecambe Bay NHS Foundation Trust, UK, for providing valuable critical review on this work.

References

1. Bushberg JT, Seibert JA, Leidholdt EM, Boone JM. *The essential physics of medical imaging*. 3rd ed. New York: Williams & Wilkins; 2011.
2. Fischmann A, Siegmann KC, Wersebe A, Claussen CD, Müller-Schimpfle M. Comparison of full-field digital mammography and film-screen mammography: image quality and lesion detection. *Br J Radiol* 2005;**78**:312–5.
3. Lee L, Stickland V, Wilson R, Evans A. *Fundamental of mammography*. 2nd ed. London: Churchill Livingstone; 2003.
4. Tucker AK, Ng YY, editors. *Textbook of mammography*. 2nd ed. London: Churchill Livingstone; 2001.
5. Hogg P, Szczepura K, Kelly S, Taylor J. Blurred digital mammography images. *Radiography* 2012;**18**(1):55–6.
6. Hogg P, Kelly J, Millington S, Willcock C, McGeever G, Tinston S, et al. Paddle motion analysis. In: *East of England Conference; 2012 December; University of Cambridge, UK*. National Health Service Breast Screening Programme; 2012.
7. Kelly J, Hogg P, Millington S, Sanderud A, Willcock C, McGeever G, et al. Paddle motion analysis preliminary research. In: *United Kingdom Radiological Congress (UKRC); 2012 June 25–27; Manchester, UK*. British Institute of Radiology; 2012.
8. Hauge I, Hogg P, Szczepura K, McGill G, Connolly P, Mercer C. The readout thickness versus the measured thickness for a range of screen film mammography and full-field digital mammography units. *Med Phys* 2012;**39**(1):263–71.
9. Ma WK, Hogg P, Kelly J, Millington S. Mammography machine paddle movement analysis. In: *A multicentre study. United Kingdom Radiological Congress (UKRC); 2012 June 25–27; Manchester, UK*. British Institute of Radiology; 2012.
10. Geerligs M, Peters GWM, Ackermans PAJ, Oomens CWJ, Baaijens FPT. Does subcutaneous adipose tissue behave as an (anti-)thixotropic material? *J Biomech* 2010;**43**:1153–9.
11. IPEM (Institute of Physics and Engineering in Medicine). *The commissioning and routine testing of mammographic X-ray systems: a technical quality control protocol*. Report no. 89. York: IPEM; 2005.
12. Yap KH, Guan L, Perry SW, Wong HS. *Adaptive image processing: a computational intelligence perspective*. 2nd ed. Florence: CRC Press; 2009.
13. Rasband WS. *ImageJ, U.S. National institutes of health, Bethesda, Maryland, USA*; 1997–2014. Available at: http://imagej.nih.gov/ij.
14. Hicks C. *Research methods for clinical therapists: applied project design and analysis*. 5th ed. Edinburgh: Churchill Livingstone; 2009.

What is the minimum amount of simulated breast movement required for visual detection of blurring : An exploratory investigation?

Ma, WK, Aspin, R, Hogg, P, Kelly, J and Millington, S

http://dx.doi.org/10.1259/bjr.20150126

Full paper

What is the minimum amount of simulated breast movement required for visual detection of blurring: an exploratory investigation?

ABSTRACT

Background: Image blurring in mammography can cause significant image degradation and interpretational problems. A potential source is due to paddle movement during image formation. Paddle movement has been shown to be as much as 1.5mm. No study has yet been performed to determine how much motion would be noticeable, visually.

Objectives: To determine the minimum amount of simulated breast movement at which blurring can be detected visually.

Method: 25 artefact free mammogram images were selected. Mathematical simulation software was created to mimic the effect of blurring produced by breast movement during exposure. Motion simulation was imposed to 15 levels, from 0.1mm to 1.5mm stepping through 0.1mm increments. 15 degraded images and 1 without blurring were de-identified, randomized and assessed on a blinded basis by two clinical experts to determine presence or absence of blurring. Statistical testing was carried out to determine the consistency between the two observers.

Results: The probability of simulated blurred image detection is highest for the Gaussian method and lowest for soft edged mask estimation.

Conclusion: The amount of simulated breast movement at which blurring can be detected visually for Gaussian blur, hard edge mask estimation, and soft edge mask estimation are 0.4mm,

0.8mm and 0.7mm respectively. Cohen's Kappa for all the levels of simulated blurring is 0.689 ($p<0.05$).

Advances in knowledge: This research establishes the concept of using probability to represent visual detection of blurring rather than defining a hard cut-off level.

Keywords: motion simulation, mammography, Gaussian distribution, blurring, paddle movement

List of Figure Captions

Figure 1: One of the 25 blur free images

Figure 2a: Simulation of pixel accumulation during motion, enacted as a hard edged block function. Figure 2b: Analysis of diagonal section (bottom left to top right) of accumulated pixel intensity, showing distribution of intensity due to accumulation of pixel representation as a hard edged block function (green line) and equivalent Gaussian function (black line) within the section.

Figure 3a: Simulation of pixel accumulation during motion, enacted as a soft edged block function. Figure 3b: Analysis of diagonal section (bottom left to top right) of accumulated pixel intensity, showing distribution of intensity due to accumulation of pixel representation as a soft edged block function (green line) and equivalent Gaussian function (black line) within the section.

Figure 4: Gaussian mask for 1.5mm simulated motion

Figure 5: Hard edged pixel mask for1.5mm simulated motion

Figure 6: Soft edged pixel mask for 1.5mm simulated motion

Figure 7: Blurred image generated by Gaussian for 1.5mm simulated motion

Figure 8: Blurred image generated by hard edged estimation for 1.5mm simulated motion

Figure 9: Blurred image generated by soft edged estimation for 1.5mm simulated motion

INTRODUCTION

Image blurring in mammography causes image degradation which can lead to problems with interpretation. Blurring has been detected during routine clinical practice and according to the results of a local audit it was the reason behind 87% of repeat images [1]. Within the UK, blurred mammograms have been increasingly noticed, particularly since the introduction of full field digital mammography (FFDM) [1]. Image blurring was probably present on conventional film but it was easier to detect by FFDM due to improvements in contrast resolution. A study by Saunders et al [2] shows that presence of noise and blurring would significantly reduce lesion detection accuracy; blurring may mask certain types of lesion which can result in false negative or false positive outcomes.

Image blurring may be caused by a number of factors such as geometric distortion from the finite focal spot size, digitizer blur, patient movement and under-compression [3, 4]. Studies have shown that using too little compression can result in blurring; also one study has demonstrated compression force is not evenly distributed across the breast and for the medio-lateral oblique view (MLO) a lot of compression is lost in the pectoral muscle leading to under-compression in the rest of the breast [4].

Human perception of blurring could be affected by the distribution of contrast across different spatial frequencies. For instance, if the high spatial frequencies are filtered by a low-pass spatial filter the image will appear blurred while the image will appear sharp if low spatial frequencies are filtered by a high-pass spatial filter. Psychophysical studies suggest that perception of blurring can be controlled by adaptive adjustment of the spatial frequencies [5]. Literature on motion perception concurred with the psychophysical findings and suggests that image processing algorithms could affect observer's perception on motion because the noise

suppression for these processing algorithms not only changes the spatial frequencies but also reduces sharp transitions between pixel intensities; these modifications affect how human observers perceive motion in the presence of image degradation [6, 7].

Blurring can result in mammography images needing to be repeated; this increases client radiation dose and anxiety. Recently paddle movement has been suggested as a potential source of blurring. Ma et al [8] observed movement attributed to the paddle using an experimental approach in which metal ball-bearing diameters altered during compression of a deformable breast phantom in FFDM; change in diameter was considered to be the result of paddle motion. In a multicenter study the extent of the paddle movement was observed to be as much as 1.5mm during the acquisition / exposure period, in the vertical plane [9].

Whilst these observations have been reported, no study has yet investigated how much motion needs to occur before the effect is visually noticeable on a mammogram. Therefore, the aim of this exploratory investigation was to determine the minimum amount of breast movement which needs to occur for blurring to be visually evident. Software based image processing has been used to replicate the visual effect of breast movement. This study is a compromise because of the practical difficulties encountered when trying to control motion to 0.1mm precision on a FFDM mammographic machine so a physical approach for creating motion was not adopted.

METHOD

Image acquisition

Mammography images were acquired on a Selenia Dimensions (Hologic, Bedford, USA) FFDM machine within the National Health Breast Screening Programme (NHSBSP). Routine equipment quality assurance (QA) had been performed and the results complied with manufacturer specifications [10].

Images selection

Images were only included if blur was not present [11, 12]. Blur free images were identified by selecting images in which breast anatomical structures had distinct / sharp edges (Figure 1). Hundreds of images were reviewed initially on 5MPx monitors within the breast unit and 100 met the inclusion criteria. These had been scrutinized by imaging practitioners as part of the routine clinical processes for breast screening within the UK and also through additional quality review as part of this study. A university professor who regularly conducts and publishes research into dose and image quality optimisation identified the 25 images which were included in this study. Selection of the final 25 images did not involve the observers who later assessed the 1200 images for absence / presence of blurring.

Figure 1: One of the 25 blur free images

Motion simulation

It is extremely difficult to control submillimeter movement of a mammogram accurately in a physical study. Software was therefore developed and validated to simulate motion in mammogram image datasets. Research by Ma et al [8] suggests the amount of movement during a mammography exposure in a female breast ranges from 0.4mm to 1.5mm, in the vertical plane. Our software motion simulation was designed to impose 15 levels of motion, from 0.1mm to 1.5mm stepping through 0.1mm. Using this approach it is possible to create 15 blurred images for each image.

Blurring was created by the accumulated pixel points moving under random motion. After sampling blurred image data from real patient images we identified three mathematical techniques which are suitable to simulate motion blurring: Gaussian, hard edge mask estimation, and soft edge mask estimation [13, 14]. Currently, there is a paucity of literature about motion

simulation techniques therefore all three mathematical simulation techniques were used in this study.

Evaluation of pixel motion was made by accumulating the pixel intensity of randomized micro steps, within 1.5 mm of motion boundary. Propagation of the pixel intensity to the accumulation plane was initially enacted as hard edged block pixel and soft edged block pixel respectively, with a further refinement to apply a Gaussian distribution centered on the pixel step position, with mask dimension proportional to the original pixel size. The resultant accumulation of intensity was sampled by a diagonal section of the spread pixel to determine the profile of intensity spread due to motion. Matching this to the standard Gaussian distribution, commonly used to enact blurring in image processing, showed that for the motion enacted by the actual pixel a significantly steeper drop-off and narrower spread of intensity was presented (Figures 2 to 3).

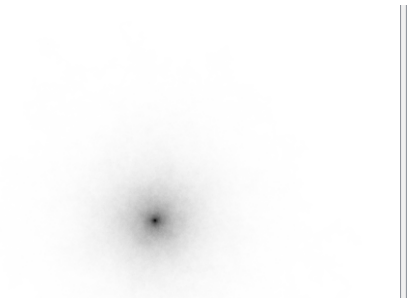

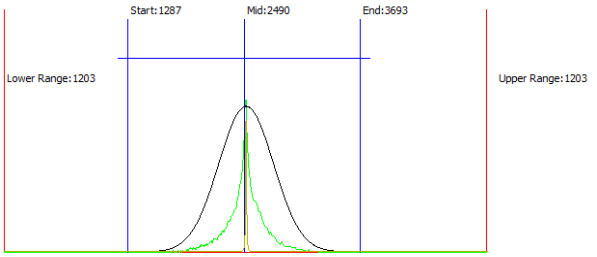

Figure 2a: Simulation of pixel accumulation during motion, enacted as a hard edged block function.
Figure 2b:Analysis of diagonal section (bottom left to top right) of accumulated pixel intensity, showing distribution of intensity due to accumulation of pixel representation as a hard edged block function (green line) and equivalent Gaussian function (black line) within the section.

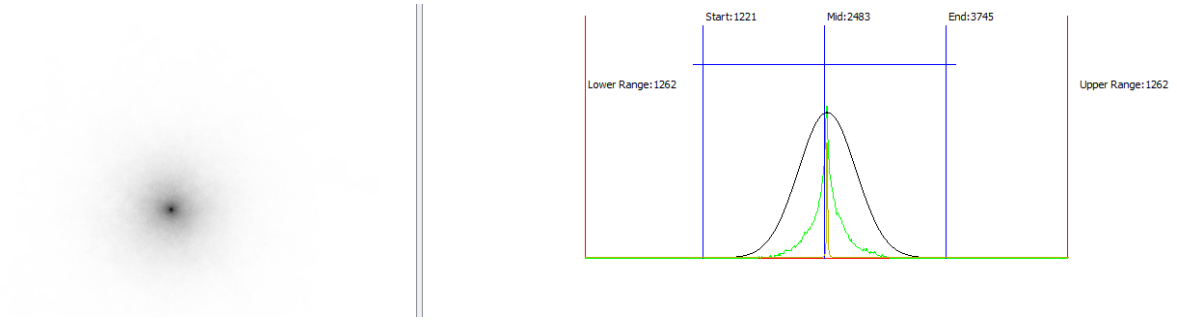

Figure 3a: simulation of pixel accumulation during motion, enacted as a soft edged block function.
Figure 3b: Analysis of diagonal section (bottom left to top right) of accumulated pixel intensity, showing distribution of intensity due to accumulation of pixel representation as a soft edged block function (green line) and equivalent Gaussian function (black line) within the section.

Averaged data from multiple runs of this experiment was evaluated using curve fitting processes to determine a curve function to represent the transition. This function was used to populate convolution masks for enacting blurring in the sample images (Figures 4 to 6). Blurred images were generated for all three approaches (Figures 7 to 9) by applying the convolution masks to the source images.

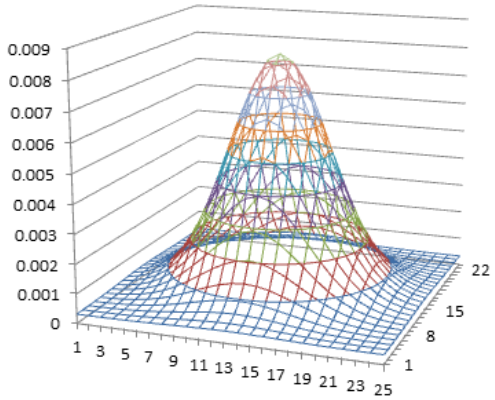

Figure 4: Gaussian mask for 1.5mm simulated motion

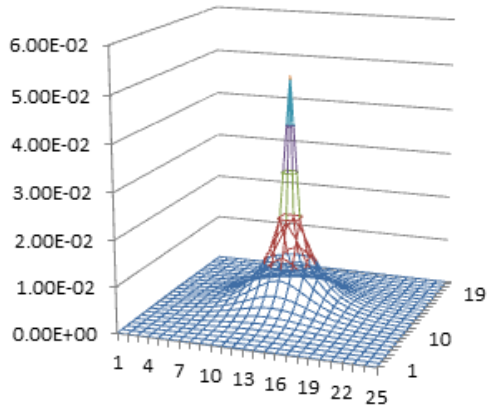

Figure 5: Hard edged pixel mask for1.5mm simulated motion

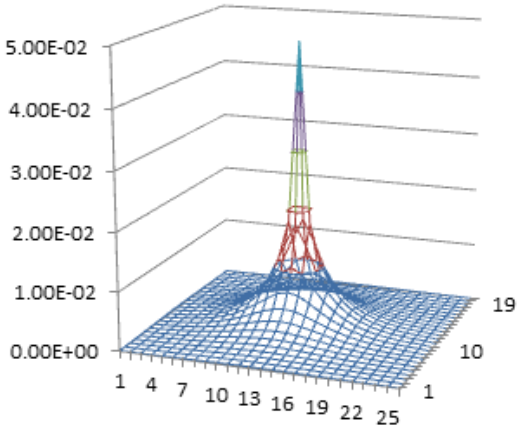

Figure 6: Soft edged pixel mask for 1.5mm simulated motion

Figure 7: Blurred image generated by Gaussian for 1.5mm simulated motion

Figure 8: Blurred image generated by hard edge mask estimation for 1.5mm simulated motion

Figure 9: Blurred image generated by soft edge mask estimation for 1.5mm simulated motion

For each source image (image without blurring), 15 processed images were created with between 0.1 and 1.5mm of simulated movement and these were exported as a randomized Digital Imaging and Communications in Medicine (DICOM) sequence for evaluation by two observers.

Visual assessment of images

MediViewer viewing software (Schaef Systemtechnik, Petersaurach, Germany) was used to display the images. 1200 images were reviewed for the 3 simulation methods; 25 DICOM images sets and 15 levels of motion plus 1 without blurring (3x25x16). Ambient light level in the reading room was set to be less than 10 lux [15]. On a blinded and individual basis the images were displayed in a random order to the two observers. The two observers were qualified radiographers with specialist postgraduate qualifications in mammography imaging; they had been trained to interpret mammograms and they had been doing this role independently for 7 and 15 years, respectively. As part of this role they participate annually in the PERFORMS (Loughborough University, UK) [16] image reading analysis; this independent analysis has

always resulted in their scores being well above the expected mark for interpreting mammography images within the NHSBSP. Both reviewers therefore had proven technical and clinical skills in image quality appraisal from technical and diagnostic points of view.

Presence or absence of blurring was a purely binary decision - indicating whether it was present (yes) or not (no). Kappa analysis was carried out to determine variability between the two observers. The presence of motion blurring was assessed by the observers with reference to the guidelines published by the National Health Service Breast Screening Programme (NHSBSP) and through determining whether breast anatomical structures had distinct / sharp edges [17]. To minimize eye strain / fatigue the observers did not score images for longer than 30 minutes in any one session. Images were viewed on a 21.3 inch LCD monitor (EIZO, Ishikawa, Japan) with a resolution of 2560x1920 (5 megapixels). The viewing monitors were calibrated to the DICOM Grayscale Standard Display Function (GSDF) [18].

RESULTS

The probability of detecting blurring for Gaussian blur, hard edge mask estimation, and soft edge mask estimation are shown in tables 1 to 3. All the non-motion images were identified correctly by the observers. Cohen's Kappa (K) for all the levels of simulated blurring is 0.689 ($p<0.05$), representing good agreement for the two observers [19]. The average probability of detecting blurring rises from 40% (0.1mm) to 92% (0.3mm) for Gaussian blurring (table 1); from 10% (0.1mm) to 98% (0.7mm) for hard edge mask estimation (table 2) and from 4% (0.1mm) to 98% (0.6mm) for soft edge mask estimation (table 3). The average probability of detecting blurring is the highest in Gaussian blur (40%) which means when the amount of breast movement is 0.1 mm there is 40 % chance that the blurring can be detected visually. The amount of simulated breast

movement at which 100% of blurred images can be detected visually for Gaussian blur, hard edge mask estimation, and soft edge mask estimation are 0.4mm, 0.8mm and 0.7mm respectively.

Table 1: Probability of detecting blurring for Gaussian blurring

Movement (mm)	0.1	0.2	0.3	0.4	0.5	0.6	0.7	0.8	0.9	1.0	1.1	1.2	1.3	1.4	1.5
Observer 1 Probability (%)	24	64	84	100	100	100	100	100	100	100	100	100	100	100	100
Observer 2 Probability (%)	56	100	100	100	100	100	100	100	100	100	100	100	100	100	100
Average Probability (%)	40	82	92	100	100	100	100	100	100	100	100	100	100	100	100

Table 2: Probability of detecting blurring for hard edged mask estimation

Movement (mm)	0.1	0.2	0.3	0.4	0.5	0.6	0.7	0.8	0.9	1.0	1.1	1.2	1.3	1.4	1.5
Observer 1 Probability (%)	12	28	32	56	72	72	96	100	100	100	100	100	100	100	100
Observer 2 Probability (%)	8	80	84	88	100	100	100	100	100	100	100	100	100	100	100
Average Probability (%)	10	54	58	72	86	86	98	100	100	100	100	100	100	100	100

Table 3: Probability of detecting blurring for soft edged mask estimation

Movement (mm)	0.1	0.2	0.3	0.4	0.5	0.6	0.7	0.8	0.9	1.0	1.1	1.2	1.3	1.4	1.5
Observer 1 Probability	8	32	52	72	96	96	100	100	100	100	100	100	100	100	100

(%)															
Observer 2 Probability (%)	0	60	96	100	100	100	100	100	100	100	100	100	100	100	100
Average Probability (%)	4	46	74	86	98	98	100	100	100	100	100	100	100	100	100

DISCUSSION

The rationale for choosing the image algorithms

The Gaussian algorithm was chosen as it is the standard approach for image blurring; it replicates the effect of putting a translucent film over the image and scatters light uniformly. Initial review by the clinicians showed that this was similar to the blurring effect seen, but that it was creating too much blur for the movement levels.

The pixel walking application was then setup to examine what happens to a point in the breast under motion during the [pixel] acquisition. The hard edged mask estimation made the assumption that a single point in the image would map to a single pixel at every point of its motion. The soft edged mask estimation further refined this by applying a soft edge to the breast tissue feature in effect at the tissue moved a part captured by a single pixel could, after a small movement step, occupy a space sampled by several pixels. Validation was also performed by calculation against grid images to ensure the amount of spread (size of mask) was appropriate.

Blurring masks

While the convolution mask used in the Gaussian blurring approach is the same size as for the other approaches, with the size of the mask defined by the level of motion simulated, the more gradual spread of the function creates a greater distribution of the pixel intensity within the

specific motion. Gaussian blurring is commonly used to simulate blurring in image processing, and it assumes a model based similar to placing an opaque diffusion filter over the image. However, the blur within the images here is based on an actual motion of the subject during the time the pixel was captured. Therefore it is not a good fit for replicating the characteristic blur seen in these image types. The simulation process we undertook, which replicates the subject motion as a stochastic sampling process, shows that the profile of distribution within a motion based blur is characterized by a function in which the intensity drop off is much more rapid (Figures 2 & 3). This means that for the same level of simulated motion, application of a Gaussian based function delivers a greater level of visual blurring than our evaluated mask suggests, explaining why the detection of blur within the Gaussian image sequences is more detectable for smaller levels of motion.

The two simulated convolution masks evolved as part of an iterative process. The initial prototype considered a sample of the same size as the capture pixel which was moved during the simulated walking by fixed step sizes of the same unit. This demonstrated the discrepancy between the general case Gaussian mask profile and motion based simulation within the characteristics of the imaging system. Given this initial validation a refined variant of the simulation process was evolved in which a soft edged subject point was translated by variable step sizes within the motion walking process to more accurately reflect the analog nature of motion within the imaging process. For completeness in the evaluation, images from both the initial prototype and the refined (soft-edged) approach were used. The more subtle simulation of motion within the soft edged approach delivered a slightly more diffuse distribution of the pixel blur, which makes the perception of blur slightly more prevalent at lower motion levels (Table 3)

than for the hard-edged approach (Table 2), but this latter approach is more reflective of the actual physical effect of motion within the imaging process.

Perception of blurring

Visual perception of blurring can vary between individuals, factors such as visual acuity, experience/ability and Circadian rhythm variations can account for these differences [20]. Consequently, in this study we used probability to represent blurring detection rather than defining a hard cut-off level. The level of agreement between the two observers is reasonable (k =0.698), however their level of agreement was not perfect (k =1). Nevertheless, the level of agreement is good and provides a basis upon which conclusions can be drawn. Further research needs conducting to identify and assess the factors which may affect the ability of observers to visually detect blurring.

FFDM imaging and display systems resolution

In this study we have shown that only small amounts of simulated motion is needed in FFDM images for blurring to be seen visually. If our simulation models reflect actual motion then our results could have clinical importance, as they could help to explain why there has been an increase in blurred images since the introduction of FFDM. Furthermore, as technical advances continue to be made in acquisition and display resolution then blurred images could become more problematic. Further research is needed to understand whether this would be the case.

An additional problem, related to image blurring concerns the resolution of the monitors used in clinical room, as it is here where the images are checked for technical accuracy prior to sending the client home. Though monitor specification has risen in recent years, for monitors used for checking images prior to the client leaving the actual resolution can be as low as 1.8 MPx. We

speculate that imaging practitioners might not see visual blurring on monitors at this resolution, and as local audits show it is only when images are displayed on 5MPx screens that blurring becomes apparent. This disparity might be a cause of technical recalls noted in audits. Further research needs conducting to assess higher and lower monitor resolution with respect to blurring detection. In light of this we have already commenced a project, using simulated blurred images, to investigate the effect of monitor resolution on blurring detection.

Lesion detection performance

In this study we have demonstrated that simulated blurring can be detected visually even when there is only a small amount of breast movement (e.g. 0.1mm). We have not addressed the most important question, whether blurring affects lesion detection performance and lesion characterization. Consequently, further research needs conducting to address this.

Ways to reduce blurring

Sources of blurring can be summarized into three categories: patient-, practitioner- and machine-related. Breast compression can only deal with patient related factors such as patient movement. Practitioner related factors can be minimized by good patient positioning skills, for example patient movement could be avoided through sufficient compression and good patient communication [21]. Movement at the paddle is an example of a machine-related factor; according to the research by Ma et al. [8] paddle movement is the highest in the first 10 seconds. Therefore if practitioners could wait a few seconds after the compression force ceases to be applied before making the exposure blurring could be minimized. Further research could be carried out to investigate the optimum waiting time to ceases the compression.

Limitations

One of the limitations of our work is the use of motion simulated images. Motion simulation might not fully represent real / physically blurred images because mammography image blurring may fully or partly affect the image; our software simulation only fully blurred the images. Since conducting this study we have refined our mathematical model to introduce regional blurring to better reflect clinical reality. Another limitation is the number of observers involved. Since this is an exploratory investigation only two observers and 25 original images were involved. We have already extended our work to include a larger sample of observers.

CONCLUSION

All non-motion images were identified by the observers. The probability of simulated blurred image detection is highest for the Gaussian method and lowest for soft edged mask estimation. The amount of simulated breast movement at which 100% of blurred images can be detected visually for Gaussian blur, hard edge mask estimation, and soft edge mask estimation are 0.4mm, 0.8mm and 0.7mm respectively. Our results could have clinical importance, and they re-enforce the need to minimize patient motion during the acquisition process. It is likely that image blurring will become even more apparent when improvements are made in FFDM acquisition and display systems resolution.

Conflict of interest statement

The authors have no conflict of interest.

References:

1. Kelly J, Hogg P, Szczepura K et al. The Blurring Issue in Mammography: 2011. Mammographic Imaging Seminar, 2011 December; Salford, UK: University of Salford, 2011.

2. Krupinski EA, Williams MB, Andriole K, Strauss KJ, Applegate K, Wyatt M, et al. Digital radiography image quality: image processing and display. Journal of the American College of Radiology 2007; 4(6): 389-400.

3. Highnam R, Brady JM. Computational Imaging and Vision Mammographic: Image Analysis. 1st ed. London, UK: Springer, 1999.

4. Dustler M, Andersson I, Brorson H, Fröjd P, Mattsson S, Tingberg A, ZackrissonS, Förnvik D. Breast compression in mammography: pressure distribution patterns. Acta Radiol. 2012 Nov 1;53(9):973-80.

5. Webster MA, Georgeson MA, Webster SM. Neural adjustments to image blur. Nat Neurosci 2002; 5: 839-840. doi:10.1038/nn906.

6. Massanes F, Brankov G. Motion perception in medical imaging, Proc. SPIE 7966, Medical Imaging 2011: Image Perception, Observer Performance, and Technology Assessment, 796610 (March 03, 2011); doi:10.1117/12.878417.

7. Gonzalez RC, Woods RE. Digital image processing. 3rd ed. London, UK: Pearson, 2008.

8.Ma WK, Hogg P, Kelly J, Millington S. A method to investigate image blurring due to mammography machine compression paddle movement. Radiography 2014; in press. Epub ahead of print. doi:10.1016/j.radi.2014.06.004

9. Ma WK, Brettle D, Howard D, Kelly J, Millington S, Hogg P. Extra Patient Movement During Mammographic Imaging: An Experimental Study. Br J Radiol 2014;87:20140241.

10. Moore A C, Dance D R, Evans D S, Lawinski C P, Pitcher E M, Rust A, et al. The Commissioning and Routine Testing of Mammographic X-Ray Systems: A Technical Quality Control Protocol. Report No. 89 York, UK: IPEM, 2005.

11. Taplin S, Rutter C, Finder C, Mandelson M, Houn F, White E. Screening Mammography: Clinical Image Quality and the Risk of Interval Breast Cancer. AJR 2002, 178, 797–803

12. Samei E, Performance of Digital Radiographic Detectors: Quantification and Assessment Methods. Advances in Digital Radiography: RSNA Categorical Course in Diagnostic Radiology Physics, Radiographics, 25, 2, 2005, pp 37–47. 9. Gale AG, Scott H. Measuring Radiology

13. Young S, Driggers G, Jacobs L. Signal Processing and Performance Analysis for Imaging Systems. 1st ed. New York, US: Artech House, 2008.

14. Dougherty G. Digital Image Processing for Medical Applications. 1st ed. Cambridge,UK: Cambridge University Press, 2009.

15. Perry N, Broeders M, Wolf C, Törnberg S, Holland R, Karsa L, et al. European guidelines for quality assurance in breast cancer screening and diagnosis. 4th ed. Luxembourg: European Communities, 2006.

16. Performance in Breast Screening. In M.Michell (ed.) Contemporary Issues in Cancer Imaging – Breast Cancer, Cambridge UP, Cambridge, 2010.

17. The National Health Service Breast Screening Programme. Quality assurance guidelines for mammography, vol. 63. Sheffield: NHSBSP publication; 2006.

18. National Electrical Manufacturers Association (NEMA) Digital Imaging and Communications in Medicine (DICOM) Part 14: Grayscale Standard Display Function; 2011.

19. Hicks C. Research Methods for Clinical Therapists: Applied Project Design and Analysis. 5th ed. Edinburgh, UK: Churchill Livingstone, 2009.

20. Lanca C, Lanca L, Thompson J and Hogg P, A method to assess visual function prior to conducting medical imaging research using perceptual methodologies. Radiologic Technology 2015; in press

21. Hogg P, Kelly J, Claire E. (Eds.) Digital Mammography A Holistic Approach, 1st ed. London, UK: Springer, 2015.

Blurred digital mammography images : an analysis of technical recall and observer detection performance

Ma, V, Kelly, J, Millington, S, Scragg, B, Borgan, R, Aspin, R, Costa, C and Hogg, P

http://dx.doi.org/10.1259/bjr.20160271

Full paper

Blurred digital mammography images: an analysis of technical recall and observer detection performance

Abstract

Background: Blurred images in Full Field Digital Mammography (FFDM) are a problem in the UK Breast Screening Programme. Technical recalls may be due to blurring not being seen on lower resolution monitors used for review.

Objectives: This study assesses the visual detection of blurring on a 2.3 megapixel (MP) monitor and a 5 MP report grade monitor and proposes an observer standard for the visual detection of blurring on a 5 MP reporting grade monitor.

Method: Twenty-eight observers assessed 120 images for blurring; 20 had no blurring present whilst 100 had blurring imposed through mathematical simulation at 0.2, 0.4, 0.6, 0.8 and 1.0 mm levels of motion. Technical recall rate for both monitors and angular size at each level of motion were calculated. Chi-squared (X^2) tests were used to test whether significant differences in blurring detection existed between 2.3 and 5 MP monitors.

Results: The technical recall rate for 2.3 and 5 MP monitors are 20.3 % and 9.1% respectively. Angular size for 0.2 to 1 mm motion varied from 55 to 275 arc seconds. The minimum amount of motion for visual detection of blurring in this study is 0.4 mm. For 0.2 mm simulated motion, there was no significant difference X^2 (1, N=1095) =1.61, p=0.20) in blurring detection between the 2.3 and 5 MP monitors.

Conclusion: According to this study monitors equal or below 2.3 MP are not suitable for technical review of FFDM images for the detection of blur.

Advances in knowledge: This research proposes the first observer standard for the visual detection of blurring.

Key words: Simulated motion; technical recall; monitor resolution; observer standard; blurring detection

1. Introduction

Image blurring due to motion unsharpness in full field digital mammography (FFDM) is a widely recognized problem in the UK and various explanations exist about how it occurs [1, 2]. One explanation is breast/paddle movement whilst the exposure is being made [1-4]. Other factors such as inadequate compression and patient movement together with long exposures may also cause blurring [5].

Blurring has the potential to increase false negative results as it may obscure small or low-density microcalcification cancers and larger lesions particularly in dense breast tissue. Technical repeat due to blurring increases client radiation dose, overall examination time and can raise client anxiety. Technical recall is necessary if blurring is not seen at the attendance time and it could add further to client and family anxiety [6], as unlike a technical repeat taken at the time of the initial examination the woman will have to wait several days for repeat imaging.

Little has been published about blurred mammography images. In 2000 Seddon et al. reported that over 90 % of their screening mammogram technical recalls were due to blurred images [5]. More recently blurred images were found to be a major source of technical recall in Manchester, UK [7]. In an unpublished audit in one of our breast screening units we found that 0.86 % (40

out of 4650 FFDM examinations) of clients were recalled due to image blur; this contributed almost one third (29 %) of the 3 % maximum permissible recall rate in the National Health Breast Screening Programme (NHSBSP) [8]. For some of these images the blurring could only be detected when they were displayed on 5 MP reporting grade monitors at the time of reporting. In many instances blurring was missed when the images were checked for technical accuracy at the time of imaging. We believe this discrepancy could be due to the lower quality non-diagnostic quality monitors used in clinical rooms coupled with variable and also generally brighter ambient lighting when compared to reporting rooms. Interestingly, a good deal of research emphasis has been placed on the evaluation of reporting grade monitors and the environment in which they sit [9-11], but surprisingly little has been placed on the evaluation of technical review monitors used within mammography imaging rooms or X-ray imaging rooms generally. In the context of breast screening, only one study in 2016 by Kinnear and Mercer [12] was found which reported the ability of observers to visually detect image blurring in FFDM images on 5 MP and 1 MP monitors; the lower resolution monitor resulted in a lower visual detection rate for blurred images. Kinnear and Mercer's study represents an important first step and our study builds on this in various ways. First, our study has a much larger group of observers thereby enabling inter observer differences to be considered; second, simulation of blurring is used in which the exact amount of blurring is known; third, image selection went through a rigorous and carefully documented evidence-based approach; finally, the images were displayed in a room where the ambient lighting was controlled and standardized.

Aside monitor resolution, it is possible that observer ability to visually identify blur will also affect technical recall rates. Currently no performance data exists on observer ability to detect blur. However, early work by Ma et al [3] suggested that 0.4 mm of simulated blur can be

visually detected on 5 MP reporting grade monitors. Limitations of Ma et al's study relates to the low number of observers used and the observers being experienced image readers who are not representative of the practitioners who undertake mammography imaging.

Our study has two aims: to investigate whether there is a difference in the visual detection of blurring between a 2.3 MP technical review monitor and a 5 MP reporting grade monitor; to propose an observer standard for the visual detection of blurring on reporting grade 5 MP monitors.

2. Materials and methods

Mammography images were acquired in 2014 on a Selenia Dimensions FFDM unit (Hologic®, Bedford, MA) which has a 24 cm x 29 cm amorphous silicon (a-Si) thin-film transistor (TFT) image receptor with 70 micron pixel size and spatial resolution of 7.1 lp/mm [13] within the UK Breast Screening Programme. Two experienced image readers independently reviewed a number of images using published quality criteria [14] to identify twenty normal and artifact free FFDM images. These comprised of craniocaudal (CC) and mediolateral oblique (MLO) images. Mathematical simulation software [3] with a soft-edge mask was used to simulate the effect of motion in the 20 images. Soft-edge mask simulates motion by applying a mathematical algorithm known as convolution function based on a Gaussian distributed pixel under simulated motion [15, 16]. Motion blurring was added to the images by accumulating the pixel intensity of randomized microsteps within 1.5mm motion boundary [3]. The soft-edge mask method was chosen because it best represents the physical process that caused the blurring effect.

Simulated blurring was imposed to the 20 artifact free FFDM images from 0.2 to 1.0 mm at 0.2 mm increments. 120 images were available for use - 100 with five levels of simulated motion and 20 with no blur. Figures 1 and 2 show examples of FFDM images with and without simulated blur imposed.

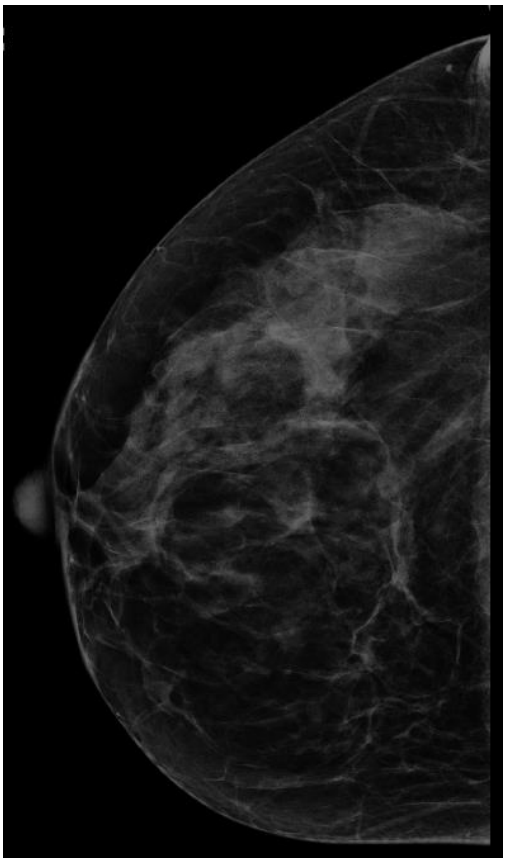

Figure 1: FFDM image with no blur

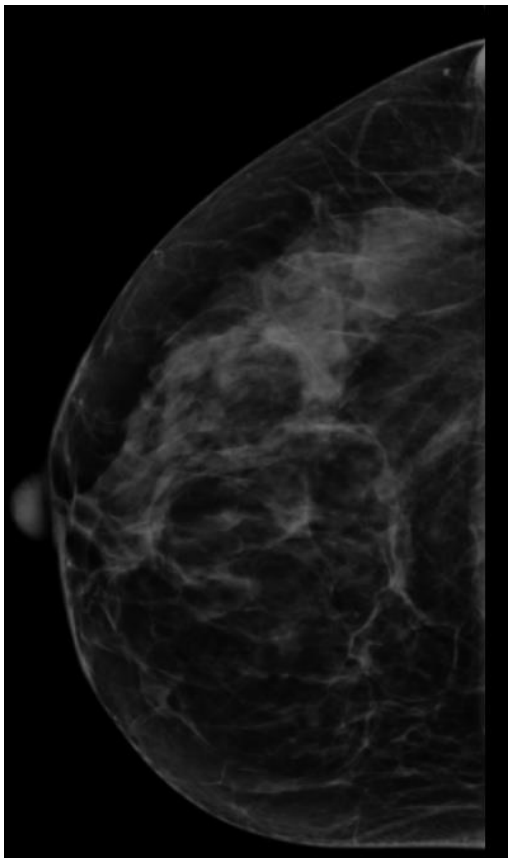

Figure 2: FFDM image with 1 mm simulated blur

The 120 images were de-identified, randomized and displayed at full screen size on a 24 inch 2.3 MP monitor (NEC, Multisync 243wm) with 0.27 mm pixel pitch and 1920 x 1200 display resolution; and a 21.3 inch 5 MP monitor (NDS, Dome E5) with 0.17 mm pixel pitch and 2560 x 2048 display resolution. Both monitors were calibrated to the DICOM Grayscale Standard

Display Function [17]. Dimmed ambient lighting (less than 10 lux) was used for both monitor viewing sessions, being consistent with that employed in normal image reading conditions [14]. Images were displayed using MediViewer (Schaef Systemtechnik, Petersaurach, Germany). No interpolation method was used to map image pixels onto the display pixels. Observers were blinded to the type of monitor used as both monitors have similar dimensions and appearance; and information about the monitor was not displayed anywhere. Images were viewed on a blinded basis by 28 observers without knowing the amount of blurring. Window width and level was set to values agreed by consensus between two experienced FFDM image readers prior to the observers commencing the study; width and levels were set to give image appearances similar to those seen in routine practice.

In clinical practice distance between the monitor and observer's eye is not standardized or controlled. This is because observers constantly change the distance between their eye and the monitor when viewing images. Our study allows this variation of distance to be preserved by positioning the chair such that observers' eye to monitor distance would not exceed 75 cm. A viewing distance of 75 cm was chosen because it is within the viewing range (64 to 89 cm) which maintains the extraocular muscles in a more relaxed state and minimizes eye strain [18]. However, we did not control or measure the distance from eyes to monitors as this was not the focus of our study. Two calculations on angular size will be performed, one at 30 cm and one at 75 cm, as these are likely to be the extremes of distance that observers might view images.

Angular size is a measurement that describes how large an object appears from a given point of view, defining the distance between the two ends of an object. The capacity to identify blurring depends on the potentialities of the human visual system. To identify the minimum amount of

blurring that can be detected by the observer the angular size for each level of motion was calculated with the equation shown below [19]:

$$\text{Angular size in degree} = 57.3 \times \text{physical size/viewing distance}$$

Where physical size is the level of motion in mm.

Twenty-six radiographers qualified in mammography imaging and two radiologists ('observers') from two breast screening centres in the North West of England (UK) were invited to review the 120 images on the 2.3 MP technical review monitor and the 5 MP reporting grade monitor. None of the observers reported visual pathologies and image evaluation was conducted with optical correction if glasses had been prescribed previously. The observers were approached individually and asked if they would be willing to participate; of those that agreed they were provided with written information about the research before conducting it. This study was classified as service evaluation in both breast screening centres; Clinical Audit Department permission was granted formally on this basis from both hospitals. Anonymity was provided by one coordinating staff member within each centre assigning a unique code to each observer; only the observer and coordinating staff member knew the code. Feedback was given only on an individual basis to each observer. Observers' age varied from 26 to 59 years (mean = 44.5, SD = 8.3 years). Mammography experience varied from 0.4 to 25 years (mean and median experience was 9.9 years and 10 years respectively, SD = 4.9 years, interquartile range = 7.5 years).

The observers were not permitted to magnify the images or adjust the window width and level. Image manipulation was not permitted due to the need to tightly control the viewing conditions to exclude sources of error [20-22]. If the observers were allowed to manipulate images based on

their personal preferences in display then the study could be comparing the ability of the observers to manipulate images as well as detect blurring on the two monitors.

For each image the observers had to indicate whether blurring was present or not, this was a binary decision (yes = 1, no = 0). As in Mucci et al's study [23], Fleiss' kappa analysis was carried out to determine the inter-observer variability [24]. To minimize fatigue, image review sessions did not exceed 30 minutes [25] and each monitor took approximately 1 hour to complete, therefore 4 viewing sessions were required (approximately 2 hours per observer was needed) to review the images on the 2.3 and 5 MP monitors. Due to clinical demands, data collection had to be conducted over an eight month period. Experimental conditions and observer training for the experiments were overseen and controlled/standardized by two members of staff – one in each clinical centre. Also, all observers underwent a training exercise to help them identify blurred and non-blurred images. This exercise was conducted by an experienced image reader using a 5 MP reporting grade monitor; for this exercise clinical FFDM images were drawn from each of the two screening programmes to train the observers. These images contained blurred and non-blurred examples.

Blurring detection rate at each level of motion for 2.3 and 5 MP monitors was calculated. The equation for blurring detection rate (BD) is shown below.

$$BD = Ni/Nb$$

Where Ni is the number of blurred mammograms identified by the observers; Nb is the number of blurred mammograms.

Chi-squared (X^2) test was used to determine whether significant differences in blurring detection rate existed between the 2.3 and 5 MP monitors. The influence of level of motion, monitor resolution, observers' experience and age on blurring detection was modeled in a logistical regression model.

Technical recall rate at each level of motion for 2.3 and 5 MP monitors was calculated according to the NHSBSP recommendations [26]. In this study, the number of mammograms required to repeat (Nr) was estimated by the number of blurred mammograms missed by the observers (Nm) which is equal to the difference between the number of blurred mammograms (Nb) and the number of blurred mammograms identified by the observers (Ni).

The equation for technical recall rate (TC) is shown below.

$$TC = Nr/Nt$$

$$= Nm/Nt$$

$$= (Nb-Ni)/Nt$$

Where TC is the technical recall rate; Nr is the number of mammograms required to repeat; Nt is the total number of mammograms taken; Nb is the number of blurred mammograms and Ni is the number of blurred mammograms identified by the observers.

The upper quartile for the blurring detection rate on the 5 MP monitor was calculated to develop the observer standard for the visual detection of blurring. The upper quartile was used to set the minimum standard for blur detection because it represents the highest 25 percent of the data. If the blurring detection rate is at 75th percentile it means 75 percent of the observers would perform the same as or less than this level and 25 percent would perform better than this level.

3. Results

The average blurring detection rate for the 2.3 and 5 MP monitors are shown in Figure 3. All the non-motion images were identified correctly. As can be seen in Figure 3 the blurring detection rate increases with simulated motion and monitor resolution. The 5 MP monitor has a higher average blurring detection rate than the 2.3 MP monitor.

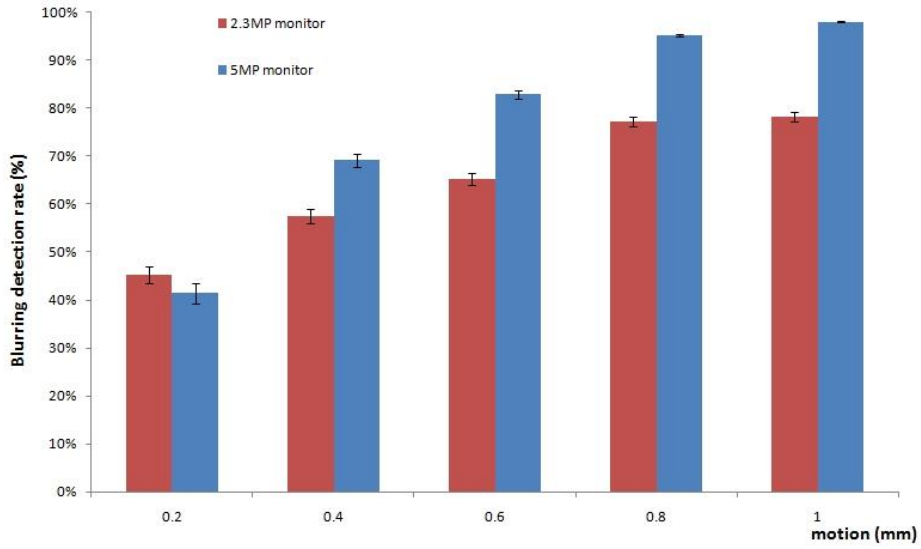

Figure 3. Blurring detection rate against level of motion, the error bars represent the standard errors.

Chi-Squared (X^2) test revealed that there was no significant difference in blurring detection between the 2.3 and 5 MP monitors for 0.2 mm motion, X^2 (1, N=1095) =1.61, p=0.20). While there were significant differences in blurring detection between 2.3 and 5 MP monitors for 0.4 mm (X^2 (1, N=1095) = 17.50, p<0.001), 0.6 mm (X^2 (1, N=1095) = 44.44, p<0.001), 0.8 mm (X^2 (1, N=1095) = 75.26, p<0.001) and 1 mm (X^2 (1, N=1095) = 108.32, p<0.001) motion.

Fleiss' kappa for 5 MP and 2.3 MP monitors is 0.48 and 0.11 respectively and the mean kappa is 0.26. A kappa of 1 indicates perfect agreement where a kappa of 0 indicates agreement equal to chance [24].

Cohen's d was used to measure the effect size for factors in the logistical regression model. The Cohen's d values for level of motion, monitor resolution, observers' experience and age are 0.38, 0.35, 0.09 and 0.05 respectively. Cohen's d of 0.2 can be consider as "small" effect, around 0.5 as "medium" effect and larger than 0.8 as "large" effect [27].Therefore, the Cohen's d value

indicated that in this study observers' experience and age are not good predictors for blurring detection.

The angular size for each level of motion for viewing distances of 30 cm and 75 cm is summarized in Table 1. As can be seen, the angular size increases with the level of motion and it is bigger when the observers are closer to the monitor (30 cm). Individuals with 20/20 vision have the ability to recognize a pixel if the angular size is equal or larger than 60 arc seconds. The angular size for 0.2 mm motion at 75 cm is 55 arc seconds which is smaller than the threshold and such a small change cannot be identified by the human eye [27, 28].With this in mind, we propose the minimum amount of motion required for visual detection of blurring in this study is 0.4 mm.

The technical recall rates for 2.3 and 5 MP monitors were calculated and summarized in Table 2. As can be seen in Table 2, the technical recall rate decreased with the level of motion and monitor resolution. The technical recall rate for the 2.3 MP monitor varies from 3.6 % to 7.1 % and for the 5 MP monitor it varies from 0.3 % to 5.1 %. The 2.3 MP monitor has a higher overall technical recall rate (20.3 %) compared to 5MP monitor (9.1 %). For example, at 1 mm motion the recall rate for 2.3 and 5 MP monitors are 3.6 % and 0.3 % respectively which means for 1000 clients the number of recall would be 36 and 3 respectively.

The upper quartile for the blurring detection rates on the 5 MP monitor are summarized in Table 3. The observer standard for the minimum standard of blurring detection at 0.4, 0.6, 0.8 and 1.00 mm level of motion is 96 %, 100 %, 100 % and 100 % respectively.

4. Discussion

The results from the monitor comparison study confirm that a monitor with lower resolution (eg 2.3 MP) would likely have a poorer visual detection rate for FFDM image blurring compared with a higher resolution reporting grade monitor (5 MP). The number of blurred images missed by the observers (Nm) for the lower resolution monitor is higher than the number in the higher resolution monitor, which leads to a higher technical recall rate for the lower resolution monitor.

In clinical practice as some technical review monitors have resolutions as low as 1 MP [12], we can confidently propose that such monitors would have even poorer blurred image visual detection rates than the one used in our study (2.3 MP). Further work is needed to determine the minimum specifications of a technical review monitor for use in imaging rooms for which technical recall rates could be suitably low for clinical purposes. It is worth noting that our data suggests that there is a 55 % reduction in the technical recall rate if a 5 MP reporting grade monitor is used for checking images in the clinical rooms. This would reduce the need for additional time slots for appointments as well as the cost of the administrative overhead for booking the appointments. Also it would minimize client/client family anxiety and costs for the re-attendance.

Resolution acuity refers to the smallest amount of spatial detail necessary to distinguish a difference between patterns or features in a visible target [28]. Individuals with 20/20 vision have the ability to recognize a minimal angle of resolution (MAR) subtended by the components of the stimulus, which has an angular size of 60 arc seconds [28, 29]. At 0.2 mm of simulated blurring there is no significant difference (X^2 (1, N=1095) =1.61, p=0.20) in blurring detection between the 2.3 and 5.0 MP monitors. One of the possible explanations is that the human visual system is not able to resolve this level of detail at a distance of 75 cm as the angular size is less than 60 arc seconds.

Angular size calculations demonstrate that blur of 0.2 motion is not possible to identify if the viewing distance is increased to 75 cm, independently of the monitor used. The impact of the visual system on diagnostic decision-making is not well understood. However, it is known that visual acuity and accommodation accuracy get worse at the end of a long radiology workday [30, 31]. Variance in the viewing distance combined with visual fatigue and a low resolution monitor can be a potential risk factor for missing the detection of blur on 2.3 MP monitors.

The selection of the motion levels used in this study was related with the early work by Ma et al [3]. Detection performance between the limits of 30 cm and 75 cm was not tested for 0.3 mm. According with our current calculations of angular size for 0.3 mm of motion it could be argued that if 0.3 mm of blurring had been used the blurring would be identifiable by the observers at 75 cm (82 arc seconds).This warrants further research to determine threshold values for detection of blurring at different distances from the monitor.

Fleiss' kappa for 2.3 MP monitors is much lower than the 5 MP monitor which suggests that using the lower resolution monitor to see blurring is more difficult compared with the higher resolution monitor. On the other hand, the mean kappa in our study is 0.26 which indicates poor agreement between observers [24]. In observer studies it is very rare to achieve perfect agreement and a range of cognitive, visual and environmental factors can be used to explain this. Also, anecdotally we know that some people find the task of differentiating blurred from non blurred images very difficult, so this could be another explanation for poor agreement. One conclusion from this could be that observers who performed less well could need additional training. This poor level of agreement raises questions about the blur detection abilities between observers which is the second aim of this study. In view of this, the observer standard developed

in our study could be used to help inform the development of competence assessment standards of observers in training programmes and in routine practice.

Intra-observer variation and inter-observer variation across professional disciplines was not included into this study. As observers only viewed each image once it is not possible to calculate the intra-observer variation. For inter-observer variation across professional disciplines the sample size for radiologists is too small (n=2) to conduct meaningful analysis. Further research is therefore warranted for intra- and inter-observer variability for different professional groups.

One of the limitations of our study is the use of motion simulation as this may not fully represent real blurring. For instance, the mathematical simulation used in our study blurs the whole image while real mammography image blurring may fully or partly affect the image. An updated version of our mathematical simulation has the ability to introduce regional blurring. Using this updated version further studies could be carried out to investigate the effect of regional blurring on observer and monitor blurring detection rates. Aside proposing an extension to our study using regional blurring it could be valuable to conduct a study using real blurred FFDM images. However, it should be noted that for real blurring it would be hard to control and identify the exact amount of blurring in the images.

Another limitation of our study is that the normal mammography screening environment might not be fully recreated in our study. For example, practitioners working in imaging rooms often do not work in levels of subdued light consistent with common reporting conditions and they probably do not have the same amount of time as image readers to scrutinize the image. Further studies could be carried out to investigate the effect of lighting and image viewing time on blurring detection rate for technical review monitors.

Finally, we did not take into account observers' previous activities. For example visual fatigue may occur if a radiologist or radiographer finished a reporting session and then immediately took part in the study. Further studies could be carried out to investigate the effect of visual fatigue on blurring detection rates and also other factors, as indicated earlier, which can impact upon observer performance.

5. Conclusions

According to our study monitors equal to or lower than 2.3 MP are not suitable for technical review of FFDM images for the detection of blur. The minimum amount of motion required for visual detection of blurring in our study is 0.4 mm and the observer standard for blur detection at 0.4, 0.6, 0.8 and 1 mm level of simulated blurring are 96 %, 100 %, 100 % and 100 % on a 5 MP monitor.

References:

1. Ma WK, Brettle D, Howard D, Kelly J, Millington S, Hogg P. Extra patient movement during mammographic imaging: An Experimental Study. Br J Radiol 2014; 87:20140241. doi: 10.1259/bjr.20140241.

2. Ma WK, McEntee MF, Mercer CE, Kelly J, Millington S, Hogg P. Analysis of motion during the breast clamping phase of mammography. Br J Radiol 2016; 89: 20150715. doi: 10.1259/bjr.20150715

3. Ma WK, Aspin R, Kelly J, S. Millington, Hogg P. What is the minimum amount of simulated breast movement required for visual detection of blurring? An exploratory investigation. Br J Radiol 2015; 88: 20150126. doi: 10.1259/bjr.20150126

4. Ma WK, Hogg P, Kelly J, Millington S. A method to investigate image blurring due to mammography machine compression paddle movement. Radiography 2015; 21:36-41. doi: 10.1016/j.radi.2014.06.004

5. Seddon D, Schofield K A, Waite C A. Investigation into possible caused of blurring in mammograms. Breast Cancer Res. 2000; 2(suppl2): A64. doi: 10.1186/bcr253\

6. Hogg P, Kelly J, Claire E, eds. Digital mammography: a holistic approach. 1st ed. London, UK: Springer; 2015

7. O'Rourke J, Mercer CE, Starr L. Programme evaluation: Technical recall and image blur within a breast screening service. Symposium Mammographicum 2014, British Institute of Radiology,UK: Bournemouth; 2014. Available from: http://www.birpublications.org/doi/pdf/10.1259/conf-symp.2014

8. NHS Cancer Screening Programmes. Consolidated guidance on standards for the NHS Breast Screening Programme. NHSBSP Publication No 60 (Version 2), UK: Sheffield; 2005.

9. Shiraishi J, Abe H, Ichikawa K, Schmidt RA, Doi K. Observer study for evaluating potential utility of a super-high-resolution LCD in the detection of clustered microcalcifications on digital mammograms. J Digit Imaging. 2010; 23(2):161-9. doi: 10.1007/s10278-009-9192-x.

10. Schueller G, Schueller-Weidekamm C, Pinker K, Memarsadeghi M, Weber M, Helbich TH. Comparison of 5-megapixel cathode ray tube monitors and 5-megapixel liquid crystal monitors for soft-copy reading in full-field digital mammography. Eur J Radiol. 2010; 76(1):68-72. doi: 10.1016/j.ejrad.2009.04.070.

11. Kamitani T, Yabuuchi H, Matsuo Y, Setoguchi T, Sakai S, Okafuji T et al. Diagnostic performance in differentiation of breast lesion on digital mammograms: comparison among hard-copy film, 3-megapixel LCD monitor, and 5-megapixel LCD monitor. Clin Imaging 2011;35(5):341-5. doi: 10.1016/j.clinimag.

12. Kinnear L, Mercer CE. A study to compare the detection of visual blurring in 1 MP and 5MP monitors within mammography clinical practice. Imaging and Therapy Practice 2016; p.23-28. ISSN 1360-5518.

13. Selenia Dimensions Mammography System datasheet; 2016 Available from: http://www.hologic.com/sites/default/files/DS-05534_rev002_SeleniaDimensions13Jan2016.pdf

14. Perry N, Broeders M, Wolf C, Törnberg S, Holland R, Karsa L. European guidelines for quality assurance in breast cancer screening and diagnosis. 4th edn. Luxembourg: European Communities; 2006.

15. Young SS, Driggers GR, Jacobs LE. Signal processing and performance analysis for imaging systems. 1st edn. New York, NY: Artech House; 2008.

16. Dougherty G. Digital image processing for medical applications. 1st edn. Cambridge, UK: Cambridge University Press; 2009.

17. National Electrical Manufacturers Association (NEMA) Digital Imaging and Communications in Medicine (DICOM) Part 14: Grayscale Standard Display Function; 2011.

18. Krupinski EA, Flynn MJ. IT reference guide for the practicing radiologist. Reston, VA: American College of Radiology; 2013. Available from: http://www.acr.org/~/media/ACR/ Documents/PDF/Advocacy/IT%20Reference%20Guide/IT%20 Ref%20Guide%20Displays.pdf

19. Legge GE, Bigelow CA. Does Print Size Matter for Reading? A review of findings from vision science and typography. J Vis. 2011;11(5):8-8.

20. Thompson JD, Chakraborty DP, Szczepura K, Tootell AK, Manning JD and Hogg P. Effect of reconstruction methods and x-ray tube current–time production nodule detection in an anthropomorphic thorax phantom: a crossed-modality JAFROC observer study, Med. Phys. 2016; 43 (3): 1265-1274.doi: 0094-2405/2016/43(3)/1265/10

21. Thompson JD, Hogg P, Manning DJ, Szczepura K, Chakraborty DP. A free-response evaluation determining value in the computed tomography attenuation correction image for revealing pulmonary incidental findings: a phantom study, AcadRadiol 2014; 21:538–545. doi:10.1016/j.acra.2014.01.003.

22. Thompson JD, Hogg P, Higham S and Manning DJ. Accurate localization of incidental findings on the computed tomography attenuation correction image: the influence of tube current variation. Nuclear Medicine Communications 2013; 34 (2):180-184. doi: 10.1097/MNM.0b013e32835c0984

23. Mucci B, Murray H, Downie A, Osborne K. Interrater variation in scoring radiological discrepancies. The British Journal of Radiology. 2013;86(1028):20130245. doi:10.1259/bjr.20130245.

24. Gwet, K L. Handbook of Inter-Rater Reliability. 4th edn. Gaithersburg, USA: Advanced Analytics; 2014.

25.Anshel JR, Visual Ergonomics in the Workplace, American Association of Occupational Health Nurses Journal 2007; 55: 414–420. doi: 10.1177/216507990705501004

26. NHS Cancer Screening Programmes. Collecting, Monitoring and Reporting Repeat Examinations. NHSBSP Good Practice Guide No 4 (Version 2), UK: Sheffield, 2006.

27. Geher G, HallS. Straight forward Statistics: Understanding the Tools of Research. 1sted. London, UK: Oxford university press; 2014

28. Glaser JS. Neuro-Ophthalmology. 3rd edn. Philadelphia: Lippincott Williams & Wilkins; 1999.

29. Healey C G. and Sawant A. On the limits of resolution and visual angle in visualization. ACM Trans. Appl. Percept 2012; 9(4). doi:10.1145/2355598.2355603

30. Safdar NM, Siddiqui KM, Qureshi F, et al. Vision and quality in the digital imaging environment: how much does the visual acuity of radiologists vary at an intermediate distance? Am J Roentgenol 2009;192:W335–W340. doi:10.2214/AJR.07.3515.

31. Krupinski EA, Berbaum KS, Caldwell RT, Schartz KM, Kim J. Long radiology workdays reduce detection and accommodation accuracy. J Am Coll Radiol 2010;7:698–704. doi:10.1016/j.jacr.2010.03.004.

Table 1: Angular size for different levels of motion

Level of motion (mm)	*Angular size (degree)*		*Angular size (arc seconds)*	
	30 cm	*75 cm*	*30 cm*	*75 cm*
0.2	*0.0382*	*0.01528*	*138*	*55*
0.4	*0.0764*	*0.03056*	*275*	*110*
0.6	*0.1146*	*0.04584*	*413*	*165*
0.8	*0.1582*	*0.06112*	*550*	*220*
1	*0.1910*	*0.07640*	*688*	*275*

Table 2: Technical recall rate (TC) for 2.3MP and 5MP monitors

Level of motion (mm)	0.4	0.6	0.8	1	Total
TC for 2.3MP monitor	7.1%	5.8%	3.8%	3.6%	20.3%
TC for 5MP monitor	5.1%	2.9%	0.8%	0.3%	9.1%

Table 3: Observer standard for the minimum standard of blurring detection for 5 MP monitor

Level of motion (mm)	0.4	0.6	0.8	1
Upper quartile (75^{th} percentile)	96%	100%	100%	100%

Closed-loop control of compression paddle motion to reduce blurring in mammograms

Ma, W, Hogg, P and Howard, D

http://dx.doi.org/10.1002/mp.12333

Full paper

Closed-loop control of compression paddle motion to reduce blurring in mammograms

AUTHORS AND AFFIFIATIONS:

***Wang Kei Ma[a], David Howard[b], Peter Hogg[a]**

***corresponding author**

Address correspondence to: Mr Wang Kei Ma. E-mail: carnby2000@gmail.com

a. Directorate of Radiography, University of Salford, Salford, UK, M5 4WT

b. School of Computing, Science & Engineering, University of Salford, Salford, UK, M5 4WT

Abstract

Background: Since the introduction of full field digital mammography (FFDM) a large number of UK breast cancer screening centers have reported blurred images, which can be caused by movement at the compression paddle during image acquisition.

Purpose: To propose and investigate the use of position feedback from the breast side of the compression paddle to reduce the settling time of breast side motion.

Method: Movement at the breast side of the paddle was measured using two calibrated linear potentiometers. A mathematical model for the compression paddle, machine drive and breast was developed using the paddle movement data. Simulation software was used to optimize the position

feedback controller parameters for different machine drive time constants and simulate the potential performance of the proposed system.

Results: The results obtained are based on simulation alone and indicate that closed-loop control of breast side paddle position dramatically reduced the settling time from over 90 seconds to less than 4 seconds. The effect of different machine drive time constants on the open-loop response is insignificant. With closed-loop control, the larger the time constant the longer the time required for the breast side motion to settle.

Conclusions: Paddle motion induced blur could be significantly reduced by implementing the proposed closed-loop control.

Keywords: Paddle motion, motion blurring, breast compression, closed-loop control, breast side motion

List of figure captions

Figure 1: Alternative control systems for breast compression: a) using only machine side position feedback; b) also using breast side position feedback.

Figure 2: Schematic diagram of the experimental setup

Figure 3: The simplest lumped parameter model of the paddle and breast

Figure 4: Models of the alternative control systems: a) conventional open-loop; b) closed-loop using breast side position feedback.

Figure 5: Experimental data for paddle movement against time for the Selenia Dimensions 18x24 cm and 24x30 cm paddles

Figure 6: Experimental data for paddle movement against time for the Lorad Selenia 18x24 cm and 24x30 cm paddles

Figure 7: The step responses of the Selenia Dimensions open-loop breast compression system for machine drive time constants (τ) of 0.1s, 0.2s and 0.4s (i.e. without breast side position feedback). The upper group of curves (τ1-τ3) are for the 24x30 cm paddle and the lower group of curves (τ4-τ6) are for the 18x24 cm paddle. Note that the differences between the three responses for each paddle are negligible.

Figure 8: The step responses of the Lorad Selenia open-loop breast compression system for machine drive time constants (τ) of 0.1s, 0.2s and 0.4s (i.e. without breast side position feedback). The upper group of curves (τ1-τ3) are for the 24x30 cm paddle and the lower group of curves (τ4-τ6) are for the 18x24 cm paddle. Note that the differences between the three responses for each paddle are negligible.

Figure 9: The step responses of the Selenia Dimensions closed-loop breast compression system for machine drive time constants (τ) of 0.1s, 0.2s and 0.4s (i.e. with breast side position feedback). The curves labelled τ1-τ3 are for the 24x30 cm paddle and the curves labelled τ4-τ6 are for the 18x24cm paddle.

Figure 10: The step responses of the Lorad Selenia closed-loop breast compression system for machine drive time constants (τ) of 0.1s, 0.2s and 0.4s (i.e. with breast side position feedback). The curves labelled τ1-τ3 are for the 24x30 cm paddle and the curves labelled τ4-τ6 are for the 18x24cm paddle.

Notation

c_b	Breast viscous friction coefficient
c_m	Motor viscous friction coefficient
C_1 and C_2	Arbitrary constants which depend on initial conditions at the start of the movement
$G_{drive}(s)_{CL}$	Machine drive closed-loop transfer function
$G_{drive}(s)_{OL}$	Machine drive open-loop transfer function
G_{dyn}	Paddle and breast 2nd order dynamics
G_{gain}	Paddle and breast steady-state gain
G_{PID}	PID controller transfer function
G_{sys}	Paddle and breast transfer function
J_m	The machine's effective inertia
k_b	Breast spring constant
k_c	Proportional gain for the machine drive control
k_m	Motor gain
k_p	Paddle spring constant
k_{prop}	Proportional gain of the PID controller
k_{integ}	Integral gain of the PID controller
k_{deriv}	Derivative gain of the PID controller
m_b	Effective mass of the breast and paddle
R	Ratio between linear velocity of the paddle ($\dot{x}_m$) and motor angular velocity ($\dot{\theta}_m$)
s	The Laplace variable
T_m	Motor torque
x_m	Machine side paddle position

x_p	Breast side paddle position
$x_{p_{ss}}$	Steady-state breast side paddle position
τ	Machine drive time constant
ω_n	System natural frequency
ζ	System damping ratio
$\dot{\theta}_m$	Motor angular velocity
λ_1 and λ_2	Empirically identified exponents that describe the motion of the paddle.

1. Introduction

Since the introduction of full field digital mammography (FFDM) a large number of UK breast cancer screening centers have identified blurred images during local audit; however, few reports have been published about the causes and possible solutions[1,2]. Blurring can be caused by a number of factors including inadequate breast compression, long exposures and patient movement[3]. Studies have also shown that image blurring can be caused by movement of the compression paddle during image acquisition[4,5,6]. Previous research into paddle motion has demonstrated that the settling time required for the compression paddle motion to become negligible is approximately 30 seconds and most of the movement occurs within the first 10 seconds, which is when the mammography image would normally be formed[6].

Current breast compression systems control the position of the machine side of the paddle (i.e. the side on which it is attached to the machine) and, if position feedback is used, it is feedback from the machine side (e.g. in the manner shown in Figure 1a). Therefore, even if the machine side motion settles quickly, there is no guarantee that the remainder of the paddle and breast do not

continue to move during image acquisition causing motion blurring. In light of this and building on the work of Ma et al[6] on paddle movement, we propose a new feedback control system with the aim of minimizing the settling time of the paddle as a whole and, hence, the breast. Referring to Figure 1b, we propose the use of position feedback from the breast side of the paddle (the right-hand side in Figure 2) so that the machine drive is controlled in such a manner that the breast side motion settles quickly. This relies on the assumption that this better reflects breast motion as a whole because, when the machine side is stationary, any change in compressed breast thickness and shape will change the amount of paddle-bend and hence the position of the breast side of the paddle.

Referring to Figure 1b, in the proposed solution, a proportional, integral and derivative (PID) controller is driven by the error in breast side paddle position. The PID controller determines the set-point for the machine side position control (inner feedback loop). PID controllers are commonly used when a fast settling time is required and can be tuned to deal with variability in the plant transfer function[9] (see footnote). This is important in this application because female breasts vary widely in terms of size, compressed thickness and density and, hence, the plant (breast) transfer function will vary from woman to woman.

Footnote: The transfer function of a linear system is defined as the ratio of the Laplace transform of the output variable to the Laplace transform of the input variable. It is an input-output description of the behavior of a system with all initial conditions assumed to be zero[7]. Transfer functions are widely used in the study of dynamic control systems because they are algebraic functions rather than differential equations, which makes the analysis simpler[8].

In this paper we present the results of a simulation study to demonstrate the potential performance of the proposed system and, in particular, the benefits associated with using feedback of the breast side paddle position.

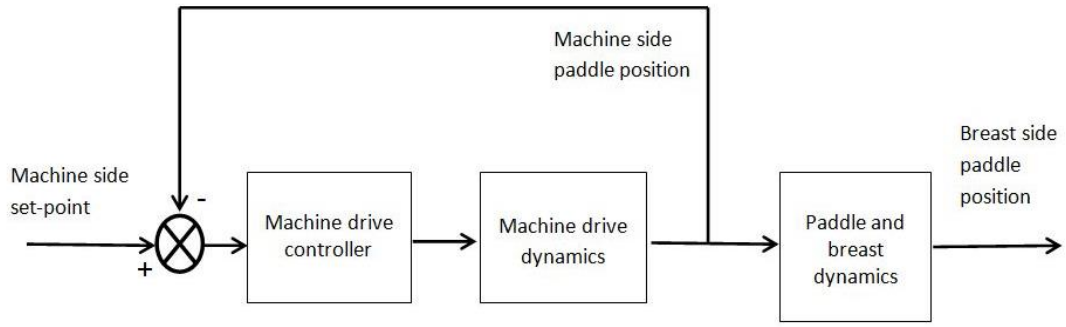

Figure 1a

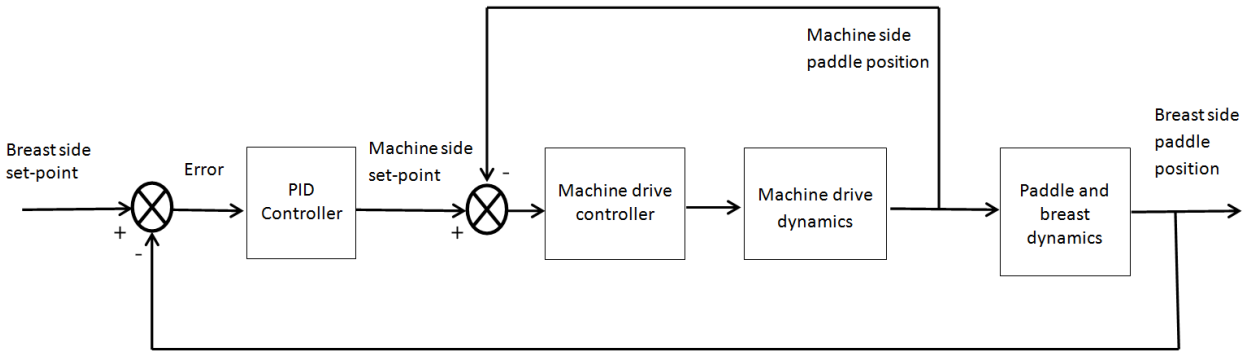

Figure 1b

Figure 1: Alternative control systems for breast compression: a) using only machine side position feedback; b) also using breast side position feedback.

2. Methods

2.1 Measurement of paddle movement

A Selenia Dimensions mammography unit (*Hologic Incorporated, Bedford, MA, USA*) and a Lorad Selenia mammography unit (*Hologic Incorporated, Bedford, MA, USA*) were used in this study, fitted with either an 18x24 cm or a 24x30 cm compression paddle. Routine equipment quality assurance (QA) was performed and the results complied with the manufacturer specifications[10]. A deformable breast phantom (*Trulife, Sheffield, United Kingdom*) with compression characteristics similar to a female breast[11] was compressed manually to approximately 80 N, after which the movement of the breast side of the paddle was recorded at 0.5 second intervals for 90 seconds. The machine side of the paddle was stationary during measurement. The movement of the breast side of the paddle was measured using two calibrated linear potentiometers (Activesensors, Dorset, United Kingdom). Figure 2 shows the experimental setup. The measurement was repeated three times to minimize the experimental uncertainties.

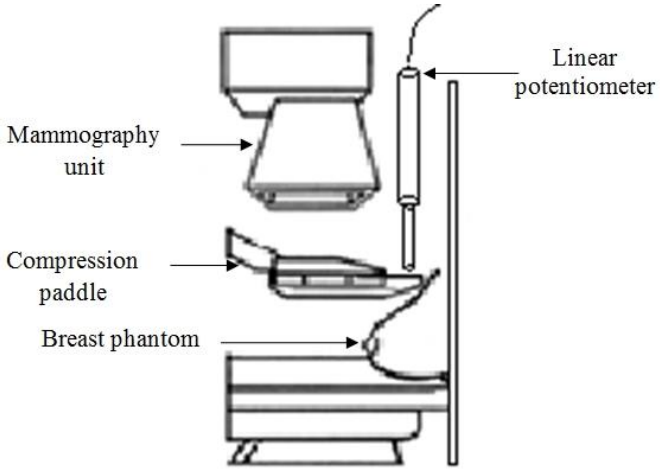

Figure 2: Schematic diagram of the experimental setup

2.2 Modeling the paddle and breast

Previous work by the authors[6] suggests that the paddle motion is that of either a 1st order system or an over-damped 2nd order system. This is also supported by the data presented in this study. To

the more appropriate of these two models, the simplest lumped parameter model was considered as shown in Figure 3. The breast is represented as being viscoelastic (c_b and k_b). The effective mass of the breast and paddle is represented by m_b. The paddle is represented by the spring k_p. In this model x_m is the machine side paddle position and x_p is the breast side paddle position.

155 Applying Newton's 2nd law we obtain:

$$k_p(x_m - x_p) - k_b x_p - c_b \dot{x}_p = m_b \ddot{x}_p \quad (1)$$

where the three terms on the left of the equation are the paddle elastic force, the breast elastic force, and the breast viscous force respectively. Rearranging equation 1 we obtain:

$$m_b \ddot{x}_p + c_b \dot{x}_p + (k_p + k_b) x_p = k_p x_m \quad (2)$$

160 Therefore we adopted an over-damped 2nd order model of the paddle and breast. Furthermore, equation 2 can be written in standard form as follows:

$$\ddot{x}_p + 2\zeta \omega_n \dot{x}_p + {\omega_n}^2 x_p = \frac{k_p}{(k_p + k_b)} {\omega_n}^2 x_m \quad (3)$$

Where $\zeta = \frac{c_b}{2\sqrt{(k_p + k_b) m_b}}$ is the system's damping ratio and $\omega_n = \sqrt{\frac{(k_p + k_b)}{m_b}}$ is the system's natural frequency.

165

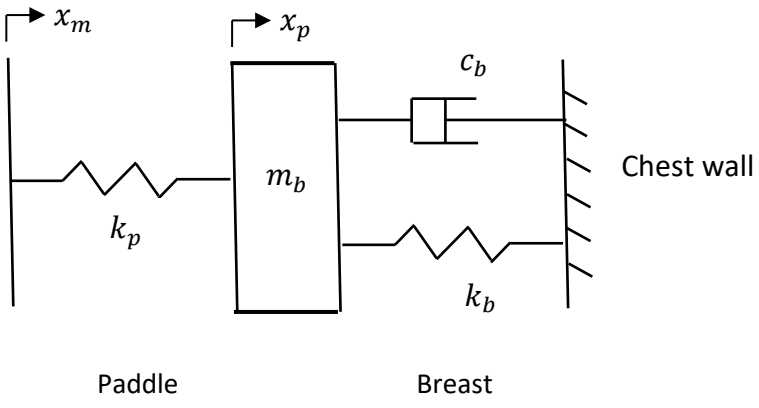

Figure 3: The simplest lumped parameter model of the paddle and breast.

Because the machine side of the paddle was stationary during our experimental measurements, the resulting motion represents the transient response only (i.e. there was no forcing function). This transient motion of the paddle and breast is the solution to the following homogeneous (or complementary) equation[12]:

$$\ddot{x}_p + 2\zeta\omega_n\dot{x}_p + \omega_n^2 x_p = 0 \quad (4)$$

Where ω_n is the system's natural frequency and ζ is its damping ratio

For over-damped 2nd order dynamics, the general solution to equation 4 is given by:

$$x_p(t) = C_1 e^{\lambda_1 t} + C_2 e^{\lambda_2 t} \quad (5)$$

Where the two exponents are given by:

$$\lambda_{1,2} = -\zeta\omega_n \pm \omega_n\sqrt{\zeta^2 - 1} \quad (6)$$

And C_1 and C_2 are arbitrary constants that depend on the initial conditions of the system at the start of the movement. The four constants in equation 5 were identified using the experimental motion data and the Mathworks curve fitting tool, which minimizes the sum of the square errors. The two values found for λ_1 and λ_2 were substituted in equations 6, which were then solved to find ω_n and ζ.

Laplace transforming both sides of equation 3 and solving for the transfer function[9] we obtain:

$$\mathrm{G_{sys}(s)} = \frac{x_p}{x_m} = \frac{k_p}{(k_b+k_p)} \frac{{\omega_n}^2}{s^2+2\zeta\omega_n s+{\omega_n}^2} \quad (7)$$

Where $\mathrm{G_{sys}(s)}$ is the paddle and breast transfer function, with the breast side paddle position (x_p) as output, the machine side paddle position (x_m) as input, and where *s* is the Laplace variable. Considering equation 7, it is clear that the model of the paddle and breast can be divided into two parts representing: a) a steady-state gain (obtained by substituting $s = 0$); and b) the 2nd order dynamics. These two parts have the following transfer functions:

$$G_{gain} = \frac{x_{p_{ss}}}{x_m} = \frac{k_p}{(k_b+k_p)}$$

$$G_{dyn}(s) = \frac{x_p}{x_{p_{ss}}} = \frac{{\omega_n}^2}{s^2+2\zeta\omega_n s+{\omega_n}^2}$$

Where $x_{p_{ss}}$ is the steady-state breast side paddle position. This assumes the breast has a linear elastic relationship which is unlikely. Furthermore, we have adopted an estimate of $G_{gain} = 0.9$ (i.e. we assume the paddle is much stiffer than the breast). However, these assumptions have little impact on the conclusions of this study as we are primarily concerned with the dynamics ($G_{dyn}(s)$), the parameters of which (ζ and ω_n) we can determine from our experimental data as described above.

2.3 Modeling the machine drive

Our aim here was to develop the simplest model of the machine drive that would allow us to compare the open-loop and closed-loop alternatives shown in Figure 1. Assuming that changes in the motor torque (T_m) propelling the machine drive can occur very quickly, and that the motor

torque overcomes viscous friction (c_m) and accelerates the machine's effective inertia (J_m), as seen by the motor, it can be shown that the following equation of motion applies:

$$J_m\ddot{\theta}_m + c_m\dot{\theta}_m = T_m \tag{8}$$

As a first approximation, if we neglect the acceleration term and include the ratio (R) between the linear velocity of the paddle ($\dot{x}_m$) and the motor angular velocity ($\dot{\theta}_m$), this simplifies equation 8 to $\dot{x}_m = k_m T_m$, where $k_m = R/c_m$. This leads to the following open-loop transfer function for the machine drive:

$$G_{drive}(s)_{OL} = \frac{x_m}{T_m} = \frac{k_m}{s} \tag{9}$$

If we assume simple closed-loop proportional control (with gain k_c), then the transfer function is given by[9]:

$$G_{drive}(s)_{CL} = \frac{x_m}{x_{m_{setpoint}}} = \frac{k_c k_m/_s}{1+k_c k_m/_s} = \frac{1}{1+\tau s} \tag{10}$$

where the time constant $\tau = 1/_{k_c k_m}$. Although a more complex model of the machine drive could be used, for our purposes we simply needed to model the machine drive's speed of response, which is determined by the time constant. Because we don't have experimental data for machine drive response and also because it will differ between machine suppliers, we have included simulation results for a range of time constants to show the effect of different machine drive dynamics.

2.4 Controller modeling and design

Referring to Figure 4, we considered two scenarios: a) conventional control where the motion of the breast side of the paddle is controlled in an open-loop manner; and b) closed-loop PID control using position feedback from the breast side of the paddle.

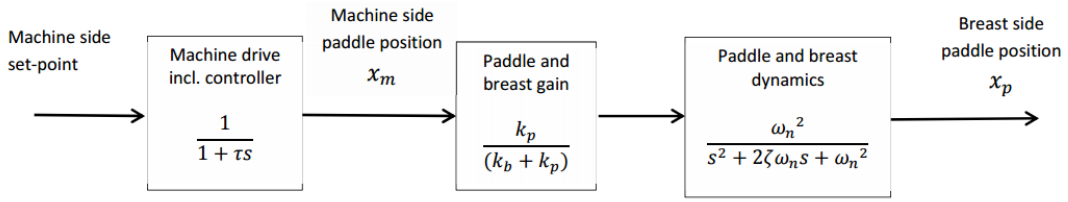

Figure 4a

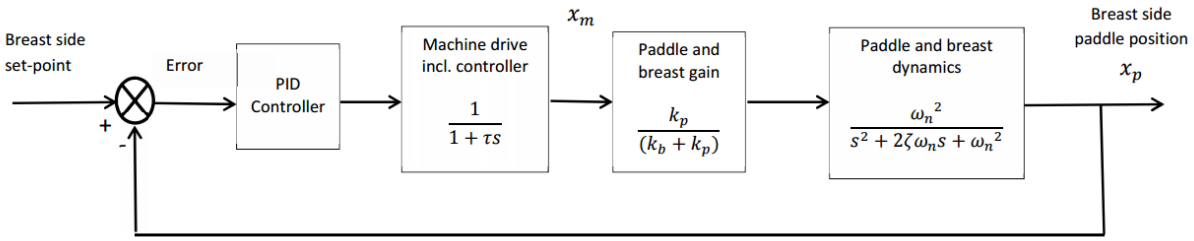

Figure 4b

Figure 4: Models of the alternative control systems: a) conventional open-loop; b) closed-loop using breast side position feedback.

Both scenarios were modeled in Mathworks Simulink and the PID controller parameters tuned to minimize the settling time of the breast side paddle motion. For the purposes of this study, in both scenarios we compare the system responses with machine drive time constants (τ) of 0.1s, 0.2s and 0.4s to determine the importance of machine drive response. In this context, $\tau = 0.4s$ is considered a conservative value, corresponding to a 95% rise time of 1.2 seconds and hence not requiring a fast servo-system. The transfer function of the PID controller is given by:

$$G_{PID} = k_{prop} + k_{integ}\frac{1}{s} + k_{deriv}s \qquad (11)$$

Where k_{prop} is the proportional gain, k_{integ} is the integral gain, and k_{deriv} is the derivative gain. The PID controller was tuned using the Mathworks Simulink response optimization tool to minimize the integral square error and also satisfy the constraint that the overshoot should be zero (because overshoot might cause breast pain).

3. Results

3.1 Experimental data and model fitting

As we expected, the paddle movement on the breast side decreased in an over-damped 2nd order manner and took approximately 80 seconds to settle (Figures 5 and 6).

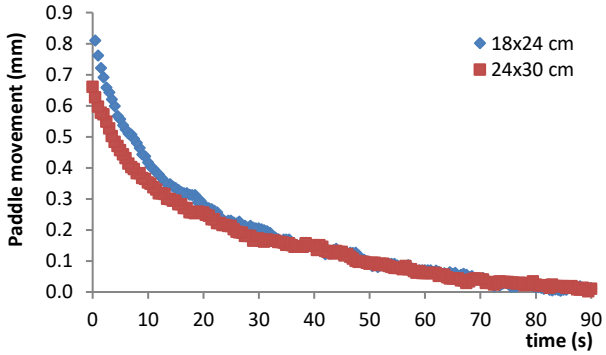

Figure 5: Experimental data for paddle movement against time for the Selenia Dimensions 18x24 cm and 24x30 cm paddles

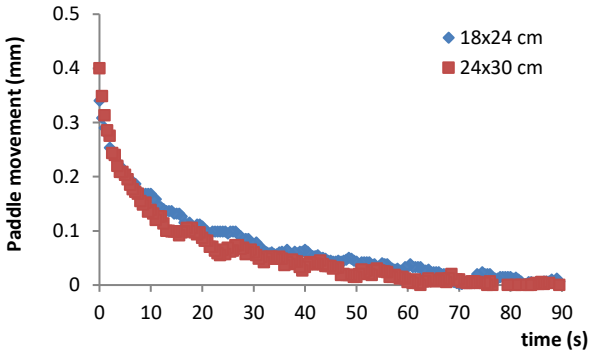

Figure 6: Experimental data for paddle movement against time for the Lorad Selenia 18x24 cm and 24x30 cm paddles

Using the curve fitting method described previously, this data was used to derive the following equations for the motion of the Selenia Dimensions and Lorad Selenia 18x24 cm and 24x30 cm paddles.

$$x_{p\ 18x24cm\ \text{Selenia}}(t) = 0.58e^{-0.036t} + 0.27e^{-0.28t} \quad (12)$$

$$x_{p\ 24x30cm\ \text{Selenia}}(t) = 0.48e^{-0.034t} + 0.18e^{-0.27t} \quad (13)$$

$$x_{p\ 18x24cm\ \mathrm{Lorad}}(t) = 0.22e^{-0.036\mathrm{t}} + 0.11e^{-0.39\mathrm{t}} \quad (14)$$

$$x_{p\ 24x30cm\ \mathrm{Lorad}}(t) = 0.21e^{-0.045\mathrm{t}} + 0.16e^{-0.32\mathrm{t}} \quad (15)$$

The coefficients of correlation (R-squared) for the Selenia Dimensions and Lorad Selenia paddles are listed in table 1.

Table 1: Coefficients of correlation (R-squared) for Selenia Dimensions and Lorad Selenia paddles

Mammography machine	Selenia Dimensions		Lorad Selenia	
Paddle size	18x24 cm	24x30 cm	18x24 cm	24x30 cm
R-squared	0.9968	0.9943	0.9874	0.9864

The two exponents in equations 12 to 15 were then used to solve for the natural frequency (ω_n) and damping ratio (ζ) of the paddle and breast. For the Selenia Dimensions paddles ω_n and ζ were found to be 0.101 rad/s and 1.565 respectively for the 18x24 cm paddle; and 0.096 rad/s and 1.591 respectively for the 24x30 cm paddle. For the Lorad Selenia paddles ω_n and ζ were found to be 0.117 rad/s and 1.799 respectively for the 18x24 cm paddle; and 0.121 rad/s and 1.531 respectively for the 24x30 cm paddle. Hence, the transfer functions for the Selenia Dimensions and Lorad Selenia paddles and breast are given by:

$$G_{dyn}(s)_{18x24cm\ Selenia} = \frac{x_P}{x_{PSS}} = \frac{0.0102}{s^2+0.3168s+0.0102} \quad (16)$$

$$G_{dyn}(s)_{24x30cm\ Selenia} = \frac{x_P}{x_{PSS}} = \frac{0.0092}{s^2+0.3049s+0.0092} \quad (17)$$

$$G_{dyn}(s)_{18x24cm\ Lorad} = \frac{x_P}{x_{PSS}} = \frac{0.0138}{s^2+0.4223s+0.0138} \quad (18)$$

$$G_{dyn}(s)_{24x30cm\ Lorad} = \frac{x_P}{x_{PSS}} = \frac{0.0146}{s^2+0.3697s+0.0146} \quad (19)$$

3.2 Controller performance

Using the Mathworks Simulink response optimization tool, PID controller gains for the Selenia Dimensions and Lorad Selenia 18x24 cm and 24x30 cm paddles were established for both scenarios (open-loop and closed-loop using breast side position feedback) and also for machine drive time constants (τ) of 0.1*s*, 0.2*s* and 0.4*s*. The PID gains and corresponding step responses for the open-loop and closed-loop systems are shown in Tables 2 and 3 and Figures 7 to 10.

Referring to Tables 2 and 3 and Figures 7 and 8, for each paddle, the open-loop step response curves for all machine drive time constants overlay one another as there are no significant differences between the curves. In other words, the effect of different machine drive time constants on the open-loop response is insignificant. However, there is a small difference between the two paddle sizes; but in both cases the settling time is very long.

Referring to Tables 2 and 3 and Figures 9 and 10, closed-loop control of breast side paddle position dramatically reduces the settling time from over 90 seconds to less than 4 seconds for a machine drive time constant of 0.4s. Furthermore, the smaller the machine drive time constant, the shorter the rise and settling times; but this effect is not as important as switching to closed-loop control in the first place. Although there are small differences between the two paddle sizes, these do not alter the observed trends or the conclusions drawn.

Table 2: PID controller gains and step response performance for Selenia Dimensions 18x24 cm and 24x30 cm paddles

290

	Machine drive time constant (τ)											
	Open-loop system						Closed-loop system					
	24x30 cm			*18x24 cm*			*24x30 cm*			*18x24 cm*		
	τ1=0.1	τ2=0.2	τ3=0.4	τ4=0.1	τ5=0.2	τ6=0.4	τ1=0.1	τ2=0.2	τ3=0.4	τ4=0.1	τ5=0.2	τ6=0.4
k_{prop}	-	-	-	-	-	-	91.96	51.39	25.99	100.77	49.66	27.11
k_{integ}	-	-	-	-	-	-	2.75	1.54	0.79	3.28	1.61	0.88
k_{deriv}	-	-	-	-	-	-	304.89	168.35	85.27	329.63	158.43	86.26
10-90% rise time	65.68	65.68	65.69	61.03	61.04	61.05	0.67	1.18	2.32	0.53	1.12	2.01
98% settling time	119.44	119.54	119.74	111.03	111.13	111.33	1.16	1.98	3.89	0.89	1.87	3.27

Table 3: PID controller gains and step response performance for Lorad Selenia 18x24 cm and 24x30cm paddles

	Machine drive time constant (τ)											
	Open-loop system						Closed-loop system					
	24x30 cm			*18x24 cm*			*24x30 cm*			*18x24 cm*		
	τ1=0.1	τ2=0.2	τ3=0.4	τ4=0.1	τ5=0.2	τ6=0.4	τ1=0.1	τ2=0.2	τ3=0.4	τ4=0.1	τ5=0.2	τ6=0.4
k_{prop}	-	-	-	-	-	-	42.78	33.13	22.26	98.20	51.55	28.41
k_{integ}	-	-	-	-	-	-	1.69	1.31	0.90	3.20	1.73	0.95
k_{deriv}	-	-	-	-	-	-	114.61	89.30	61.30	232.03	123.28	69.04
10-90% rise time	49.78	49.78	49.78	62.11	62.11	62.10	1.24	1.45	2.00	0.56	1.06	1.87
98% settling time	90.60	90.70	90.90	112.65	112.75	112.95	2.22	2.55	3.26	0.94	1.74	3.01

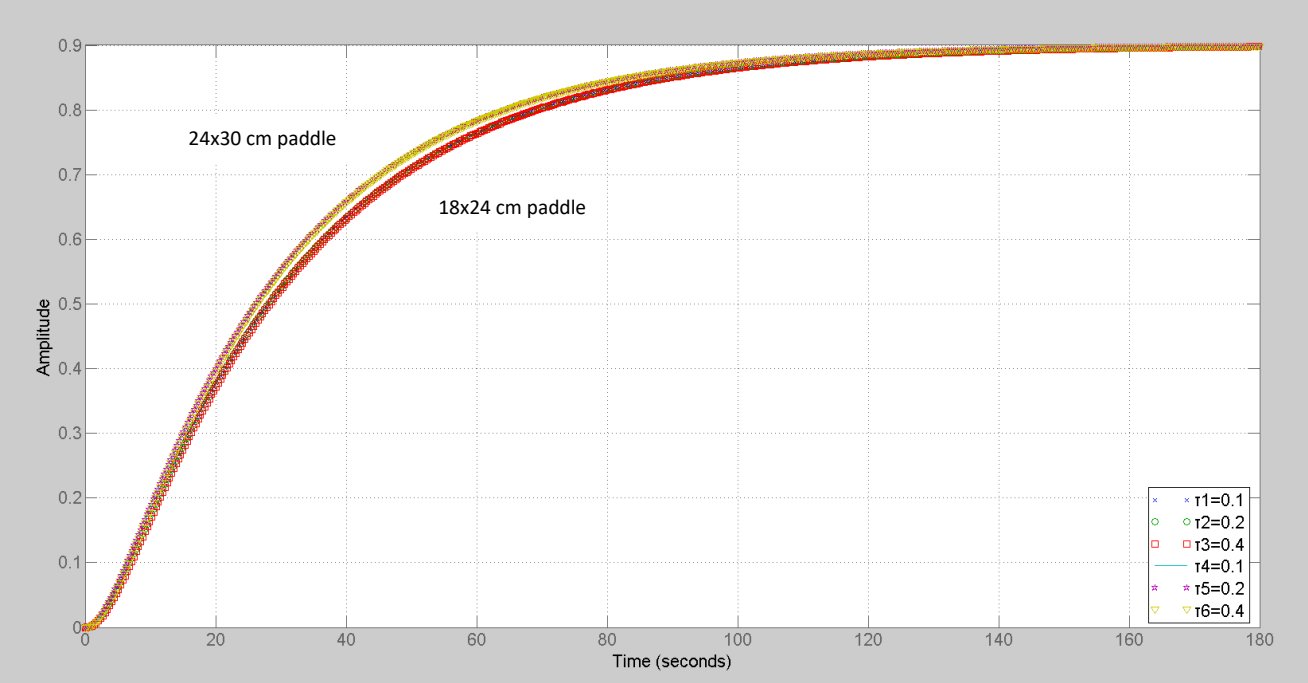

Figure 7: The step responses of the Selenia Dimensions open-loop breast compression system for machine drive time constants (τ) of 0.1s, 0.2s and 0.4s (i.e. without breast side position feedback). The upper group of curves (τ1- τ3) are for the 24x30 cm paddle and the lower group of curves (τ4- τ6) are for the 18x24 cm paddle. Note that the differences between the three responses for each paddle are negligible.

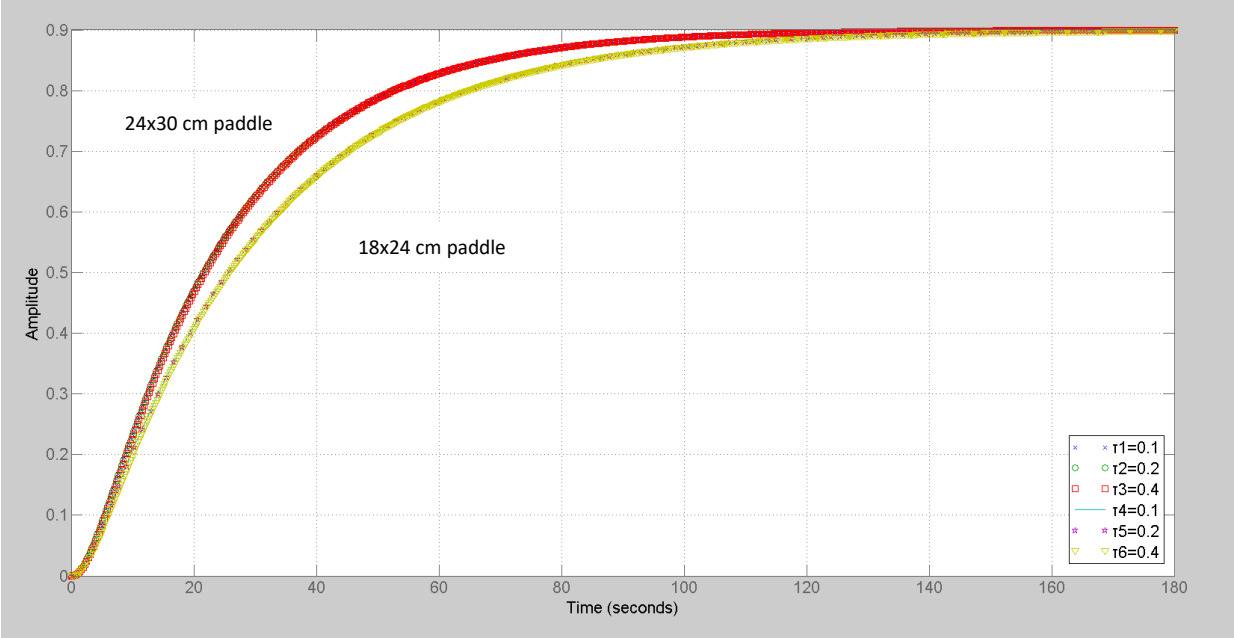

Figure 8: The step responses of the Lorad Selenia open-loop breast compression system for machine drive time constants (τ) of 0.1s, 0.2s and 0.4s (i.e. without breast side position feedback). The upper group of curves (τ1- τ3) are for the 24x30 cm paddle and the lower group of curves (τ4- τ6) are for the 18x24 cm paddle. Note that the differences between the three responses for each paddle are negligible.

295

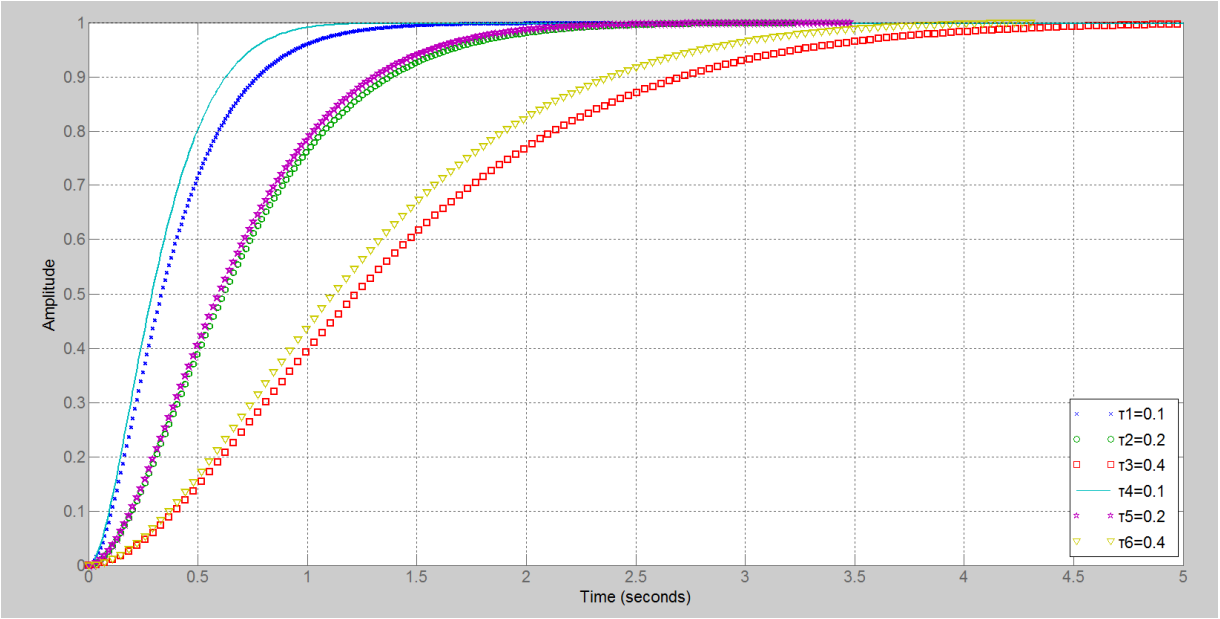

Figure 9: The step responses of the Selenia Dimensions closed-loop breast compression system for machine drive time constants (τ) of 0.1s, 0.2s and 0.4s (i.e. with breast side position feedback). The curves labelled τ1- τ3 are for the 24x30 cm paddle and the curves labelled τ4- τ6 are for the 18x24 cm paddle.

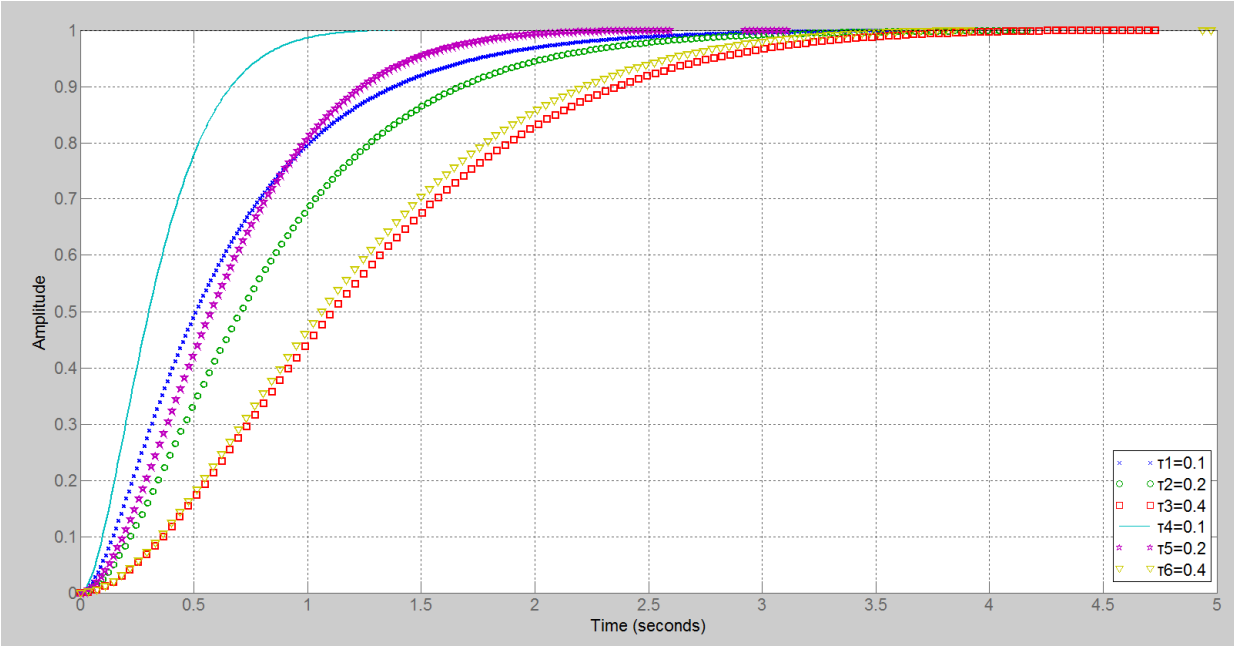

Figure 10: The step responses of the Lorad Selenia closed-loop breast compression system for machine drive time constants (τ) of 0.1s, 0.2s and 0.4s (i.e. with breast side position feedback). The curves labelled τ1- τ3 are for the 24x30 cm paddle and the curves labelled τ4- τ6 are for the 18x24 cm paddle.

4. Discussion

4.1 Clinical implications of the results

Current breast compression systems use open-loop control of breast side paddle position and, referring to Tables 2 and 3, our simulation results indicate a settling time of almost 2 minutes. This means that it is highly likely that there will still be paddle movement during image acquisition, which could cause blurring of the mammogram. Conversely, we have shown that closed-loop control of breast side paddle position dramatically reduces the settling time to less than 4 seconds (even for a slow machine drive where $\tau = 0.4s$). Therefore, it is possible that paddle motion induced blur could be significantly reduced by implementing the proposed closed-loop control of breast side paddle position.

4.2 Study limitations

This preliminary study is based on simulation alone and the results will need to be validated against in-vivo measurements taken during mammogram acquisition. However, this would require a physical prototype of a closed-loop controller using breast side paddle position feedback. The aim of the simulation study reported here was to justify the creation of such a prototype for the next stage of our work. Furthermore, we assume that the motion of the breast side of the paddle reflects breast motion as a whole. Again, physical prototyping and an experimental study would be required to confirm this.

A simple machine drive model was used in this study and this was not validated against experimental results. However, it can be reasonably assumed that the response of the machine

drive will be much faster than that of the paddle and breast (e.g. a machine drive time constant of 0.4s or less). This means that changes in the machine drive dynamics have only a small effect compared to the dramatic reduction in settling time (over 80 seconds) achieved by using closed-loop control and, therefore, such changes do not alter the overall conclusions of this study. We have included results for three different machine drive time constants to demonstrate this.

The breast and paddle model used in this study is a simplified linear model. In reality, the breast is likely to have non-linear visco-elastic characteristics. However, the experimental results shown in Figures 5 and 6 support our decision to approximate the dynamic response (G_{dyn}) to that of a linear 2nd order system. The steady-state gain ($G_{gain} = 0.9$) is less relevant in the context of settling time and changing its value would not alter the results as the PID gains would simply change accordingly.

In practice, female breasts vary widely in terms of size, compressed thickness and density (which depends on the mix of glandular and fatty tissues) and, hence, the plant (breast) transfer function will vary from woman to woman. Therefore, the proposed closed-loop controller would have to be able to deal with this. It may be possible to tune the PID controller so that it is robust to this variability in the plant transfer function. If this is not possible, then adaptive control techniques could be investigated. In adaptive control, the controller gains are automatically adjusted to suit different system dynamics (breast characteristics in this case). These could be based on a gain scheduling approach that uses fixed look-up tables that define how the controller gains should vary as a function of certain system parameters (breast characteristics). Alternatively, an automatic model estimation approach could be adopted using sensor data captured during breast compression.

5. Conclusions

Paddle motion induced blur could be significantly reduced by implementing the proposed closed-loop control of breast side paddle position. With a machine drive time constant of 0.4s, the settling time is reduced from over 90 seconds for the open-loop system to less than 4 seconds for the closed-loop system. Reducing the machine drive time constant further reduces the settling time of the closed-loop system, but this effect is not as important as switching to closed-loop control in the first place. Although there are small differences between the two paddle sizes, these do not alter the observed trends or the conclusions drawn.

Conflict of interest statement:

The authors have no conflict of interest.

References

[1]P.Hogg, K.Szczepura, J.KellyandJ.Taylor,"Blurred digital mammography images,"Radiography.**18**, 55–56 (2012).

[2]P.Hogg, J.Kelly, S.Millington, C.Willcock, G.McGeever and S.Tinston, et al.,"Paddlemotionanalysis," East of England Conference, Cambridge, UK. National Health Service Breast Screening Programme, (2012).

[3]D.Seddon, K.A.Schofieldand C.A.Waite,"Investigation into possible caused of blurring in mammograms," Breast Cancer Res.**2(suppl2)**, A64(2000).doi: 10.1186/bcr253

[4]W.K. Ma, R.Aspin, J.Kelly, S. MillingtonandP.Hogg,"What is the minimum amount of simulated breast movement required for visual detection of blurring? An exploratory investigation."Br J Radiol.**88**, 20150126 (2015).doi: 10.1259/bjr.20150126

[5]W.K.Ma, P.Hogg, J.Kelly and S.Millington."A method to investigate image blurring due to mammography machine compression paddle movement,"Radiography.**21**, 36-41.(2015).doi:10.1016/j.radi.2014.06.004

[6]W.K.Ma, D.Brettle, D.Howard, J.Kelly, S.Millington and P. Hogg."Extra patient movement during mammographic Imaging: An Experimental Study," Br J Radiol.**87**, 20140241. (2014).doi: 10.1259/bjr.20140241

[7]R. C. Dorf and R. H. Bishop, *Modern Control Systems*,12th ed.(Pearson, London, 2010)

[8]CW de Silva, *Modeling and Control of Engineering Systems,*1st ed.(CRC Press , Boca Raton ,2009)

[9]G.F.Franklin, J.D.Powell and A.E.Naeini, *Feedback Control of Dynamic System*, 7th ed.(Pearson, London, 2014)

[10]A.C.Moore, D.R.Dance, D.S.Evans, C.P.Lawinski, E.M.Pitcher and A.Rust, et al., *The Commissioning and Routine Testing of Mammographic X-Ray Systems: A Technical Quality Control Protocol,* Report No. 89(IPEM, York, 2005)

[11]I.Hauge, P.Hogg, K.Szczepura, P. Connolly, G.McGill and C.Mercer. "The readout thickness versus the measured thickness for a range of screen film mammography and full field digital mammography units", Med.Phys.**39**(1), 263–271 (2012).

[12] D. Zill, W. Wright, *Advanced Engineering Mathematics,* 5th ed.(Jones & Bartlett Learning, London, 2012)